# On the Variability of the Snowpack of the Washington Cascades

Joseph H. Casola

A dissertation
submitted in partial fulfillment of the
requirements for the degree of

Doctor of Philosophy

University of Washington

2009

Program Authorized to Offer Degree:
Atmospheric Sciences

University of Washington
Graduate School

This is to certify that I have examined this copy of a doctoral dissertation by

Joseph H. Casola

and have found that it is complete and satisfactory in all respects,
and that any and all revision required by the final
examining committee have been made.

Co-Chair of the Supervisory Committee:

_____

John M. Wallace

Co-Chair of the Supervisory Committee:

_____

Edward L. Miles

Reading Committee:

_____

John M. Wallace

_____

Edward L. Miles

_____

Mark T. Stoelinga

Date: _____

Signature: _____

Date: _____

University of Washington

## Abstract

On the Variability of the Snowpack of the Washington Cascades

Joseph H. Casola

Co-Chair of the Supervisory Committee:
Professor, John M. Wallace
Atmospheric Sciences

Co-Chair of the Supervisory Committee:
Virginia and Prentice Bloedel Professor of Marine Studies, Edward L. Miles
School of Marine Affairs

Because of the large year-to-year variability associated with winter precipitation in the Pacific Northwest, it is difficult to assess the impact of global warming on the Washington Cascades snowpack by estimating trends in the time series of annual snow accumulation. A more robust alternative is to estimate the temperature sensitivity of the snowpack, which can be done by 1) considering the geometry of the Cascades and the idea that warming will move the freezing level upward by an amount $\delta T/\Gamma$, where $\delta T$ represents the amount of warming and $\Gamma$ represents the mean lapse rate; and, 2) performing a regression of the observed snow-water equivalence (SWE) of the snowpack at the end of the winter upon the observed mean winter temperature. Both methods indicate that 1°C of warming would lead to a loss of approximately 20% of the mean SWE observed on April 1.

Estimates of the sensitivity can be used to attribute past or future losses of snowpack to warming, or to calculate the change in the frequency of occurrence of winters exhibiting low snowpack.

Characterizing the processes of accumulation and melt at the daily and monthly time scales can also yield useful information on how warming can affect the snowpack. Daily indices representing the accumulation and melt of snowpack are computed from observations made at snowpack telemetry (SNOTEL) stations. Inspection of the indices reveals that 1) a relatively large proportion of snowfall occurs during a relatively small number of winter days; 2) large accumulation events exhibit enhanced westerly flow aloft, aimed directly at the Cascades; 3) melt is rare from December through March and the amount of SWE lost is typically small; and, 4) daily melt during the spring is proportional to daily mean temperature. These results are consistent with considerations of the energy balance of the snowpack.

The results of this study are applied to the management of Seattle City Light's (SCL) hydroelectric dams, which are located along the Skagit River in the Cascades. SCL's long-term planning and season-to-season operations could be refined by consideration of the intraseasonal variability of snowpack and by anticipating the impact of global warming on snowpack.

# Table of Contents

# List of Figures

**Figure** **Page**



***Chapter 4***



***Chapter 5***

# List of Tables

# Acknowledgements

Without the helpful advice of my dissertation committee (Mike Wallace, Ed Miles, Mark Stoelinga, Dennis Hartmann, Dennis Lettenmaier, and Russ McDuff) this work could not have been completed. I sincerely appreciate their efforts over the past several years.

# Dedication

To my family, who have always encouraged me to pursue my passion and curiosity.

To Kris, for all the love and support.  I am very lucky to have you.

# 1. INTRODUCTION

In Washington, and more generally across the arid Western United States, snowpack plays an integral role in maintaining streamflow during relatively dry spring and summer months. In addition, snowpack provides natural storage for water supply and hydroelectric energy. The functioning of vital ecosystems as well as the economy depends on the amount of snow that accumulates during the winter and the timing and rate of melt in the spring and summer.

## *1.1 Snow Surveying and Water Supply Forecasting*

The value of monitoring the conditions of the snowpack was established by the pioneering efforts of James Edward Church in the early part of the 20th century. Church, a professor of classics and art history at the university of Nevada, Reno, repeatedly climbed Mount Rose, which is located along the California-Nevada border in the Sierra Nevada Mountains, to record the meteorological conditions and measure the snowpack. He established the Mount Rose weather observatory in 1906 (at the time, one of the highest weather stations in the world) and developed the protocol and instruments for sampling the depth and water-equivalence of the snowpack (for details, see Church 1908 and Church 1912). Church used observations of the spring snowpack to provide forecasts of streamflow for the watershed as well as water levels in Lake Tahoe.

Today, snow surveys conducted throughout the West still use the same type of equipment and techniques developed by Dr. Church. These measurements, along with those made at unmanned, remote stations in the Snowpack Telemetry

(SNOTEL) network, provide the foundation for statistical streamflow forecasts across the West. In recent years, numerical simulations of watershed hydrology are playing a growing role in water resource forecasting (Garen and Marks 2005).

*1.2 Global Warming and Snowpack*

In order to assess the impact of global warming on snowpack, analysts have examined both the historical snow survey measurements and performed hydrological model simulations driven by the output of global climate models. For the Cascades, the trends in the historical record do not provide a robust or reliable indication of the impact of warming. Trends estimated beginning in mid-century and ending in the early 2000's show dramatic declines in snowpack (Mote et al. 2008), while trends estimated for the period of the late 1970's to the early 2000's exhibit little decline or even an increase (Stoelinga et al. 2009). As explained in Chapter 2, trend analysis is of limited value in assessing the impacts of global warming because it is difficult to separate the portion of the trend attributable to global warming and the portion associated with "natural" variability. For the case of snowpack, the influence of natural variability, primarily associated with large swings in year-to-year precipitation, is more important than the influence of temperature.

Making use of hydrological simulation models, it is possible to directly compare the snowpack simulated for a base climate state with that for a warmer climate with the same day-to-day and month-to-month variability. Such an experiment clearly distinguishes between the effect of warming and the influence of

natural variability on snowpack. Barnett et al. (2009) and Salathé et al. (2009) have both performed model experiments for the Cascades; the former study focuses on the period 1950-1999; the latter study focuses on anticipated changes occurring between the late 20th century and the 2040's. While both studies show dramatic losses of snowpack related to warming, the results are sensitive to the global climate model employed. The estimated losses due to warming can vary by a factor or 2, which is much larger than the ratio of the rates of warming in the two models that were used. This high sensitivity suggests that experiments at the regional-scale involving coupled climate-hydrological models are currently subject to considerable uncertainty.

*1.3 Outline of Dissertation*

Measurements made for the purposes of water supply forecasting can be used to elucidate the role of temperature during the accumulation and melting of the snowpack. The investigation presented in this dissertation covers a range of temporal scales, from the daily to the interannual, focusing on two sets of questions:

**1) How will global warming affect the snowpack of the Washington Cascades?** How does it affect the amount of accumulation over the winter? How might it affect the rate of ablation in the spring and summer?

**2) What are the characteristics of the day-to-day and month-to-month variability of the snowpack?** What is the relationship between individual

accumulation events and the snow-water equivalent of the snowpack at the end of the winter? Are there preferred times during the winter for accumulation to occur? What is shape and strength of the atmospheric circulation in the North Pacific during large accumulation events? How can knowledge of the daily and monthly variability be applied to in-season forecasts of the snowpack?

By improving our understanding of the processes orchestrating the response of the snowpack to temperature changes, either over the long-term due to global warming or as part of the progression from winter to spring during a typical water year, the hydroclimatological research community can better answer questions posed to it by water and hydroelectric water managers.

The dissertation is organized as follows: Chapter 2 examines the sensitivity of spring snowpack of the Washington Cascades to warming. The methods and results also appear in Casola et al. (2009). Chapter 3 focuses on the observations made by the Snowpack Telemetry network (SNOTEL) in the Washington Cascades, quantifying the contribution of individual accumulation events to the end-of-season snowpack, identifying the circulation patterns that accompany these events, and relating daily mean temperature to the rate of ablation during the spring and summer. Chapter 4 considers the energy balance of the winter snowpack, demonstrating that the findings in the previous chapters are theoretically consistent with the equations typically used to model snowpack. Chapter 5 applies the results of Chapters 2 and 3 to the planning and operations of Seattle City Light, which owns

and maintains a series of dams in the Skagit watershed that are fed by snowmelt from the Cascades.

The work presented in this dissertation aims to provide insight into the relationship between the regional climate and snowpack. More broadly, it is hoped that this type of investigation can advance the methodology for characterizing how climate variability or climate change can affect a natural resource at the sub-continental scale.

## 2. SENSITIVITY OF ACCUMULATION TO GLOBAL WARMING

### *2.1 Introduction*

Estimating the impact of global warming on the snowpack of the western United States is crucially important for managing water and energy resources, as well as for maintaining the health of a variety of sensitive ecosystems. Specifically, the snowpack of the Washington Cascades provides a significant portion of the electricity and water supply of Washington State, and supplies summer streamflow upon which agricultural activities and riparian fauna rely.

In this chapter, three methods for assessing the impact of warming on snowpack will be discussed: trend analysis, fingerprinting, and sensitivity analysis. Two variants of the sensitivity analysis are pursued here, one based on geometrical considerations and the other based on regression analysis. The results indicate that in the absence of a warming-induced increase in precipitation the Cascades exhibit a sensitivity of approximately 20% of April 1 snow-water equivalent (SWE) lost for 1°C of warming[1]. At the conclusion of this chapter, this value of the sensitivity is employed to estimate past and future losses of snowpack as well as the increase in the frequency of occurrence of extremely low snowpack years that are attributable to global warming.

---

[1] In this work, only the direct effect of warming on the snowpack will be considered, as described in Section 2.2. In Casola et al. (2009), the examination of daily Snowpack Telemetry (SNOTEL) records indicates that the increase in precipitation accompanying warming could reduce the sensitivity to 16% of April 1 SWE lost for 1°C of warming.

*2.2 Previous Work*

A common technique for estimating the impact of warming on snowpack (or other hydrologic resources) is to examine a recent time series of snowpack. Most often, the time series representing the snowpack is drawn from measurements of the April 1 SWE, traditionally used as a measure of annual snow accumulation. Several studies have shown significant decreases in April 1 SWE for the periods beginning in the mid-20$^{th}$ century and ending in the late 1990's or early 2000's (Groisman et al. 2004; Mote et al. 2005; Regonda et al. 2005; Mote et al. 2008). These studies typically argue that warming is likely to have played a role in the decrease of spring SWE – the decline in snowpack cannot be explained by changes in precipitation alone (Hamlet et al. 2005), and that changes in other hydrologic variables, such as the advance in the timing of peak streamflow (Stewart et al. 2005) or the decrease in the fraction of precipitation falling as snow (Knowles et al. 2006), are also indicative of warming.

Despite the strong evidence for the contribution of warming to the decline of snowpack in the Cascades, and over the western US in general, examination of time series of snowpack alone do not provide a robust, quantitative estimate of the impact of warming. Depending on the choice of period of record, the sign and magnitude of the trend that can be fit to the snowpack time series are highly sensitive to the analysis protocol. For example, a decline is observed for the 1950-2006 period but not over the last 30 years (Fig. 2.1 and Table 2.1). Similarly, examination of proxies of spring snowpack on longer time scales indicate that the snowpack experiences strong interannual and interdecadal variability (Stoelinga et

al. 2009) that obscure the identification of a trend within the time series. This variability in the snowpack time series is associated with the variability in precipitation; regression of the time series of snowpack shown in Fig. 2.1 upon observations of mean wintertime precipitation made at nearby US Historical Climate Network (HCN) stations[2] yields a fraction of explained variance of $r^2$=0.41. In contrast, a similar regression using observations of mean winter temperature made at the same stations demonstrates that temperature plays a secondary role ($r^2$=0.29). Thus, trend analysis provides only limited information for assessing the impact of warming on snowpack.

Recently, work by Barnett et al. (2008) has explored a fingerprinting method for isolating the effect of temperature on snowpack and other hydrologic variables. Fingerprinting compares the observations of a given set of hydrological variables to a prescribed spatial-temporal pattern (the fingerprint) representing the influence of anthropogenic warming. In Barnett et al. (2008), the fingerprint was generated by comparing the winter temperature, the fraction of precipitation falling as snow, and the timing of streamflow that is output from control and greenhouse-gas-forced runs of a general circulation model. By projecting the fingerprint onto the observations, the strength of the signal that is specifically attributable to warming can be calculated.

---

[2] The HCN stations used were Blaine, Clearbrook, and Sedro-Wooley for the period 1950-2005. The correlation between mean winter precipitation and mean winter temperature for these stations is nearly zero ($r^2$=0.04). Thus, the correlation between snowpack and precipitation can be considered nearly independent of the correlation between snowpack and temperature.

Despite the conceptual appeal of the fingerprinting technique, there still exist issues in using the results of Barnett et al. (2008) to estimate the impact of warming on the snowpack. Based on the fingerprints generated from two different global circulation models, the strength of the signal detected in the observations differs by a factor of 2. Given this level of uncertainty, it is difficult to derive a quantitative estimate of the impact of warming on the snowpack of the Cascades region.

Estimating sensitivity is an alternative to trend analysis and fingerprinting. Like fingerprinting, sensitivity studies attempt to isolate the effect of temperature on snowpack from the effect of other variables, such as precipitation, that are largely driven by natural or internal mechanisms. Sensitivity ($\lambda$) can be expressed as the constant of proportionality between a change in temperature ($\delta T$) and a change in some variable ($\delta x$) that is affected by temperature:

$$\delta x = \lambda(\delta T) \tag{2.1}$$

The sensitivity is formally defined as

$$\lambda \equiv \frac{dx}{dT} = \frac{\partial x}{\partial T} + \sum_i \frac{\partial x}{\partial y_i}\frac{dy_i}{dT} \tag{2.2}$$

where the first partial derivative represents the direct effect of changes in temperature on $x$ and the summation term represents the indirect effect of changes in temperature on $x$. An indirect effect refers to a temperature-induced change in some variable $y$ that also affects $x$. For snowpack, the response of precipitation to warming represents a potentially important indirect effect. If precipitation (taken as $y$) were to increase as a result of warming, the subsequent increase in the SWE of the spring snowpack (taken as $x$) would tend to counteract the direct effect of

warming on the snowpack. In this work, only the direct effect of temperature on the snowpack will be considered.

Several studies present estimates of the temperature sensitivity of snowpack or glaciers. Howat and Tulaczyk (2005) presented a model based on a regression of historical observations of snowpack in the Sierra Nevada upon historical observations of temperature and precipitation that yields an estimated 6-10% of the April 1 SWE lost per degree of warming. Rasmussen et al. (2000) demonstrated that a site at the terminus of the Blue Glacier (~1300 m elevation) would lose over 25% of its snowfall for 1°C warming. Focusing more on the spatial pattern associated of warming, both Bales et al. (2006) and Nolin and Daly (2006) created maps for the US West that highlight areas where winter temperatures are often near or just below 0°C, indicating where a small warming could result in a major conversion from snowfall to rainfall.

*2.3 Sensitivity Analysis – Geometric Approach*

The conceptual model presented by Fleagle (1991) will be utilized to estimate the impact of warming on the snowpack of the Cascades. Fleagle (1991) argued that warming would result in a loss of snowpack by raising the climatological snowline. By comparing the area covered by snow prior to warming to the area covered by snow after warming, the sensitivity is calculated. What follows is an elaboration of Fleagle's model. Specifically, two improvements have been made: 1) the distribution of area with elevation is taken into account, and 2)

the increase in SWE with increasing elevation is considered. Fleagle's analysis assumed that SWE is constant above the snowline.

The volume of water contained by the snowpack (snow water storage, SWS) can be written as

$$SWS = \int S(z)A(z)dz \tag{2.3}$$

where *S(z)* represents the mean April 1 SWE as a function of elevation and *A(z) dz* represents the differential area lying between elevation contours *z* and *z+dz*. The function *A(z)* is equal to the derivative of the so-called "hypsometric curve," which represents the fractional amount of area that lies above a certain elevation in a drainage basin. Essentially, the hypsometric curve is the cumulative distribution function for the distribution of area with respect to elevation; *A(z)* is the corresponding probability density function.

This analysis is focused on the west-facing slopes of the Cascades that drain into the Puget Sound (Fig. 2.2). The hypsometric curve and *A(z)* for this region are shown in Fig. 2.3. For the range of elevations from 500 m to 1200 m, the value of *A(z)* is nearly constant. This signifies that the terrain has the same properties as a sloping plane surface, for which the areas between any two elevation contours *z* and *z+dz* would be equal. For the elevations greater than 1200 m, *A(z)* decreases nearly linearly with increasing elevation. This distribution is indicative of terrain that is more conical shaped, for which the amount of area between evenly spaced contours would shrink linearly with increasing elevation. If there existed a plateau within the basin, *A(z)* could increase with increasing elevation for some range of elevations just

below it. The Skagit watershed (see Chapter 5) displays such a feature in its *A(z)* curve.

Following Fleagle (1991), the effect of warming would be to raise the snowline by an amount equal to $\delta T/\Gamma$. Assuming that the moist adiabatic lapse rate (–6.5°C/km) represents the typical winter conditions of the Cascades, a 1°C warming would raise the mean snowline by approximately 150 m. Referencing the Snowpack Telemetry observations (SNOTEL, Chapter 3), the lowest station in the Cascades is Huckleberry Creek, located at an elevation 610 m. Its mean April 1 SWE is less than 2 cm; of the 9 years of data for this site, only 3 exhibit an April 1 SWE greater than 0 cm. Thus, 600 m will be used as the climatological snowline for the current climate and 600 m + 150 m = 750 m will be used as the future snowline following 1°C warming. Using these values for $\Gamma$ and the snowline with a constant value for *S(z)*, repeating the same analysis that Fleagle (1991) performed, the decline in April 1 SWE for Cascades is equal simply to the relative change in the snow-covered area as the snowline moves from 600 m to 750 m. This reduction represents a 12% loss of mean April 1 SWE for a 1°C warming.

Taking the analysis a step further, one can imagine that *S(z)* is not a constant above the snowline, but rather the SWE increases linearly with increasing elevation. Such a distribution is motivated by the enhancement of precipitation due to orographic forcing, as well as the large excursions of the freezing level through the winter. Both mechanisms provide for greater amounts of snow accumulation at higher elevations. Output from hydrological models also confirms the general tendency for mean April 1 SWE to increase with increasing elevation in the

Washington Cascades (Casola et al. 2009). To account for this height dependence, $S(z)$ can be replaced by $mz$, where $m$ is a constant, and Eqn. 2.3 can be rearranged to obtain

$$SWS = m\int_{z_B}^{z_T}(z - z_B)A(z)dz \qquad (2.4)$$

where $z_B$ corresponds to the base of the snow accumulation region and $z_T$ represents the top of the snow accumulation region. By setting $\Delta z$ equal to the amount the snowline is raised by warming, the change in SWS resulting from warming is

$$\Delta SWS = -m\int_{z_B}^{z_B+\Delta z}(z - z_B)A(z)dz - m\Delta z\int_{z_B+\Delta z}^{z_T}A(z)dz \qquad (2.5)$$

Within the small elevation range of $z_B$ to $z_B+\Delta z$, $A(z)$ is nearly constant and approximately equal to $A(z_B)$. Thus, the first term in Eqn. 2.5 can be rewritten as $A(z_B)m(\Delta z)^2/2$. Dividing through by the original SWS yields an expression for the sensitivity:

$$\frac{\Delta SWS}{SWS} = \frac{-\Delta z\left(A(z_B)\frac{\Delta z}{2} + \int_{z_B+\Delta z}^{z_T}A(z)dz\right)}{\int_{z_B}^{z_T}(z - z_B)A(z)dz} \qquad (2.6)$$

Notably, the rate of increase in SWE with elevation ($m$) has been cancelled out. Provided that the shape of the profile is unchanged by warming (i.e., the value of $m$ is the same both prior to and following warming), the rate of increase in SWE with respect to elevation has no bearing on the sensitivity.

Upon substituting $z_B$ = 600 m, $\Delta z$ = 150 m, $z_T$ = 3000 m, and $A(z)$ as shown in Fig. 2.3, Eqn. 2.6 yields a sensitivity of 23% of mean April 1 SWE lost for 1°C of

warming. The differences between the vertical profiles of SWS (per unit elevation) for the original climate and the 1°C climate are shown in Fig. 2.4. Altering the assumptions for $z_B$ or the lapse rate, which changes $\Delta z$, changes this estimate as shown in Table 2.2. The value used for the lapse rate has a greater impact on the sensitivity than the value used for the snowline, but the changes in sensitivity are modest in both cases.

The terms in Eqn. 2.6 represent different ways in which warming affects the snowpack. The first term corresponds to the SWE lost between $z_B$ and $z_B+\Delta z$, in other words, the area where warming causes the snow to vanish entirely on April 1. The second term corresponds to the SWE lost due to thinning throughout the snow-accumulation area, well above the snowline. For values of $\Delta z$ that are small relative to the elevation range of the snow accumulation area, the term representing thinning is considerably larger than the term representing the area that is no longer snow covered.

The geometric approach also permits estimation of the loss of snowpack accompanying a larger warming. For warming less than 3°C, the amount of SWE lost can be approximated by multiplication of the sensitivity and the amount of warming. For example, for 2°C of warming, 43% of April 1 SWE is lost, and for 3°C of warming, 59% of April 1 SWE is lost. Multiplication serves as an accurate approximation because $A(z)$ is nearly constant through most of the elevation range of snow accumulation. For warming greater than 3°C, simple multiplication yields an overestimate of the loss since $A(z)$ begins to decline with elevation. For example,

a 4°C warming, which would raise the base of the snowpack to 1200 m, leads to a 72% loss of April 1 SWE.

*2.4 Sensitivity Analysis – Regression Analysis*

A time series of observations of basin-averaged April 1 SWE (red line, Fig. 2.1) can be regressed upon observations on mean winter temperature to yield an estimate of the temperature sensitivity of the snowpack. To perform this regression, a time series of basin-averaged April 1 SWE was constructed from 24 snow course measurements[3] located throughout the Cascades (Fig. 2.2 and Table 2.3). For each water year during the period 1970-2006, the April 1 SWE observed at the snow courses was regressed upon their respective elevation. The resulting best-fit regression line is analogous to *S(z)* (see previous section) but based on the data for just one year. Then, each year's best-fit line was multiplied by the *A(z)* function and integrated with respect to *z*, yielding an estimate for the volume of water stored by the snowpack. This volume was divided by the area of the basin that is above 600 m in elevation.

Figure 2.5 shows an example of the regression of the time series of the basin-averaged April 1 SWE upon the time series of mean winter temperature observed in Washington's Climate Division 4, which represents the east slope of the Olympic Mountains and the foothills of the Cascade Mountains. The slope of the regression line indicates that the Cascade snowpack has a temperature sensitivity of 27% for

[3] These snow courses were selected from the 44 available in the region based on the fact that they had measurement for at least 33 of the 37 years in the 1970-2006 period.

1°C warming. The fit of the regression line is not particularly good ($r^2 = 0.28$), and consequently the 95% confidence interval for the slope ranges from 12% to 42%. The poor fit of the regression line reflects uncertainty from several sources. First, the use of seasonal mean values fails to capture the daily covariability between temperature and precipitation that plays an important role in determining snow accumulation. As shown in Chapter 3, a few winter days exhibiting relatively heavy precipitation while temperatures in the mountains are below freezing account for a large portion of the spring snowpack. The temperature during these heavy precipitation events has a significant impact on seasonal snowpack, while the temperature on days receiving little or no precipitation has minimal impact on the snowpack. Second, the paucity of snow courses at relatively low elevations (around 500 or 600 m) leads to uncertainty in the estimate of the basin-averaged April 1 SWE, because a sizeable proportion of the basin area is located near the base of the snowpack. Third, it is unclear which temperature record best represents conditions within the zone of accumulation. Climate Division 4 is located just upstream from the Cascades, includes a relatively large number of stations, and has been used as an indicator of temperature for previous analysis of the Cascades snowpack (Mote et al. 2008); however, the stations in that division are located in the lowlands.

To address the uncertainty in the sensitivity estimate, the regression was repeated after linearly regressing out the variability associated with the seasonal mean precipitation from the time series of the basin-average April 1 SWE. Since winter precipitation and winter temperature are largely uncorrelated in the region

($r^2$<0.01), the two can be treated as nearly independent predictors of the April 1 SWE. While regressing out the precipitation-related variability narrows the range of the 95% confidence interval for the estimate of sensitivity from 12-42% to 18-35%, the central estimate is only changed from 27% to 26%.

In addition, other temperature records can be used. Table 2.4 shows the results for the regressions using temperature and precipitation records from Washington Climate Division 5 and from selected US Historical Climate Network (HCN) stations. Climate Division 5 represents the area of the Cascades. It contains stations that are located at a higher elevation relative to those in Climate Division 4; however, fewer stations are included in Division 5. Subsequently, the variability of the temperature record is greater and the confidence intervals for the estimate of sensitivity are relatively large. The HCN stations (Table 2.5; Karl et al. 1990) have been quality controlled for use in climate studies, and are often considered superior for performing time series analysis. As it turns out, the sensitivity estimates made using the HCN stations are quite similar to those from the Climate Divisions, with the exception of the estimate associated with the subset of stations located to the East of the Cascades. It is clear that the temperatures observed at these stations, which are located primarily downstream from snow courses, have a particularly weak relationship with the snow measurements.

Overall, while there is considerable uncertainty associated with the estimates of sensitivity from the regression of the time series of the basin-averaged April 1 SWE upon various time series of winter temperature, the estimates are consistent

with the sensitivity value of 23% for 1°C warming derived from the geometric approach.

*2.5 Applying Sensitivity*

The sensitivity of the snowpack to warming can be combined with estimates of past or future warming to determine losses of April 1 SWE during those respective periods. In addition, the sensitivity can be used to build scenarios to gauge the impact of warming on the frequency of occurrence of extremely low values of April 1 SWE. For simplicity, a sensitivity value of 20% of mean April 1 SWE lost for 1°C warming will be used in the following calculations. The base value for determining losses is defined as the mean April 1 SWE of the period 1970-2006. This period was analyzed explicitly in the regression section and was represented by the profile of $S(z)$ with a base located at 600 m in the geometric approach section.

Estimating Past and Future Losses of April 1 SWE attributable to Warming

Within the Pacific Northwest, the amount of snowpack lost due to warming during the previous decades and that is expected to be lost during the coming decades has been a matter of considerable public and scientific dispute (Mote et al. 2008; Cornwall 2008). By multiplying the estimate of the temperature sensitivity by an estimate of the local warming attributable to global warming, the amount of loss for either a period in the past or the future can be calculated. However, the amount of local warming caused by a global-scale forcing, most of which is attributed to anthropogenic emissions of greenhouse gases (Solomon et al. 2007), can only be

estimated roughly. A theoretical framework for linking warming on the global scale to the climate of a much smaller region, such as the North Pacific or the Washington Cascades, does not yet exist. While models can be used to assess future changes, the representation of important regional features of climate, especially those that have a significant impact on snowpack (e.g., topography, dynamics involving the land surface, the orientation and strength of the jet stream) is an active area of research. The simulations performed for the Pacific Northwest to date demonstrate that when different global climate models are used to supply the boundary conditions for the regional domain, the climate responses can be quite different, especially with respect to winter precipitation (Salathé et al. 2007). In the future, as more simulations are preformed with a variety of global climate models coupled to regional climate models, it will hopefully be possible to quantify both the regional-scale climatic response to global warming, as well as the uncertainty associated with that response.

For this calculation, it is assumed that the contribution of global warming to the rise in winter temperatures over the Cascades is the same as the observed rise in temperatures averaged over the Northern Hemisphere as a whole – it is assumed that "a rising tide lifts all ships." For the future, it is assumed that the rate of warming experienced over the previous three decades (1970-2000) will continue for the upcoming decades (2010-2040). This is consistent with IPCC projections (Solomon et al. 2007) and regional climate modeling studies (Salathé et al. 2007). Additionally, the possibility of a distinction between temperature trends over land and ocean will be allowed for, since it could be argued that winter precipitation over

the Cascades is more strongly affected by the conditions averaged through the depth of the marine boundary layer located upstream of the mountains rather than by the local surface air temperature.

Table 2.6 shows estimates of the linear trend in surface temperature for portions of the Northern Hemisphere during the period 1977-2006. The rate of warming has been roughly twice as large over the continents as over the oceans. Distinctions between the trends based on geographical domain or season are less pronounced.

A reasonable upper bound on the amount of warming that has occurred over the period 1977-2006 is 1°C, a value representative of the zonal-mean land temperature trends (left hand column of Table 2.6). A lower bound for the warming is 0.5°C, a value representing the zonal-mean ocean temperature trends (top three estimates in the right hand column of Table 2.6). Combining these estimates with the sensitivity estimate of 20% of mean April 1 SWE lost for 1°C warming yields a loss of 10-20% of mean April 1 SWE attributable to global warming. Projecting the same rate of warming (+0.33°C/decade over land; +0.17°C/decade over the ocean) for the period 2010-2040, an additional 10-20% of loss can be expected. The cumulative loss of April 1 SWE from 1977 to 2040 ranges from approximately 20% to 40%.

If mean temperature of the North Pacific domain in Table 2.6 were used in place of hemispheric or zonal averages as the lower bound of past warming, the temperature rise would have been 0.38°C rather than 0.5°C. Evidently there has been some degree of cancellation between the hemispheric-scale warming over the

past 30 years and the dynamically-induced temperature trend over the North Pacific. If this cancellation were understood to be an integral part of the spatial signature of global warming, there would be a basis for expecting it to continue to mitigate the impacts of global warming on Cascades snowpack. Lacking dynamical support for such an interpretation, the smallness of the temperature rise over the North Pacific over the past 30 years is regarded as a consequence of regional variability and is assumed to have no predictive implications.

Changes in the Frequency of Occurrence of Extreme Events

In this section, a procedure is outlined for estimating the increase in the frequency of extremely low snowpack years attributable to global warming. This procedure models the "natural" year-to-year variations in April 1 SWE using a time series of randomly sampled values from a set of normally distributed numbers. In this "base climate," the natural variability is represented as a white noise process. To simulate the "warmed climate," a negative linear trend can be added to the white noise time series.

To demonstrate the procedure, a long time series (10,000 years) representing the natural variability in April 1 SWE has been generated (Fig. 2.6). This constitutes the base climate. While the units are arbitrary, it can be assumed that the time series represents the annual anomaly in cm of April 1 SWE for the basin; positive values indicate a year with greater than average April 1 SWE and negative values represent a year with less than average April 1 SWE. The two "free parameters" of this simple model are the standard deviation of the time series

representing the natural variability in April 1 SWE and the slope of the trend representing the impact of global warming. Both can be expressed as percentages of the mean value of April 1 SWE; a mean value for the April 1 SWE time series is assumed to be 100 cm, facilitating the conversion between percentages and dimensional units. The standard deviation of the time series has been set to 35 cm, or 35% of the mean April 1 SWE. This is equal to the coefficient of variation exhibited by 20$^{th}$ century simulations of the snowpack by the Distributed Hydrology Soil Vegetation Model (DHSVM) for the portion of the Cascades that drains into the Puget Sound (Casola et al. 2009). The impact of global warming has been modeled as a 20% loss of April 1 SWE over a 30 year interval (a line with a slope of –0.67 cm SWE/yr), consistent with the sensitivity estimates calculated in previous sections and a +0.33°C/decade warming rate.

To determine the change in the frequency of occurrence of extremely low snowpack years, a time frame and threshold for a "low snowpack year" must be chosen. For this analysis, the focus is on periods of 50 years and events in the lowest 2 percentiles of the 10,000 year time series, colloquially the "50-year low snowpack event." This threshold for low snowpack years corresponds to values of April 1 SWE that are approximately 30% of the mean. In the time series of April 1 SWE observations (Fig. 2.1), this would correspond roughly to the April 1 SWE observed in the years 1977 and 2005. Sample plots of the "simulated" snowpack time series for 50-year periods are shown in Fig. 2.7 The base climate is shown in the top panel; the linear decline in snowpack due to warming is shown in the middle

panel; and, the warmed climate (i.e., sum of the base climate and warming trend) is shown in the bottom panel.

Figure 2.8 shows that for the base climate, most of the 50-year periods exhibit 0, 1, or 2 of these events. Examination of the realizations for the warmed climate indicates that the frequency of occurrence of the low snowpack years increases to 1-5 events every 50 years. In the base climate, 35% of the 50-year periods do not contain a low-snowpack year (a year with only 30% of mean snowpack or less), whereas in the warmed climate only 5% of the 50-year periods do not exhibit a low-snowpack year. Likewise, the "worst case scenario" in the base climate corresponds to a single 50-year period experiencing 5 low snowpack winters. This situation has a probability of occurrence of less that 1% in the base climate. In contrast, this situation has a probability of occurrence greater than 10% for the warmed climate, and the "worst case scenario" in the warmed climate corresponds to a single 50-year period experiencing 9 low snowpack winters.

While this simple noise model has its limitations (e.g., the fit of the white noise model to the distribution of observed or simulated April 1 SWE values has not been assessed; alternative statistical models, such as those employing auto-regressive or shifting means processes have not been tested), it serves to illustrate an important point regarding the potential impact of warming on snowpack, which is likely applicable to other hydrological or ecological resources in regions that experience relatively large interannual variability in precipitation. In the case of snowpack, the effect of global warming is small relative to the magnitude of the variability associated with year-to-year precipitation, which is presumably driven

by natural mechanisms, unrelated to warming. This natural variability can at times act to mask the impact of warming; at other times it can act to amplify those impacts. While the interaction between the "signal" related to global warming and "noise" associated with natural variability makes the tasks of detection and attribution difficult, warming is nonetheless likely to result in a substantial change in the magnitude and frequency of occurrence of extreme events.

### *2.6 Summary*

The analysis presented in this chapter can be summarized in terms of the following main points:

- Performing trend analysis, fingerprinting, and calculating sensitivity are techniques for quantifying the impact of global warming on the snowpack of the Cascades. Given the large variability unrelated to warming inherent in observations of the regional snowpack, trend analysis is of marginal utility. Fingerprinting is valuable for detecting and attributing changes in the hydrological cycle to warming; however, the ability of the method to precisely quantify the impact of warming on the snowpack is limited by the precision of the models used to derive the fingerprint. Sensitivity methods offer an alternative that is conceptually straightforward, requires minimal computer resources, and the level of uncertainty accompanying the estimates is comparable, if not smaller, than the other methods.
- The geometric and regression approaches converge to a sensitivity value of 20% of April 1 SWE lost for 1°C of warming. This estimate only considers the

direct effect of warming on snowpack, and not any warming-induced increase in precipitation that might tend to counteract the direct effect. Arguments made in Casola et al. (2009) based on daily observations of snow accumulation and temperature demonstrate that the indirect effect should be small (approximately 4% of mean April 1 SWE) when compared to the direct effect.

- Other methods for estimating sensitivity presented in Casola et al. (2009) are also consistent with the sensitivity estimate of 20% of April 1 SWE lost for 1°C of warming. Specifically, output from a hydrological model that simulates the effect of warming on the snowpack in the Cascades portion of the Puget Sound drainage yields a loss 22% of April 1 SWE for 1°C warming; examination of snowpack, temperature, and precipitation measurements at a SNOTEL station (Olallie Meadows) that is considered representative of the Cascades as a whole indicates that 24% of the snowfall could transition to rainfall following a 1°C warming.
- The sensitivity value can be used to estimate previous and future losses of SWE due to warming. Additionally, the sensitivity value can be used to estimate increases in the magnitude and frequency of occurrence of extreme events related to warming.

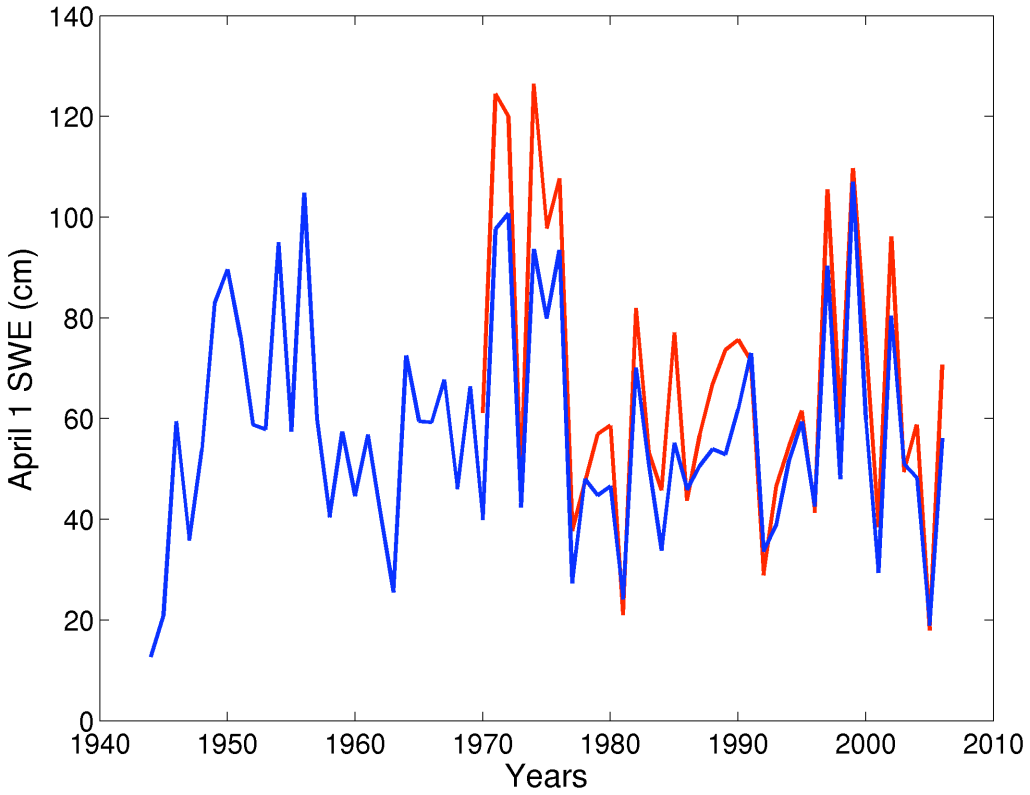


Figure 2.1. Mean of April 1 SWE observed at selected snow courses (see Table 2.3) in the Washington Cascades. The blue line represents the period from 1944-2006 and includes data from 9 snow courses, selected due to the length of their records. The red line represents the period from 1970-2006 and includes data from 24 snow courses. Despite the fact that the two time series have been constructed with a different set of snow courses, and that the data for the red line has been area-weighted (see regression section), the time series are well correlated ($r^2$=0.92).

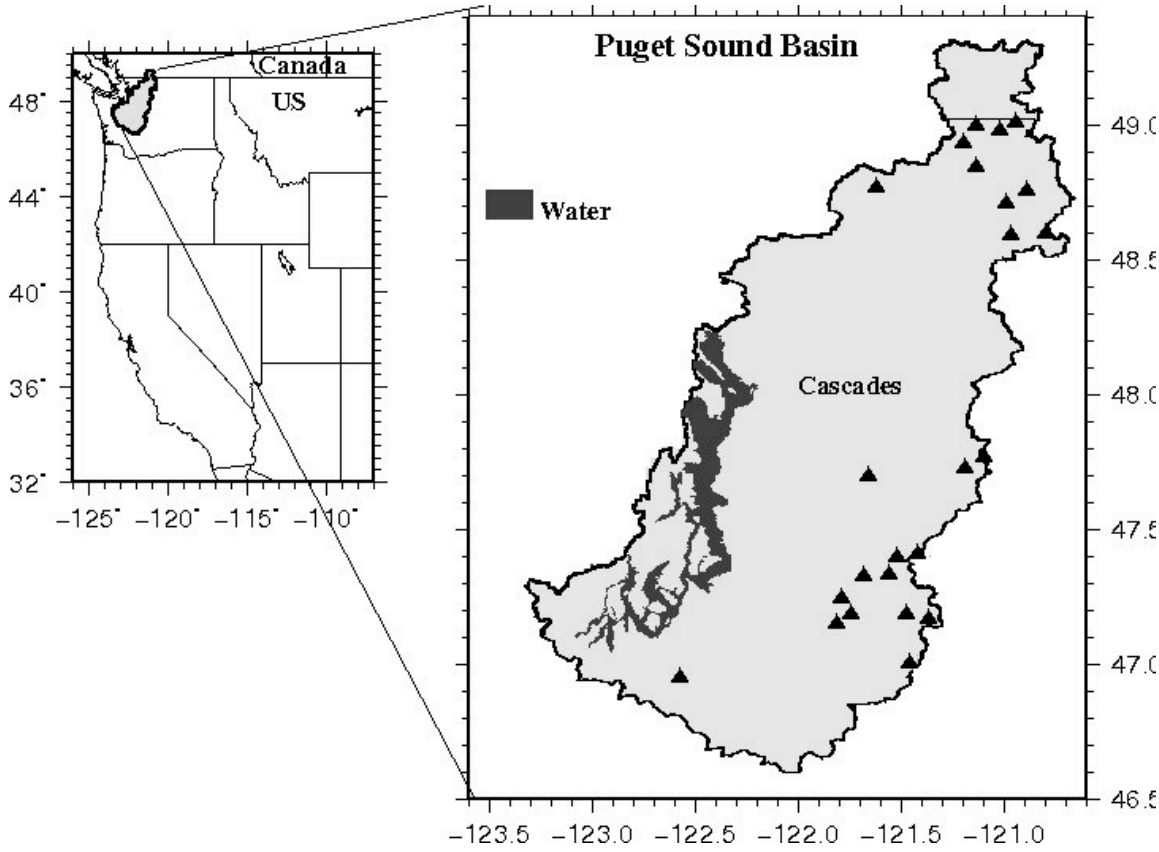


Figure 2.2. The Cascades portion of the Puget Sound drainage basin. Locations of snow courses used in the regression analysis are indicated by the triangles.

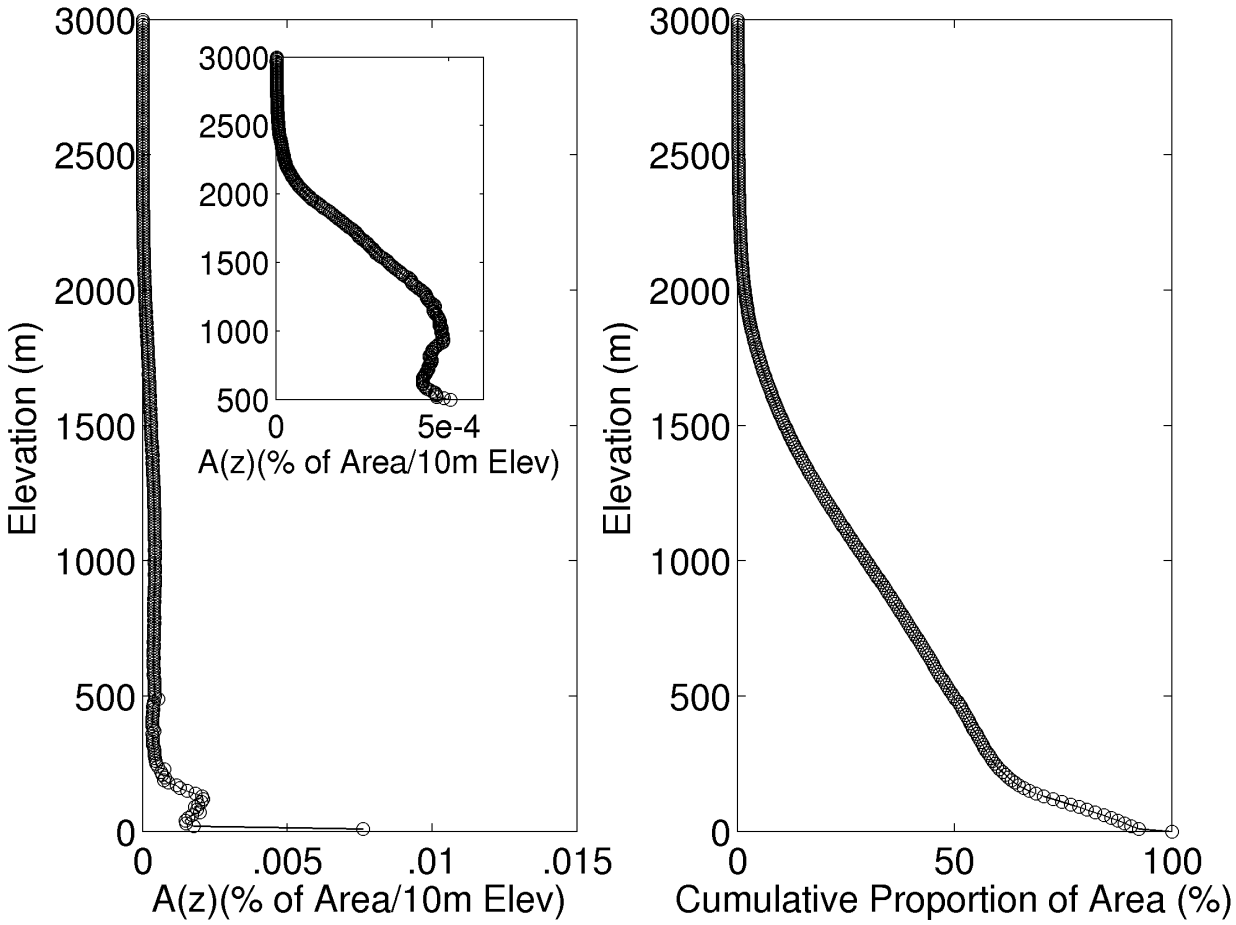


Figure 2.3. Left panel: *A(z)* for the Cascades with an inset showing an expanded plot for elevations above 500 m. Right panel: the corresponding hypsometric curve. The *A(z)* curves have been smoothed with a five-point triangular filter.

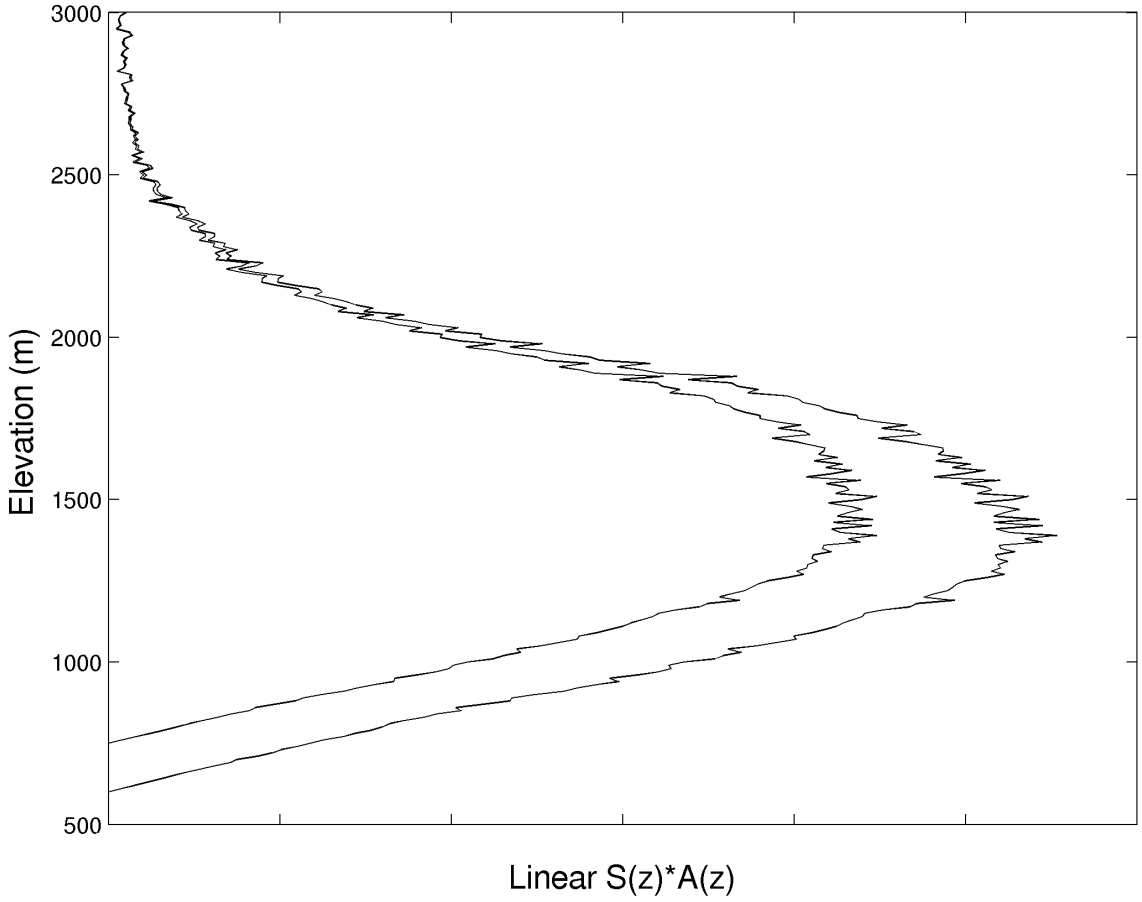


Figure 2.4. Idealized illustration of SWE loss in the Cascades, assuming a linearly increasing profile for *S(z).* Outer curve corresponds to the original climatology; inner curve corresponds to a 1°C warming and a lifting of the *S(z)* profile by ~ 150m.

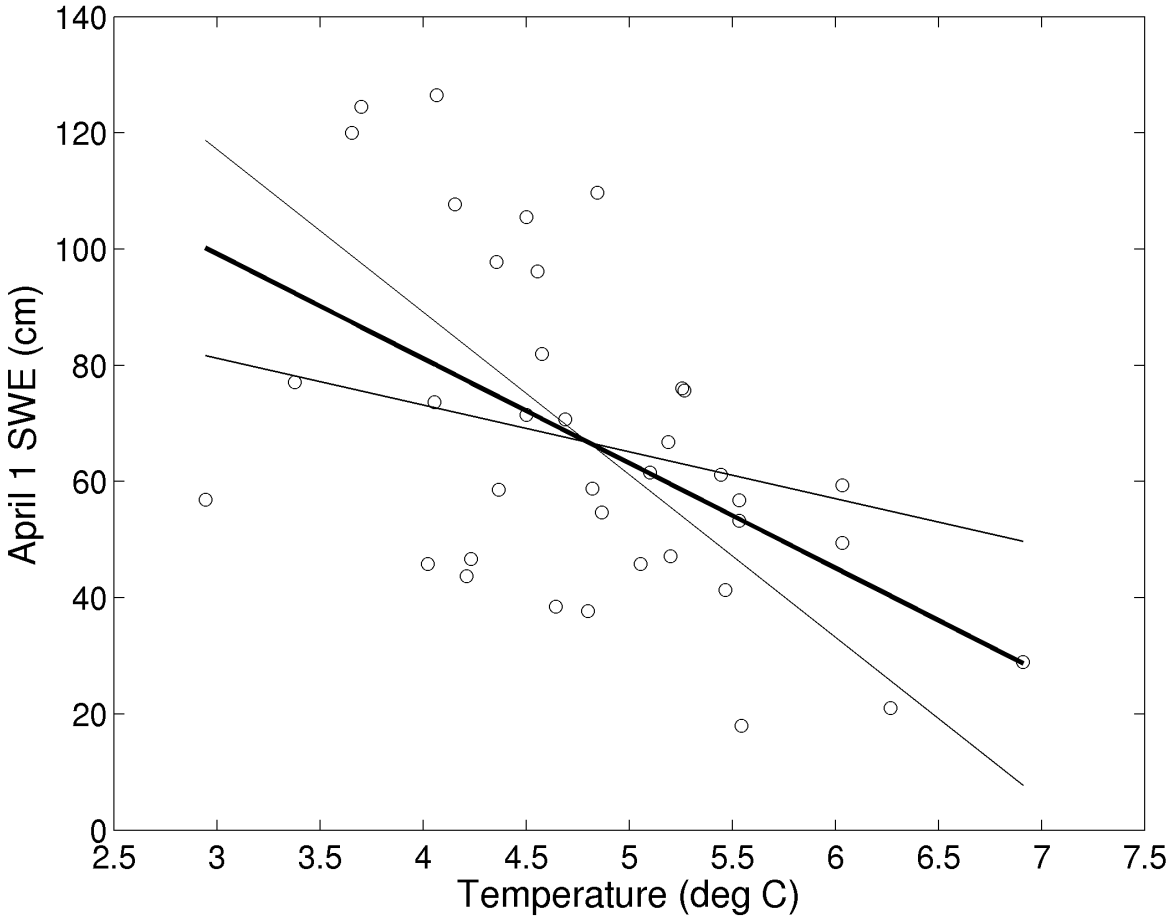


Figure 2.5. Regression of Cascades basin-integrated April 1 SWE upon mean winter (NDJFM) temperature for Washington's Climate Division 4, 1970-2006. The slope of the best-fit regression line (thick line) yields the sensitivity of the Cascade snowpack to warming. The thin lines represent the 95% confidence limits associated with the slope estimate. The basin-integrated April 1 SWE has been estimated using SWE measurements from 24 snow courses located in USGS Hydrologic Unit 1711.

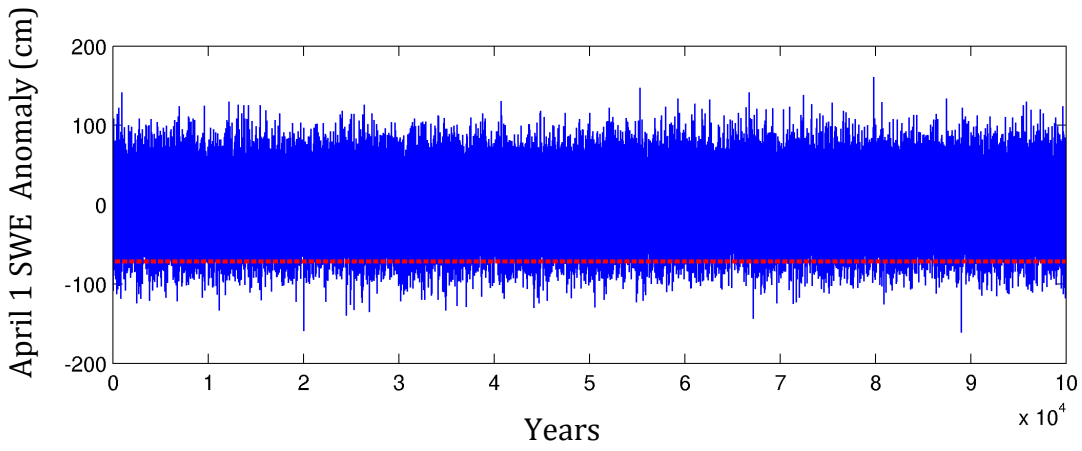


Figure 2.6. Synthetic, "white noise" time series representing annual observations of April 1 SWE anomalies (blue) for a 10,000 year period. This long time series represents the "base climate." The red, dotted line represents the threshold for low SWE years, which is equal to the lowest 2 percentiles of the 10,000 years of SWE anomaly values.

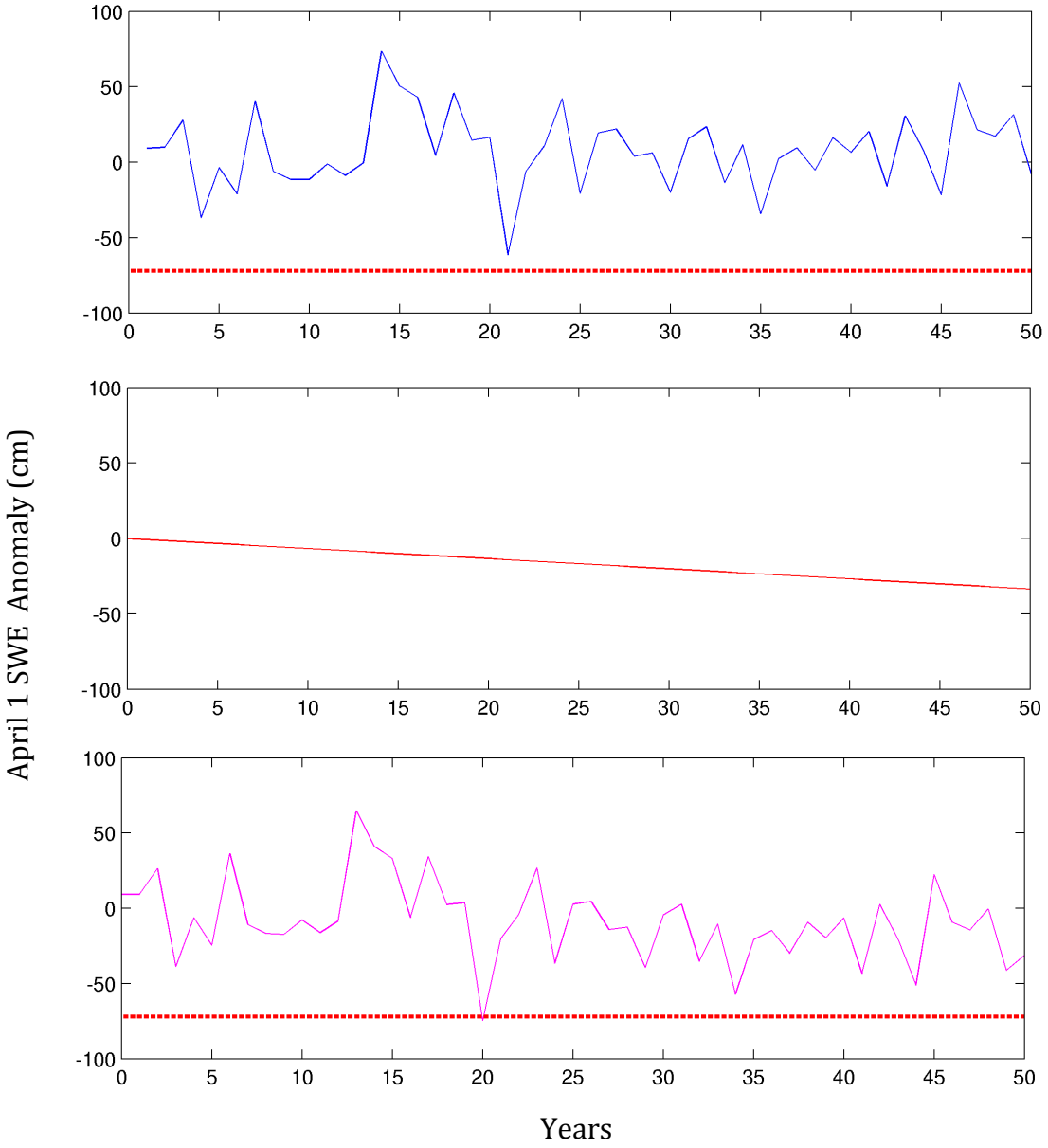


Figure 2.7. Top: An example of a 50-year period from the snowpack time series representing the "base climate" shown in Fig. 2.6. Blue line represents April 1 SWE anomalies and red, dotted line represents the threshold for low SWE years, as in Fig. 2.6. Middle: Model of the impact of global warming on the mean snowpack. Bottom: An example of the "warmed climate" (magenta) created by adding the time series from the top and middle panels. This represents the effect of global warming in the presence of large natural variability. The red, dotted line is the same as in the top panel.

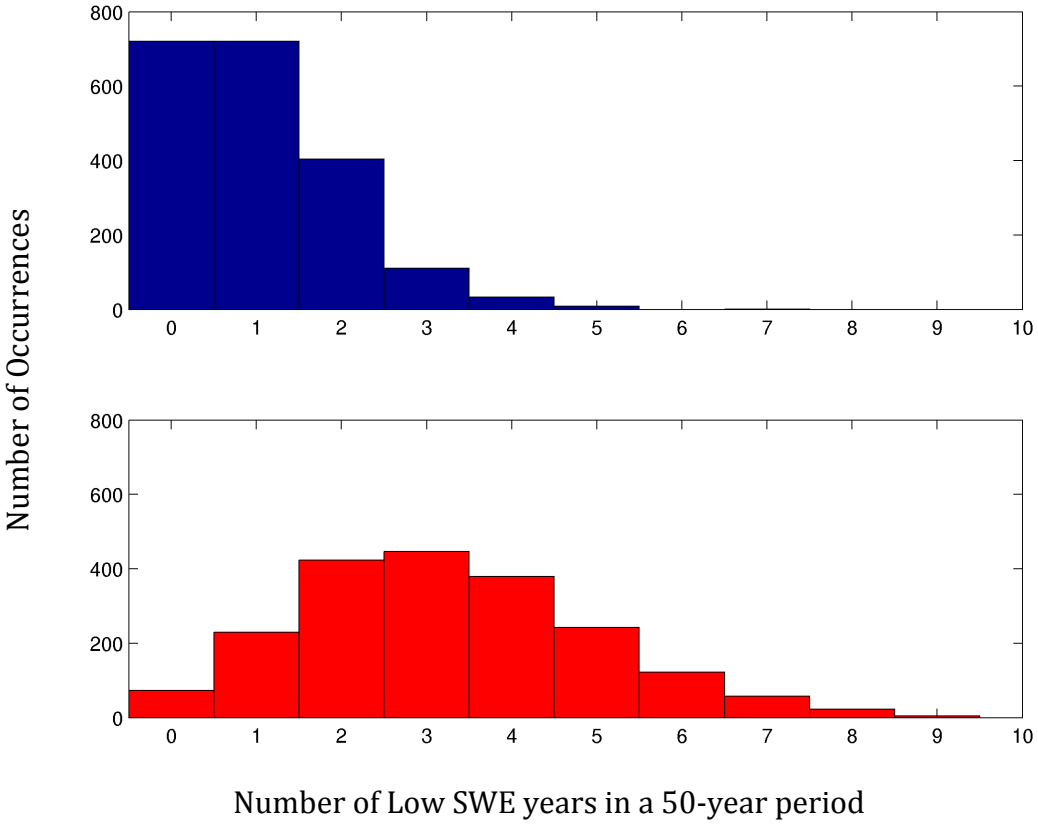


Figure 2.8. Histogram of the number of occurrences of a specified number of low SWE years in the "base climate" (top panel) and in the "warmed climate" (bottom panel).

Table 2.1. Estimates of trends in the time series of Cascades snowpack shown in Fig.1.

| | **Slope (cm/yr)** | **Slope (% of mean April 1 SWE/yr)** | **$r^2$** |
|---|---|---|---|
| 1944-2006 | -0.078 | -0.14 | <0.01 |
| 1950-2006 | -0.277 | -0.48 | 0.05 |
| 1977-2006 | +0.478 | +0.84 | 0.05 |

Table 2.2. Sensitivity estimates derived for the Cascades using the geometric approach and different assumptions regarding the lapse rate and the elevation of the base of the snowpack on April 1. All values are in percent of mean April 1 SWE lost for 1°C warming.

| | **500 m** | **600 m** | **700 m** |
|---|---|---|---|
| 7.5°/km | 19% | 20% | 22% |
| 6.5°/km | 21% | 23% | 25% |
| 5.5°/km | 25% | 27% | 29% |
| 4.5°/km | 30% | 33% | 35% |

Table 2.3. Snow courses used to estimate the basin-integrated SWE for the Cascades 1970-2006. These snow courses are located in USGS Hydrologic Unit 1711, which drains into the Puget Sound. The snow courses have April 1 SWE measurements for at least 33 of the 37 years in that period. Snow courses with asterisks (*) have been used to calculate the long time series (1944-2006) of April 1 SWE, shown in Fig. 2.1 in blue.

| Snow Course | NRCS ID | Elevation (m) | Latitude | Longitude |
|---|---|---|---|---|
| Alpine Meadow | 21B48 | 1067 | 47.77 | 121.70 |
| Beaver Creek Trail* | 21A04 | 671 | 48.82 | 121.20 |
| Beaver Pass* | 21A01 | 1122 | 48.87 | 121.25 |
| Brown Top Ridge AM* | 21A28 | 1829 | 48.92 | 121.20 |
| Cayuse Pass | 21C06 | 1615 | 46.87 | 121.52 |
| City Cabin | 21B03 | 728 | 47.32 | 121.52 |
| Corral Pass | 21B13 | 1829 | 47.02 | 121.47 |
| Cougar Mountain | 21B42 | 975 | 47.30 | 121.67 |
| Devils Park* | 20A04 | 1798 | 48.75 | 120.85 |
| Freezeout Creek Trail* | 20A01 | 1067 | 48.95 | 121.95 |
| Granite Creek* | 20A06 | 1067 | 48.60 | 120.80 |
| Grass Mountain No.2 | 21B27 | 884 | 47.22 | 121.75 |
| Lester Creek | 21B29 | 945 | 47.17 | 121.47 |
| Lynn Lake | 21B50 | 1219 | 47.20 | 121.78 |
| Marten Lake | 21A09 | 1097 | 48.77 | 121.72 |
| Meadow Cabins* | 20A08 | 579 | 48.57 | 120.93 |
| Mt. Gardner | 21B21 | 1006 | 47.37 | 121.57 |
| New Lake Hozomeen* | 21A30 | 853 | 48.95 | 121.03 |
| Olallie Meadows | 21B02 | 1105 | 47.37 | 121.45 |
| Sawmill Ridge | 21B31 | 1433 | 47.17 | 121.43 |
| Stevens Pass Pillow | 21B01 | 1241 | 47.70 | 121.08 |
| Stevens Pass Sand Shed | 21B45 | 1128 | 47.75 | 121.03 |
| Thunder Basin* | 20A07 | 732 | 48.52 | 120.98 |
| Twin Camp | 21B30 | 1250 | 47.13 | 121.78 |

Table 2.4. Sensitivity estimates derived from regression of basin-integrated April 1 SWE upon seasonal mean temperature. Basin-integrated SWE has been calculated from snow courses across the western slope of the Cascades; the temperature data used is indicated in each row. Climate Division 4 includes the east slope of the Olympic Mountains and the Cascade Foothills; Climate Division 5 includes the west slope of the Cascades. Sixteen Historical Climate Network (HCN) stations that straddle the Cascades have been used for the HCN estimates; 10 are located west of the crest of the Cascades and 6 are located east of the crest.

| **Temperature Data Used** | **Sensitivity (Range)** | **$r^2$** |
|---|---|---|
| Climate Division 4 | 27% (12-42%) | 0.28 |
| Climate Division 4, precipitation variability removed | 26% (18-35%) | |
| Climate Division 5 | 21% (8-31%) | 0.28 |
| Climate Division 5, precipitation variability removed | 17% (10-25%) | |
| Nearby US HCN stations | 18% (3-31%) | 0.15 |
| Nearby US HCN stations, West | 25% (8-39%) | 0.23 |
| Nearby US HCN stations, East | 10% (+2-22%) | 0.07 |

Table 2.5. Historical Climate Network stations used to estimate wintertime temperature in the Cascades.

| HCN Station | Cooperative Network Index | Elevation (m) | Latitude | Longitude |
|---|---|---|---|---|
| ***West*** | | | | |
| Bellingham | 0587 | 5 | 48.72 | 122.52 |
| Blaine | 0729 | 18 | 49.00 | 122.75 |
| Buckley | 0945 | 209 | 47.17 | 122.00 |
| Cedar Lake | 1233 | 475 | 47.42 | 121.73 |
| Clearbrook | 1484 | 20 | 48.97 | 122.33 |
| Everett | 2675 | 18 | 47.98 | 122.18 |
| Puyallup | 6803 | 15 | 47.20 | 122.33 |
| Seattle | 7458 | 6 | 47.65 | 122.30 |
| Sedro-Wooley | 7507 | 18 | 48.50 | 122.23 |
| Snoqualmie Falls | 7773 | 134 | 47.55 | 121.85 |
| ***East*** | | | | |
| Cle Elum | 1504 | 585 | 47.18 | 120.95 |
| Conconully | 1666 | 707 | 48.55 | 119.75 |
| Stehekin | 8059 | 387 | 48.35 | 120.72 |
| Waterville | 9012 | 799 | 47.65 | 120.07 |
| Wenatchee | 9074 | 195 | 47.42 | 120.32 |
| Winthrop | 9376 | 535 | 48.47 | 120.18 |

Table 2.6. Linear trends in surface air temperature in °C per 30 years over land (left column) and sea surface temperature over various domains in the Northern Hemisphere for the period of record 1977-2006. "North Pacific" denotes the average over the box (32.5° to 57.5°N, 142.5°E to 122.5°W). Land data based on the CRUTEM 3 data set and ocean data based on HadSST2 data set from the Climate Research Unit at the University of East Anglia (Brohan et al. 2006).

| **Domain** | **Land** | **Ocean** |
|---|---|---|
| Northern Hemisphere Annual | 0.93 | 0.52 |
| Northern Hemisphere Winter (NDJFM) | 1.04 | 0.46 |
| 45°N to 50°N Winter (NDJFM) | 1.28 | 0.55 |
| North Pacific Winter | | 0.38 |

# 3. DAILY-SCALE VARIABILITY OF THE CASCADES SNOWPACK

## *3.1 Introduction*

Understanding the atmospheric processes that control the accumulation of the snowpack during the winter is crucial for translating in-season observations into useful hydrological forecasts and for gauging the potential impact of climate change on snowpack.

Previous work examining the relationship between atmospheric variables and snowpack has focused on seasonal mean temperature and precipitation. Predictably, winters that tend to be colder and wetter than average also exhibit a snowpack with greater than average values of snow-water equivalent (SWE). Mote et al. (2008) demonstrated that regressions of annual time series of mean winter temperature and precipitation upon April 1 SWE observations explain a large portion of the year-to-year variance in SWE. However, the link between the regional circulation and the seasonal accumulation is less clear. Work in this vein has focused on the correlation between time series of climate indices and time series of April 1 SWE. The climate indices (e.g., the indices that represent the El Niño-Southern Oscillation (ENSO), the Pacific Decadal Oscillation (PDO, Mantua et al. 1997), the Pacific North-American pattern (PNA)) serve as proxy measurements of the shape and strength of the regional circulation. For example, Cayan (1996) showed that low values of April 1 SWE occur in the Pacific Northwest following winters when the PNA pattern is in its positive polarity. Mote (2006) demonstrated that April 1 SWE is positively correlated with the North Pacific Index (NPI). McCabe and Dettinger (2002) showed that by correlating maps of the 700-hPa geopotential

height field with indices of the two leading modes of spatial and temporal variability of the snowpack, the patterns derived are similar to those obtained by correlating the same data with indices of the PDO and ENSO. Clark et al. (2001) and Jin et al. (2006) demonstrated that Cold ENSO winters tend to be associated with higher values of April 1 SWE; however the reverse relationship between Warm ENSO winters and low April 1 SWE was found to be weaker.

These studies suggest some physical mechanisms for how the regional circulation can affect temperature, precipitation, and consequently snow accumulation. During the positive polarity of the PNA pattern, anomalously high pressure over the Northwest leads to positive temperature anomalies and a deflection of storms away from the region, a setup conducive to negative April 1 SWE anomalies. Warm ENSO winters, the warm phase of the PDO, and low values of the NPI are all associated with an anomalously deep Aleutian Low, which results in a shift of the storm track south of its climatological-mean position, favoring drier winters in the Northwest (Seager et al. 2009).

However, this simple schematic linking climate indicators to snowpack via seasonal mean circulation patterns is incomplete – correlation values for these indices and their predictive skill are relatively low, especially for ENSO and the PDO and asymmetries exist in the strength of the relationships for opposing phases/signs of oscillations/indices. The relationships are weak because the seasonal-mean perspective ignores the variability on shorter time scales. For example, Clark et al. (2001) and Jin et al. (2005) noted that SWE anomalies are more pronounced for Cold ENSO winters than for Warm ENSO winters; Clark et al. (2001)

explained this difference by showing that Warm ENSO winters exhibit reduced precipitation in the Northwest at the beginning and end of the winter, but increased precipitation during mid-winter. Additionally, Cayan (1996) has shown that composites of winters with anomalously high SWE exhibit a relatively weak pattern of geopotential height anomalies which suggests that high values of April 1 SWE could arise from a series of short-lived (e.g. daily) events that do not emerge in an analysis based on seasonal averages.

This chapter focuses on the daily variability of the snowpack throughout the winter season and demonstrates the episodic nature of the accumulation of the snowpack. The punctuated behavior of accumulation of the snowpack provides an explanation as to why seasonal-mean statistics are only weakly related to the spring snowpack – the meteorological conditions occurring over the region during only a small portion of the winter season can have a disproportionate influence on the amount of snowpack remaining in the spring. A few days of heavy accumulation, or conversely, the lack of such days can have a strong impact on the fate of the snowpack for the entire season. This chapter aims to characterize the frequency and magnitude of the important accumulation event days and to detail the circulation patterns that accompany these event days. In addition, the daily variability of the spring melt is investigated.

### *3.2 Previous Work on Intraseasonal Variability*

The extensive measurements undertaken by the Army Corps of Engineers (1956) at their snow laboratories during the late 1940's and early 1950's provide a

picture of the winter and spring evolution of the snowpack across the western US, and in the Pacific Northwest in particular. Taking the measurements of snow depth, SWE, temperature, precipitation, and radiation performed at the Willamette Basin Snow Laboratory as representative of the Cascades, the snowpack is typically established in November and accumulates until around the end of March. Ablation is comparable to accumulation in April. In May and June, ablation dominates and accumulation is close to zero. The snowpack has vanished by July.

Serreze et al. (1999, 2001) have examined Snowpack Telemetry station (SNOTEL) data, providing a day-to-day and month-to-month picture of the evolution of the winter and spring snowpack. For the Pacific Northwest, December and January tend to be the snowiest months despite the fact that precipitation tends to peak in November. The difference in the timing of peak snowfall and precipitation results from the fact that it is often too warm across the range of elevations of the Cascades during the early winter for precipitation to fall as snow. Additionally, they reported that snow accumulation is not normally distributed, a few rather large events account for a disproportionate total of the season-ending total; years with high April 1 SWE tend to exhibit more snow days and the periods of high accumulation tend to be of a greater magnitude.

### *3.3 Characteristics of the SNOTEL network in the Washington Cascades*

The snowpack data used in this study were collected by the portion of the SNOTEL network located in the Washington Cascades (Fig. 3.1). SNOTEL stations provide daily measurements of the SWE, temperature, and precipitation. The data

collected by the network are quality controlled and disseminated by the National Resource Conservation Service (NRCS), a division of the US Department of Agriculture. A photograph of a typical SNOTEL site is shown in Fig. 3.2. A temperature sensor and a storage precipitation gauge provide measurements of temperature and precipitation, respectively. SWE measurements are taken using a "snow pillow," which is subject to a pressure that is determined by the weight of the overlying snowpack. Measurements are taken approximately every 15 minutes, but only the daily summaries, which include minimum temperature, maximum temperature, mean temperature, year-to-date precipitation, year-to-date SWE, and daily precipitation are quality controlled by the NRCS and made available on their website (www.wcc.nrcs.usda.gov/snow/)[1].

In this study, the daily summary values of temperature, precipitation, and SWE are the examined. The data were downloaded between August 31, 2007 and September 7, 2007 from the NRCS website. They contain observations extending back as far as October 1978 for some stations. The latest data examined are from September 2006 (Table 3.1).

*3.4 Snow Climatology of the SNOTEL stations*

For the 46 SNOTEL stations located in the Washington Cascades, values for the mean April 1 SWE, mean winter precipitation, and mean winter temperature are

[1] Of note, the measurements of temperature, year-to-date precipitation, and year-to-date SWE listed for any particular day are "summarized" at 12 AM Pacific Standard Time (1 AM Pacific Daylight Time) on that day, based on the measurements performed during the previous 24 hours. However, the daily precipitation listed that same day is the total for the following 24-hour period and is not synchronous with the other time series (T. Pagano, personal communication).

shown in Figs. 3.3, 3.4, and 3.5. In these statistics, winter is defined as the 150 days beginning on November 1; and April 1 SWE is calculated as the SWE present on the 150th day of the winter season. The actual date of April 1 falls on either the 151st or 152nd day following November 1, depending on the occurrence of a leap year. It was considered preferable to use the same number of days rather than to use the calendar date to define the SWE at the end of each winter season. Likewise in the following analyses, "months" are defined as consecutive 30-day periods (e.g., "November" is the first 30 days of the winter; "December" is the next 30 days of the winter), rather than by the actual calendar dates.

These figures indicate that the coldest, wettest stations exhibit the highest values of April 1 SWE, as expected. While elevation appears to be a strong control on temperature (Fig. 3.5, correlation coefficient = 0.75), with the higher elevations exhibiting the lowest temperatures; elevation does not appear to have a strong effect on precipitation (Fig. 3.4): several low elevation stations are relatively wet and several high elevation stations are relatively dry. Hence, it is clear that precipitation, and by extension snow accumulation, are controlled by other factors (e.g., aspect, slope, geometry of nearby topography, presence of vegetation) that affect the meteorology of a particular site.[2]

The relationship of elevation to snowfall efficiency is shown in Fig. 3.6. Snowfall efficiency is defined as the sum of any daily SWE increases recorded by the

[2] The weak relationship between elevation and precipitation arises in part due to the relatively small sample size involved (46 stations). If data were available at a higher spatial resolution, precipitation would be observed to increase with increasing elevation.

snow pillow[3], divided by the sum of winter precipitation recorded by the precipitation gauge. The relatively large value of the correlation coefficient (0.83) between elevation and snowfall efficiency reflects the strong relationship between elevation and temperature. Since SWE lost via ablation does not detract from the snowfall efficiency, this plot isolates the effect of temperature on the phase of the precipitation from its effect on ablation. It should be noted that several of the highest elevation stations exhibit SWE-to-precipitation ratio values greater than 1, which is not physically possible. The presence of such values is due to the fact that precipitation gauges are subject to some degree of undercatch (Colle et al. 2000; Yang et al. 1998).

The elevation dependence of ablation (i.e., the ratio of April 1 SWE to the total winter snowfall) is shown in Fig. 3.7. The snowfall was calculated by summing all the daily SWE increases occurring during the winter, as described above for the snowfall efficiency. At stations where the value of this ratio approaches 1, the April 1 SWE is nearly equal to the daily gains in water-equivalent from winter storms, indicating that loss of SWE from the snow pillow during the winter is rare and results in the loss of only a small proportion of the total snowfall. The majority of the SNOTEL stations exhibit ratio values of 0.8 or greater. However, some of the stations at the lowest elevations exhibit ratio values ranging down to below 0.2,

[3] It should be noted that the snow pillow measurements only record the weight of the overlying material, which could include something other than snow (e.g. tree debris, animals). Also, rainfall that is incorporated into the snowpack could also be included. However, it is assumed that the data examined corresponds to snow. The rainfall sequestered by the snowpack is discussed explicitly in Chapter 4. During the winter, the storage of rainfall by the snowpack is likely temporary, as the rain will freeze once temperatures drop below zero. In the spring, the presence of liquid in the snowpack is likely less transient.

indicating that most of the SWE that fell during the winter has been removed from the snowpack via melt or sublimation prior to April 1.

*3.5 Formulating an Index of Daily Snow Accumulation and Loss*

In order to quantify the relative role of accumulation and loss in establishing the spring snowpack and to identify the dates of important gain and loss events, daily indices representing accumulation and loss were calculated to represent the Washington Cascade SNOTEL stations. The indices were calculated using the 26 stations (Table 3.1) with periods of record that began in October 1982 or earlier. The starting point of 1982 is considered a near-optimal trade-off between the number of eligible stations and the length of record – beginning a year earlier would reduce the number of eligible stations to 23, while beginning a year later would only increase the number of stations to 27.

For each of the 26 eligible stations, the time series of the daily derivative of SWE was calculated (e.g., for Day *X*, the daily derivative is equal to the SWE measured on Day *X+1* minus the SWE measured on Day *X*) for each water year, beginning November 1. The daily derivative is positive for days experiencing accumulation and negative for days experiencing loss. October was excluded from the analysis since snowpack rarely accumulates during this month across much of the range of elevations of the Cascades. Even when snow does fall in the Cascades during October, it is often ablated relatively quickly.

To obtain an accumulation time series that is representative of the Cascades as a whole, the derivative time series is reset to zero on all days on which it is less

than zero. Then, the 26 time series for the individual stations are averaged to yield a single time series for the Cascades as whole. The loss index is generated in an analogous manner by replacing all positive values in the daily derivative time series by zeros prior to averaging. Calculating the accumulation and loss time series separately prevents losses at one station from offsetting gains at another station. Figure 3.8 shows examples of the accumulation and loss time series for the 2003 water year.

Two other methods of generating a daily time series representing accumulation and loss for the Cascades were attempted; however, all three methods yield nearly identical time series ($r>0.95$ between any pair). The first alternative attempted was to standardize the accumulation and loss time series at each SNOTEL station by dividing by the standard deviation of days with non-zero values. Then, the standardized time series from all SNOTEL stations were averaged to yield a time series representative of the Cascades. The second alternative was to perform Principal Component Analysis on the correlation matrix formed by the daily derivative time series from each of the 26 SNOTEL stations. The leading mode explains $\sim 50\%$ of the variance of the data represented by the correlation matrix, and its EOF has positive loadings for all SNOTEL stations.

That all 3 methods yield nearly identical time series indicates that the temporal covariance among the SNOTEL stations is relatively high. Despite the fact that precipitation varies markedly from station to station, all stations experience the same sequence of daily increases and decreases in SWE. This is to be expected since the weather systems as well as the more slowly-evolving regional circulation

patterns that affect snowpack in the Washington Cascades are much larger in spatial scale than the Cascades themselves. The time series generated from the simple averaging of the unnormalized SWE data is used throughout this work, because it is the easiest to interpret.

Adding together the accumulation and loss and summing over the winter season yields an annual time series of April 1 SWE. This time series is similar to the area-weighted April 1 SWE estimates derived from a variety of snow courses (Fig. 2.1 and Table 2.3; see Chapter 2 for a description of the area-weighting algorithm) located on the west slopes of the Cascades (Fig. 3.9) – the correlation coefficient between the two time series is equal to 0.95. Since most of the stations in the SNOTEL network are situated at relatively high elevations (>1000 m), it is understandable that the April 1 SWE estimates are consistently higher than the estimates from the snow course data.

*3.6 The Timing and Magnitude of Daily Accumulation and Loss Events*

Investigation of the daily time series of accumulation and loss demonstrate the following: 1) accumulation and melt events occurring on just a few days of each winter account for a large percentage of the total seasonal snowfall or loss; 2) the magnitude of the seasonal snowfall derived from large accumulation events is well correlated with the total seasonal snowfall on a yearly basis; 3) the largest accumulation events can occur in almost any winter month, but usually happen in December, January or February; and, 4) loss during mid-winter is rare and much smaller than the total snowfall, except for some of the lowest SWE seasons.

The first two of these conclusions are evident from an inspection of Fig. 3.10, which shows both the fraction of total seasonal snowfall accounted for by sum of the *n* largest events and the square of the correlation between the total seasonal snowfall and the sum of the *n* largest events during that season. The total seasonal snowfall is equal to the sum of the accumulation index from November 1 through the 150$^{th}$ day following November 1 (March 29 or 30, depending on the leap year); the loss index is not included in the calculation. For the fraction of annual snowfall accounted for by the *n* largest events (blue circles), the mean of the fractions for each of the 24 years is plotted in Fig. 3.10. On average, the largest accumulation event accounts for only a few percent of the total seasonal snowfall; however, the curve rises steeply as *n* increases. Almost 30% of the total seasonal snowfall is accounted for by the 10 largest accumulation events and nearly 50% by just over 20 accumulation events.

The high degree of correlation between the amount of SWE delivered by large accumulation events and total seasonal snowfall is evidenced by the shape of the red curve in Fig. 3.10. The size of the largest individual day's accumulation explains over half of the variance in the total seasonal snowfall during the 24-year period of record, and over 80% of the variance is explained by the sum of the 10 largest events.

To examine the evolution of accumulation and loss of snowpack during the winter, daily means were calculated for the accumulation and loss indices and plotted as a function of calendar date, shown in Fig. 3.11. Accumulation dominates from November through March, while losses are relatively small in magnitude and

infrequent. Beginning in April, loss becomes more important and accumulation is reduced. By May, the snowpack is ablating rapidly. The entire snowpack has usually melted out by the end of July, when both accumulation and loss are equal to zero.

Figure 3.12 shows the timing and magnitude of the large accumulation events. For each year, the accumulation events have been ranked and sorted into 10-day bins based upon the timing of their occurrence. Generally, the large events occur more often in December, January, and February. There is a decrease in the frequency of occurrence for the bin representing the end of December; however, no physical reason is apparent. It is likely a result of sampling variability. The lower plot in Fig. 3.12 shows the amount of accumulation occurring for the large events. The top 20 events all involve 1 cm SWE/day or more, while the top 5 events range from over 2 cm SWE/day to nearly 7 cm SWE/day.

Temperature measurements are often unavailable for stations prior to the water year of 1990. In order to compare temperature to accumulation and loss, the accumulation and loss time series were recalculated for the more recent period of November 1989 to March 2006. In the shorter, more recent period four more stations to be eligible for the accumulation and loss time series – a total of 30 stations. Daily temperature time series were calculated to accompany the accumulation and loss time series. The temperature time series was calculated as the daily mean of temperature observed at the 30 SNOTEL stations.

The role of temperature in controlling the accumulation and loss during the progression of the winter and spring is shown the histograms in Fig. 3.13. For each

30-day period during the season (note that 30-day periods only roughly refer to the calendar months), the daily accumulation and loss occurring during the 17-year period of record (Nov. 1989-March 2006) were binned according to the value of the mean daily temperature time series. To accompany these histograms, Fig. 3.14 shows histograms of the daily mean temperature during each month of the season.

Figures 3.13 and 3.14 show that a large portion of accumulation during the winter is occurring at temperatures just below 0°C. For all months, the bin exhibiting the highest accumulation falls somewhere between –5°C and 0°C. The distribution about the peak bin is near-normal; deviations from normality likely result from a few particularly large events. Losses from December through March are rare. Interestingly, accumulation can occur on days when the mean temperature is above zero for the collection of SNOTEL stations. The days in this category are likely ones on which snow was accumulating at higher elevations while it was raining at lower elevations. Also, it may indicate days in which snowfall occurred when the temperature was below that of the daily mean, or when the rain that fell (see Chapter 4) was incorporated into the snowpack. Overall, even when temperatures are relatively warm during the mid-winter, the amount of loss that occurs during these months is far less than the amount of accumulation, indicating that the SWE contained by the snowpack exhibits some resilience to above-zero temperatures.

To compare the month-to-month behavior of individual SNOTEL stations to that of the index representing the Cascades as a whole, histograms for snowfall versus temperature were made for Pope Ridge (Fig. 3.15, top panels), a relatively

low elevation station, and Corral Pass (Fig. 3.16, top panels), a relatively high elevation station. The histograms for the individual stations show that the cutoff between accumulation and loss at 0°C is somewhat sharper than for the histograms for the index. This supports the first explanation offered above –when the daily mean temperature associated with the index is above-freezing, accumulation occurring likely represents snowfall at higher elevations, where temperatures are likely below that of the mean for the 30 SNOTEL stations. However, both stations also exhibit *some* accumulation occurring on days with above-freezing temperatures, so the second explanation should not be completely discarded. Additionally, the individual stations exhibit differences in the timing of accumulation and loss. At Pope Ridge, accumulation dominates during the mid-winter; loss begins occurring in March; April and May are dominated by loss; the snowpack has typically melted by June. In comparison Corral Pass, exhibits a delay of one month: accumulation dominates through March, while loss does not begin to become apparent until April. Loss dominates through May, June, and July, until the snowpack has completely ablated. The difference in timing is clearly a result of a difference in temperature (Figs. 3.15 and 3.16, bottom panels), as the Corral Pass station is typically several degrees colder than the Pope Ridge station in all months.

### *3.7 The Circulations Associated with Daily Accumulation Events*

Composite circulation patterns were generated based on a subset of the largest winter accumulation events. Figures 3.17 shows the maps of the 500-hPa and 850-hPa geopotential height fields for the 10 largest wintertime accumulation

events taken from each winter for the water years 1983-2006; Fig. 3.18 shows the map of the *u*-component of the wind on the 850-hPa pressure surface for the same events.

The 500-hPa and 850-hPa levels were chosen because of their relationship with the large-scale circulation and moisture flux. The 500-hPa geopotential height surface is often considered the "steering level" for storms, because the planetary-scale flow pattern (~thousands of km) appearing at this level indicates the paths that storms are likely to take. The planetary-wave configuration persists for several days to weeks, and can hence be used to define and identify "weather types" or "weather regimes" (Casola and Wallace 2007). The 850-hPa geopotential height surface is close to the elevation of many of the SNOTEL stations (1000-1500 m). The orientation and strength of the flow at 850-hPa provides an indication of the advection of temperature and moisture in the Cascades.

The maps are based on the NCEP/NCAR Reanalysis (Kalnay et al. 1996). In order to synchronize the geopotential height data with the timing of the SNOTEL measurements, which are taken at 12 am Pacific Standard Time/1 am Pacific Daylight Time, 6-hourly data were used. The circulation pattern for each day was calculated as the mean of the 06Z, 12Z, and 18Z for the previous calendar day and the 00Z data for that calendar day. The horizontal resolution of the NCEP/NCAR Reanalysis data is 2.5° latitude by 2.5° longitude.

For the large accumulation events, the maps (Fig. 3.17) indicate an offshore trough in the 500-hPa height field and a closed low in the 850-hPa height field centered along the North American west coast just north of 50°N. The anomaly

maps indicate that the centers of the features are co-located. In addition, the anomaly maps at both levels exhibit a strong north-south dipole. These dipole patterns are similar to the mean winter surface flow associated with high SWE winters shown by Stoelinga et al. (2009).

The dipole pattern is accompanied by enhanced onshore flow, which is clearly seen in the composite maps of the *u*-component of the winds at the 850-hPa pressure level in Fig. 3.18. Anomalous westerly flow with winds ~ 8 m/s stronger than the climatological-mean is impinging on the Washington Cascades. As suggested by the 850-hPa geopotential height field maps, the anomalous winds have a west-southwesterly orientation.

*3.8 Temperature-Dependence of Late Winter and Spring Losses*

As stated previously and shown in Fig. 3.13, ablation of the snowpack (in a basin-averaged sense) begins in March and persists through April, May, and June. By July, most of the snowpack has typically vanished. The rate of daily loss of SWE during late winter and spring is strongly controlled by the daily mean temperature as shown in Figs. 3.19 and 3.20. These figures were generated by plotting the magnitude of daily loss versus the daily mean temperature; days where the basin-averaged SWE was particularly low (<10 cm) were excluded from the plots. The same data as used to construct Fig. 3.13 were used to make these plots, with daily data available for the period November 1989-July 2006. A summary of the regression coefficients and slope values associated with these plots is shown in Table 3.2.

Whether the "melt season" is considered to run from March through June or April through June has little bearing on the value of the slope of the regression line (about –0.14 cm SWE/°C/day) or the variance explained by the regression ($r^2 \sim 0.6$). Also, whether non-ablation days (the days when the daily index of loss was equal to zero) are included or excluded from the regression has a minimal impact on these estimates. However, there is more diversity among the regression results for the individual months. The slope of the regression line for the March data is the smallest (–0.045 cm SWE/°C/day) and explains a relatively small portion of the variance of the daily melt data ($r^2=0.28$). The slopes of the regression lines are more similar for April and May (–0.12 cm SWE/°C/day and –0.15 cm SWE/°C/day, respectively) as is the strength of the regression relationship ($r^2=0.54$ and $r^2=0.62$, respectively). June exhibits a slope value (–0.11 cm SWE/°C/day) that is slightly smaller than the slope values associated with April and May, and the regression explains less of the variance in the daily loss data ($r^2=0.29$). While the strength of the regression is considerably weaker for June data, for the temperatures typically experienced in June (5°C to 15°C, Fig. 3.20), the loss estimates generated using the regression equation from June are intermediate between those generated from the regression equations associated with April and May. That the results for April and May are similar to the results for the season as a whole makes sense, given that over 60% of the SWE losses from March through June occur in those months. Adding the losses occurring in June increases this proportion to 90% of the SWE loss.

The relationship between daily SWE loss and daily mean temperature was also examined for a station at relatively low elevation, Pope Ridge (elevation 1079

m), and a station at relatively high elevation Corral Pass (elevation 1829 m). The scatter plot for the entire melt season at Pope Ridge is shown in Fig. 3.21; similar plots for individual months are shown in Fig. 3.22. Similar plots for Corral Pass are shown in Figs. 3.23 and 3.24. Summaries of the results of the regressions of daily melt upon daily temperature for the two stations are shown in Tables 3.3 and 3.4.

As noted in Section 3.6, the individual stations demonstrate that the melt season is not synchronized for areas located at low and high elevation. Despite the difference in timing of melt, the regression of daily loss upon daily mean temperature yields results that are similar to but slightly less than that of the entire basin: for Pope Ridge, the slope value is –0.17 cm SWE/°C/day; for Corral Pass, the slope value is –0.19 cm SWE/°C/day. For the individual stations, the regression is slightly weaker than for the basin-averaged data ($r^2$=0.46 for Pope Ridge; $r^2$=0.53 for Corral Pass), and excluding non-ablating days makes a larger difference for the regressions statistics. For the individual months, the estimates of the slopes increase throughout the melt season.

Overall, the regression relationships demonstrate that temperature is a key control on the rate of ablation throughout the range of elevation of the snowpack. This will be exploited in the following section to construct a "forecast model" for the melt season. The model can also be used to estimate the sensitivity of late winter and spring melt to global warming, providing a complementary estimate to that of the sensitivity of accumulation to warming presented in Chapter 2.

*3.9 A Degree-Day Model for Spring Snowmelt*

A "degree-day" or "temperature index" approach to estimating snowmelt has been widely used in the hydrological literature (Army Corps of Engineers 1956; American Society of Civil Engineers 1996). In such an approach, snowmelt is proportional to a measure of the daily temperature (typically the mean or maximum) and a constant of proportionality, or "melt factor." The melt factor represents the relationship between energy flux (see Chapter 4) and temperature. It provides a simpler alternative to estimating each term in an energy balance equation, which may require measurements that may not be readily available, such as those for solar insolation, albedo of the snowpack, and wind speed.

Using the regression relationship for the Cascades index discussed in Section 3.8, predictions of daily snowmelt for the spring (April –June) were made using the following degree-day equations

$$\Delta SWE_i = -0.1408 \text{ cm SWE/°C} * (T_{MEAN})_i - 0.4701 \text{ cm SWE} \quad (3.1)$$

$$L_i = \Sigma \, \Delta SWE_n \text{ (for } n=1 \text{ to } i) \quad (3.2)$$

where the daily loss of SWE on the *i*th day of spring is defined as $\Delta SWE_i$, the daily mean temperature on the *i*th day of spring is $(T_{MEAN})_i$, and the cumulative amount of SWE lost by the *i*th day following April 1 is defined as $L_i$ ($SWE_i$, Eqn. 3.2).

Daily predictions of snowmelt have been made for waters years 1990-2006 by inputting observed daily mean temperatures for April-June into equations 3.1 and 3.2. The model predictions are compared to observed daily losses of SWE in

the top panels of Figs. 3.25 and 3.26; cumulative losses of SWE are shown in Fig. 3.27. It is clear that some systematic biases exist for the degree-day model: the model tends to overpredict the amount of snowmelt early in the season, as evidenced by the negative residuals occurring in April (Fig. 3.26) and the tendency for the model to exhibit a SWE trajectory below that of the observations during April (Fig. 3.27). This bias is an expected consequence of using a single melt factor for the entirety of the spring. In the early spring, it is likely that the snowpack is not yet "ripe:" it is likely still below 0°C, or at least portions of the snowpack are below 0°C. Thus, the melt efficiency during the early spring is likely to be somewhat less than later in the season. Essentially, if the snowpack is not isothermal at 0°C, it retains some "memory" of the prior cold conditions – only through a period of above-freezing temperatures can this memory be erased.

The memory of the snowpack can be incorporated into the degree-day model by modifying the temperature time series used in the regression with daily snowmelt. Rather than using the daily mean temperature, a time series was constructed using the weighted average of the mean temperatures experienced during the previous days:

$$(T_{E\text{-}FOLD})_i = \frac{(T_{MEAN})_i + e^{-1}(T_{MEAN})_{i-1} + e^{-2}(T_{MEAN})_{i-2} + e^{-3}(T_{MEAN})_{i-3}}{1 + e^{-1} + e^{-2} + e^{-3}} \qquad (3.3)$$

Equation 3.3 applies a 1-day *e*-folding time to the temperature time series. Use of such an equation permits the temperature on prior days to influence the amount of

melt occurring on a particular day; however, the influence of the preceding days decreases exponentially as one goes farther into the past. Weightings for the days prior to Day *i-3* are negligible.

Regressing the $T_{E\text{-}FOLD}$ time series upon daily melt for April-June yields the following relationship,

$$\Delta SWE_i = -0.1551 \text{ cm SWE/°C} * (T_{E\text{-}FOLD})_i - 0.4170 \text{ cm SWE} \quad (3.4)$$

which serves as the basis for an updated degree-day snowmelt model. The strength of this regression ($r^2$=0.64) is very similar to that of the initial regression using $T_{MEAN}$. Cumulative losses of SWE are still calculated using Eqn. 3.2

The bottom panels of Figs. 3.25 and 3.26 show that the degree-day model that allows for the memory of the snowpack performs better than the initial degree-day model[4]. The sum of the squared residuals for the entire spring is reduced from 310 $cm^2$ to 280 $cm^2$; for the first 30 days of the spring, the sum of the squared residuals is reduced from 73 $cm^2$ to 50 $cm^2$. In addition, the size of the bias is reduced during this early season period, with the mean (median) of the residuals being reduced from –0.13 cm (–0.17 cm) to –0.09 cm (–0.13 cm). The updated model provides a relatively accurate representation of the rate of the seasonal melt

[4] Physically, it is likely that memory becomes unimportant later in the spring and summer. Once the snowpack is isothermal and 0°C, the heat flux to the snowpack (see Chapter 4) can be used for melt, rather than raising the temperature of the snowpack. Experiments made by applying the memory only during April, or by shortening the *e*-folding time of the memory in May and June produced results that were nearly identical to those from the use of a 1-day *e*-folding time throughout the melt season.

of the snowpack (Fig. 3.28). Further experiments with 2-day and 5-day *e*-folding times did not show significant improvements when compared to the model based on a 1-day *e*-folding time. In particular, the model based on a 5-day *e*-folding time exhibited a weak relationship between weighted-temperature and daily melt ($r^2$ = 0.15), and consequently its predictions of daily snowmelt are quite poor.

The degree-day model was further tested using the observations of 2007 and 2008, which are independent from the data used to construct the model. The observed daily melt and predictions from the degree-day model using a 1-day *e*-folding time is shown in Fig. 3.29; the residuals associated with the model predictions are show in Fig. 3.30; and, the observed cumulative losses and predicted cumulative losses are shown in Fig. 3.31.

For 2007, the model yields a very close approximation of the snowmelt over the spring season: there is a slight overprediction of melt during April; nearly compensating overpredictions and underpredictions of daily melt in May; and June contains a consistent overprediction, reflecting that very little snowpack is remaining in the Cascades. At this point in the season, nearly half of the stations used to compute the index had melted out, and the original regression relationship, and more generally, the index itself, is not a proper representation of the basin snowpack.

For 2008, the model predictions track the observed cumulative losses quite well until May. In May several events are substantially underpredicted by the model; in particular, a large melt event occurring in late May that lasts for several days (>3 cm of loss each day) is underpredicted by the model by nearly 2 cm each

day. It should be noted that losses of this magnitude are among the largest daily losses in the record used to construct the model (see Fig. 3.25); it should not be expected that a regression-based model would accurately simulate such an extreme event. With the exception of this period of underprediction, the model captures the melt behavior during the rest of the spring reasonably well. The overprediction issue observed in June 2007 is not repeated in 2008, as the majority of the basin's stations still have snow during June.

The degree-day model elucidates how various "milestones" related to the spring snowmelt are sensitive to warming. First, simply examining the mean rate of warming between March and May (~2.9°C per month) provides a measure of the sensitivity of the date of the initiation of the melt season. For a 1°C warming, the date would move approximately 10 days earlier in the water year (1°C/(2.9°C month$^{-1}$)). Thus, for a 3°C warming it is likely that melting would begin in March, and April would likely resemble May in today's climate, which is dominated by melt. Second, the advance of the melt-out date can be estimated by using the model. The simulated melt out date for a spring exhibiting temperatures equal to the daily mean observed over the period 1990-2006 can be compared to the simulated melt out date for a spring exhibiting temperatures that are 1°C warmer than the observed daily mean. This comparison indicates that the melt-out date is advanced approximately 7 days for 1°C of warming. Third, the sensitivity of the melt-out to the amount of April 1 SWE can also be estimated. For an additional 8 cm of SWE of April 1 SWE (approximately 10% more SWE than the long-term mean of April 1

SWE), the melt-out date is pushed back approximately 5 days later in the water year.

*3.10 Summary*

Investigation of the measurements made by the SNOTEL network in the Washington Cascades yielded the following key results regarding the day-to-day and month-to-month variability of the snowpack:

- Accumulation occurring over a relatively small number of days during the winter has a large impact on the April 1 SWE. Nearly 50% of the April 1 SWE accumulates over just the 20 heaviest snow days. Additionally, the amount of snow falling during these heavy accumulation events is strongly correlated with the April 1 SWE.
- Loss is infrequent and much smaller than accumulation during most of the winter.
- Large accumulation events are characterized by enhanced on-shore flow impinging on the Cascades. This flow is generated by a deep low located around 50°N latitude and just west of the North American west coast. The low is evident at both the "steering level" of storms (500-hPa geopotential height surface) and at an altitude similar to many of the SNOTEL stations (~ 1000 m; roughly the height of the 850-hPa geopotential height surface).
- The rate of melt in the spring is strongly associated with the daily mean temperature. This relationship can be observed using the index for SWE loss representing the Cascades as a whole or by using observations at individual

stations. The largest difference among stations appears to be that of timing – lower elevation stations exhibit significant losses beginning in March, while higher elevation stations exhibit loss beginning in April.

- A degree-day model has been proposed for predicting the daily melt of SWE in the Cascades during the spring. This model yields a reasonable match to daily observations of melt and the overall rate of melt throughout the season. When a thermal "memory" is incorporated into the model, overpredictions of snowmelt during April are significantly reduced.
- The dates of the initiation of spring melt and of melt-out are both sensitive to warming. While melt typically begins sometime in April, a 3°C warming would likely shift the onset of melting into March. During the spring, a 1°C warming is likely to abbreviate the melt season by just over 2 weeks, as a reduction in mean April 1 SWE of 16% (see Chapter 2) would account for approximately 8 days of advance, and the acceleration of spring melt would account for 7 days of advance.

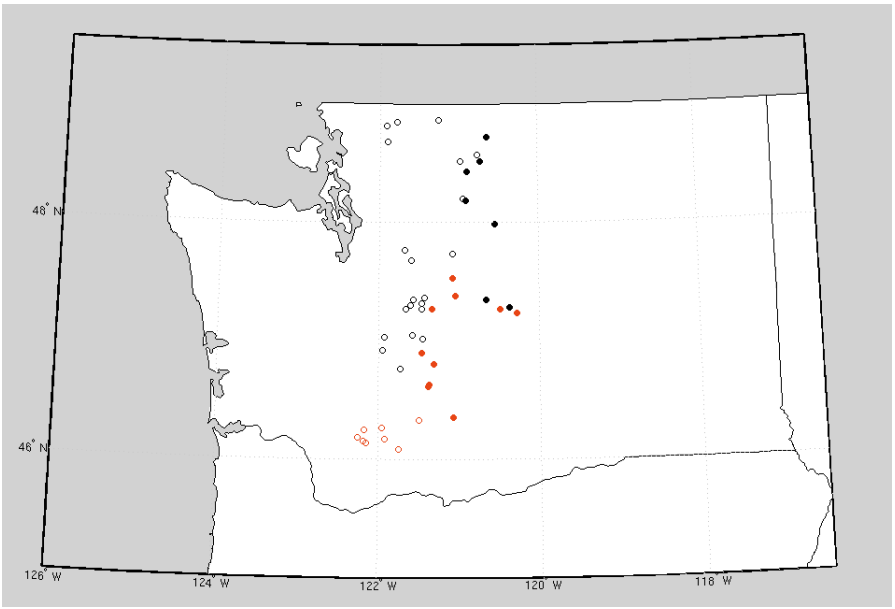


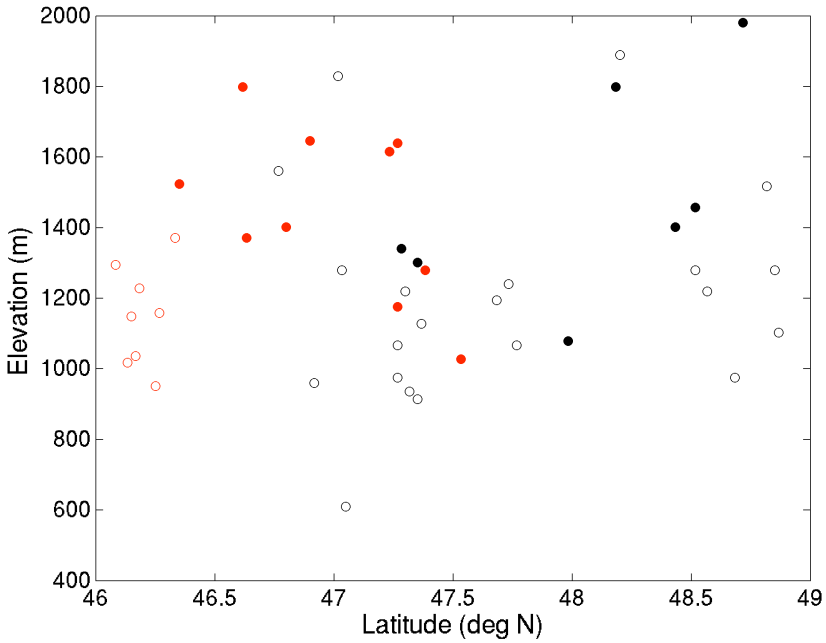


Figure 3.1. Locations of 46 SNOTEL stations in the Washington Cascades. Open (filled) circles denote stations west (east) of the crest of the Cascades. Open black circles correspond to the Puget Sound drainage, closed black circles correspond to the Upper Columbia drainage, open red circles correspond to the Lower Columbia drainage, closed red circles correspond to the Yakima drainage.

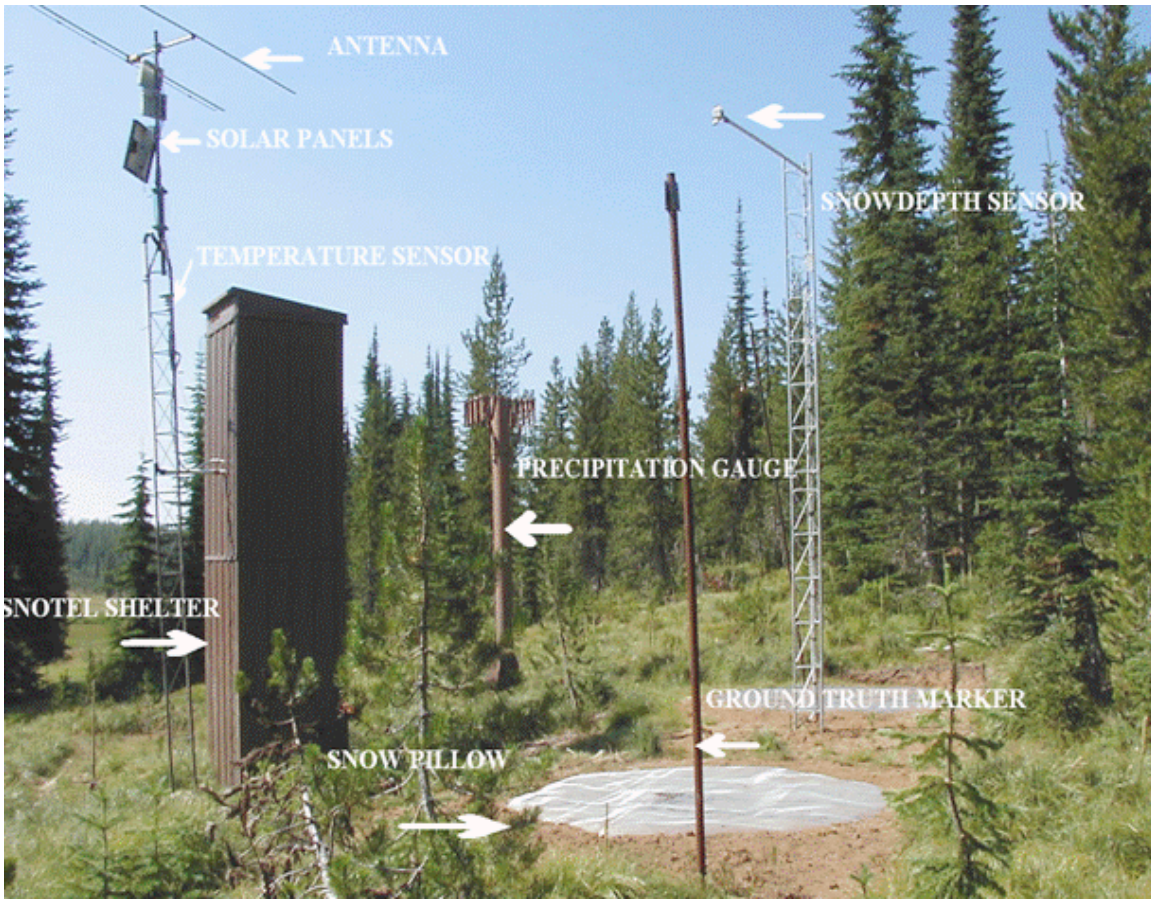


Figure 3.2. Example of a Snowpack Telemetry (SNOTEL) station. Photograph was taken of the Craters Meadow SNOTEL station located in the Clearwater Basin, Idaho. Photograph credit: National Resource Conservation Service, US Department of Agriculture (http://www.id.nrcs.usda.gov/snow/siteinfo/typical_snotel.html)

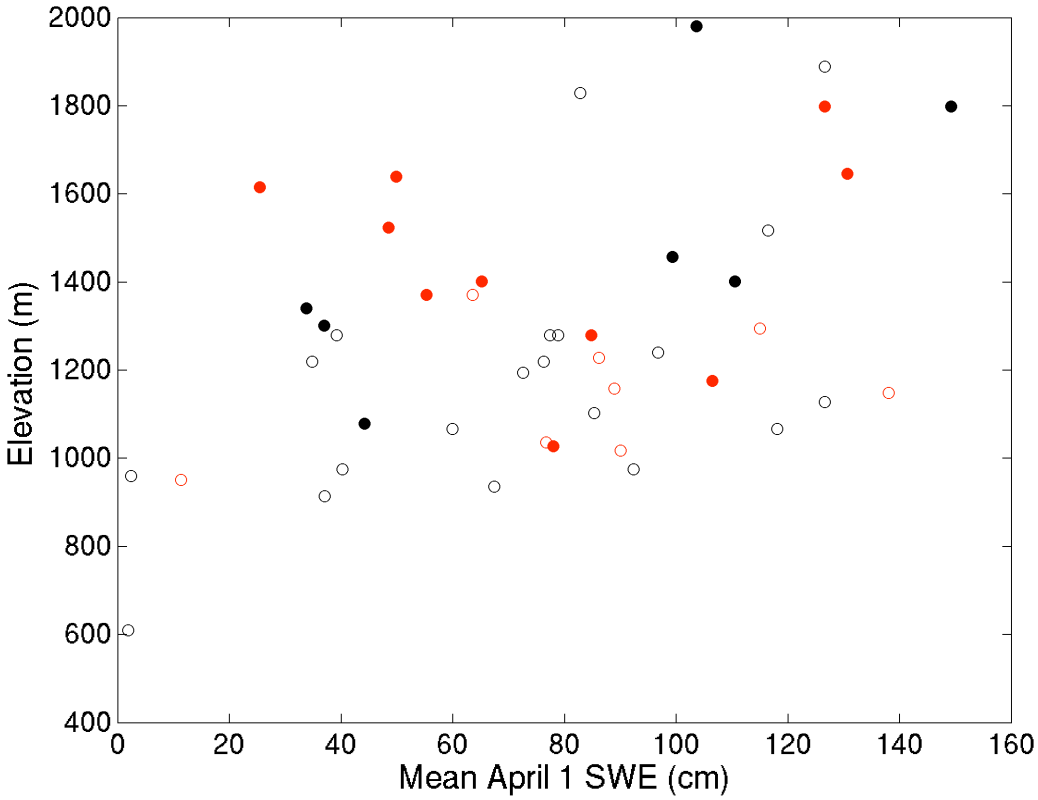


Figure 3.3. Mean April 1 SWE versus Elevation for SNOTEL stations located in the Washington Cascades. Note: Length of record varies by station between 4 and 28 seasons. Circles denote hydrologic sub-basin, as shown in Fig. 3.1.

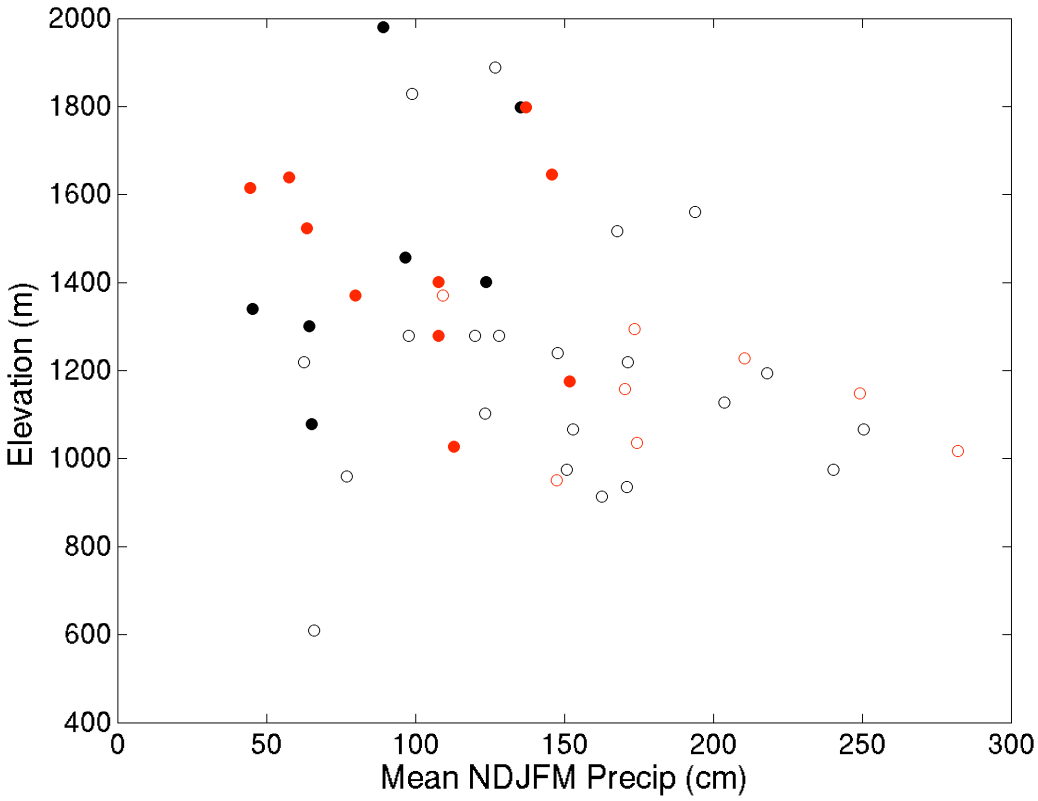


Figure 3.4. Mean Winter Precipitation (November-March) versus Elevation for SNOTEL stations located in the Washington Cascades. Note: Length of record varies by station between 4 and 28 seasons. Circles denote hydrologic sub-basin, as shown in Fig. 3.1.

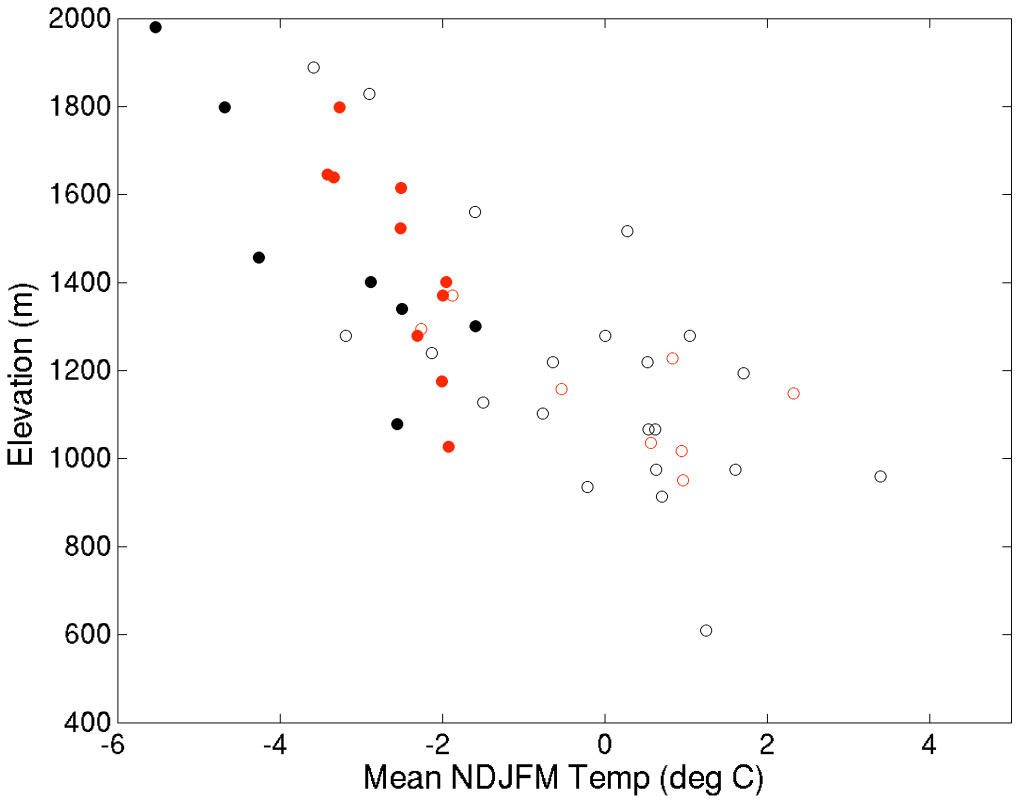


Figure 3.5. Mean Winter Temperature (November-March) versus Elevation for SNOTEL stations located in the Washington Cascades. Note: Length of record varies by station between 4 and 28 seasons. Circles denote hydrologic sub-basin, as shown in Fig. 3.1.

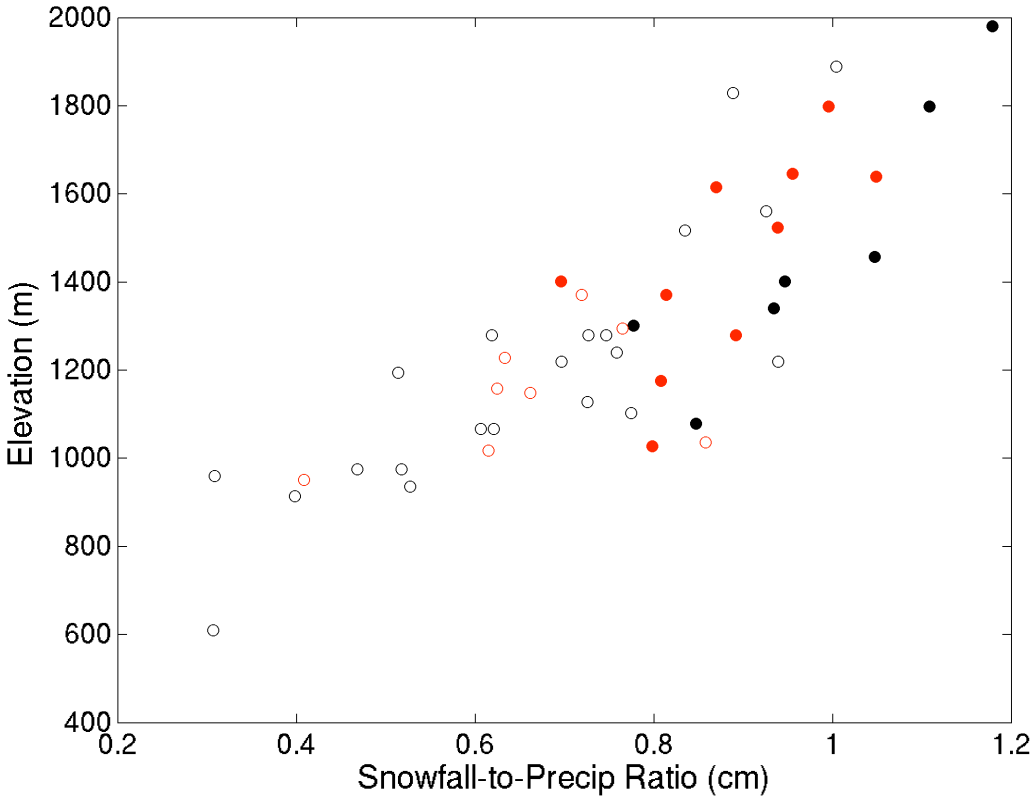


Figure 3.6. Ratio of Snowfall-to-Precipitation versus Elevation for SNOTEL stations located in the Washington Cascades. The winter Snowfall is equal to the sum of all daily increases in SWE recorded by the snow pillow for November through March. Precipitation is equal to the accumulated precipitation recorded by the precipitation gauge during the same period. Note: Length of record varies by station between 4 and 28 seasons. Circles denote hydrologic sub-basin, as shown in Fig. 3.1.

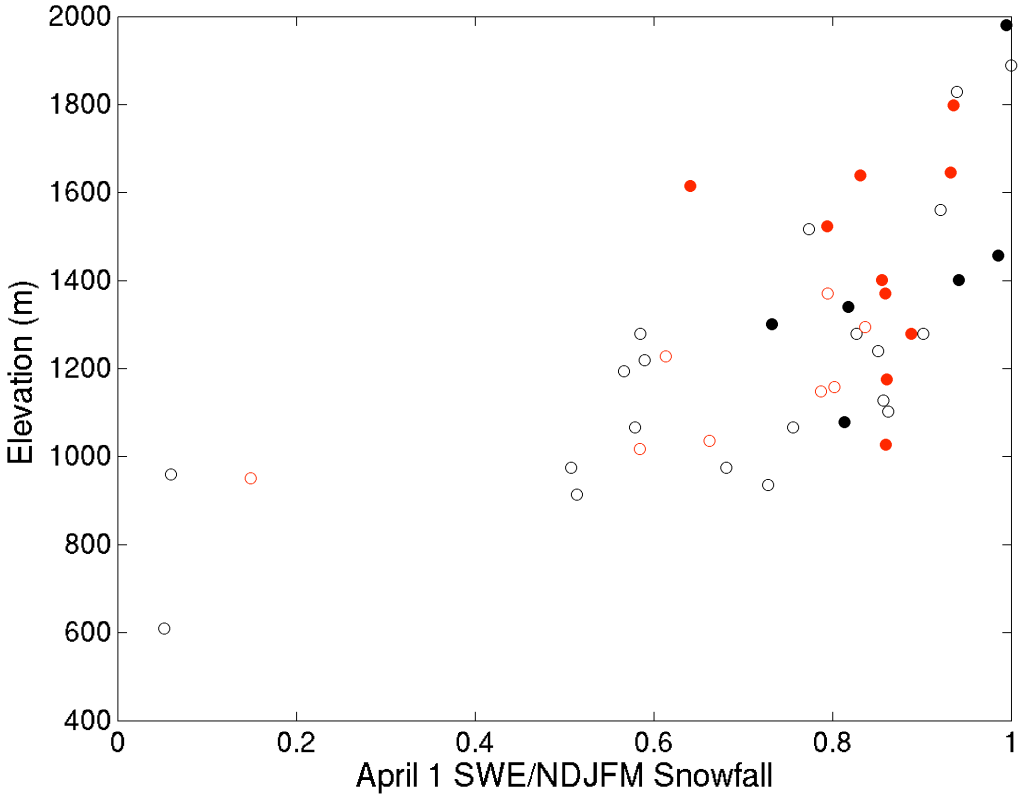


Figure 3.7. Ratio of April 1 SWE to Winter Snowfall at SNOTEL stations located in the Washington Cascades. Note: Length of record varies by station between 4 and 28 seasons. Circles denote hydrologic sub-basin, as shown in Fig. 3.1.

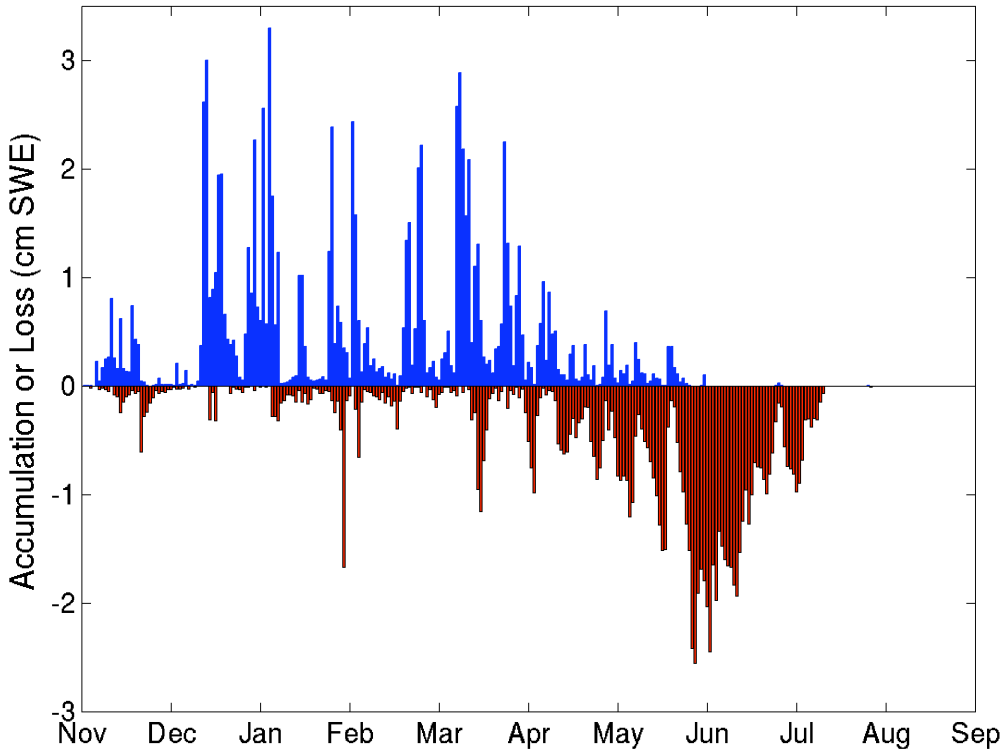


Figure 3.8. Examples of the daily accumulation (blue bars) and loss (red bars) indices for the 2003 water year (November 2002 to September 2003).

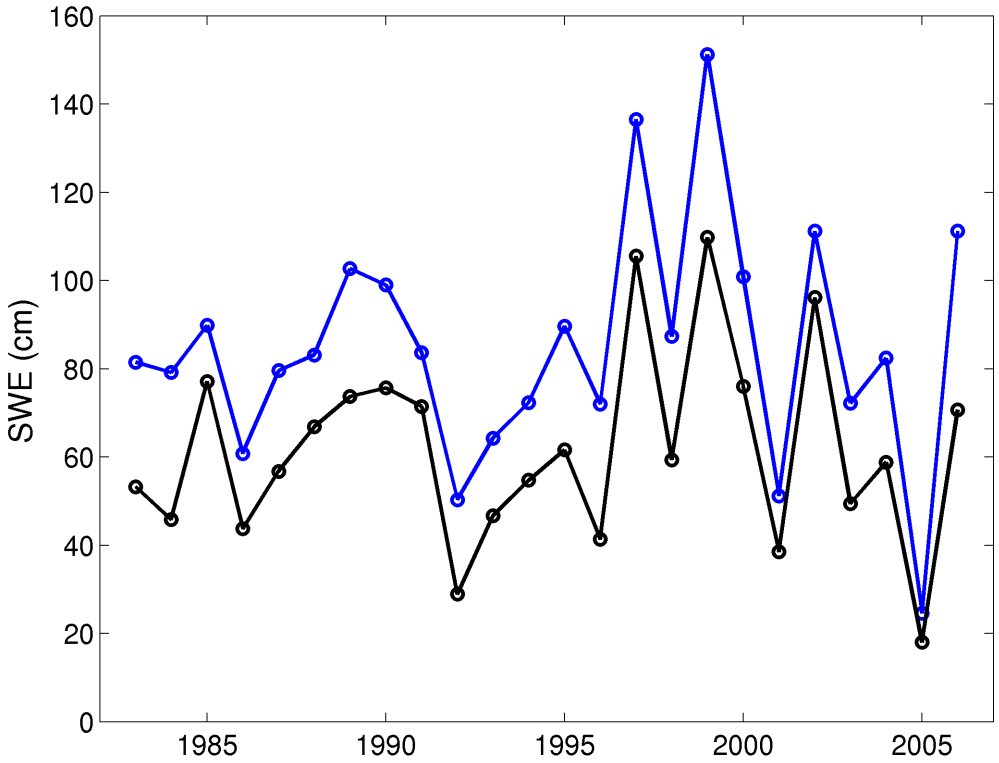


Figure 3.9. Time series of April 1 SWE generated form SNOTEL daily accumulation and loss (blue) data and time series of April 1 SWE generated from area-weighted snow course data (black, see Casola et al. 2009).

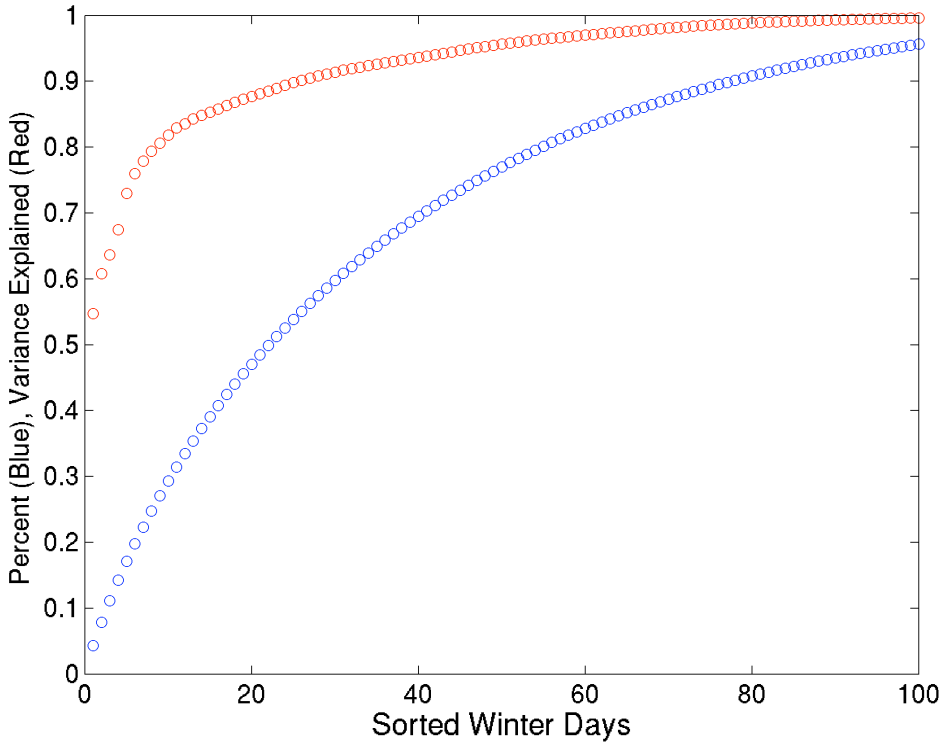


Figure 3.10. Fraction of annual snowfall accounted for by *n* largest events (blue circles) and fraction of variance of the time series of annual snowfall explained by the time series of the snowfall associated with the *n* largest events (red circles).

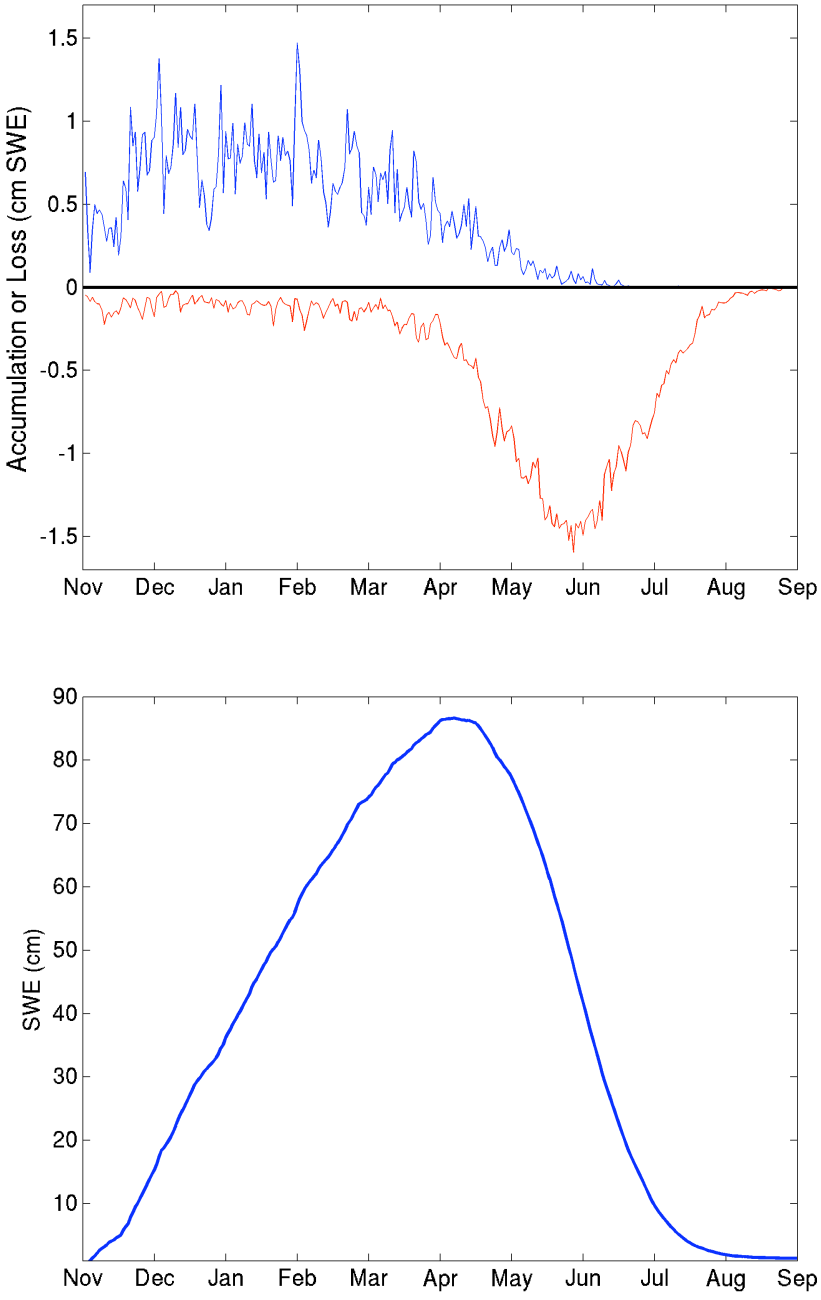


Figure 3.11. Top – Daily mean of the accumulation (blue) and loss (red) time series for the water years 1990-2006. Bottom – Mean of accumulated SWE for the water years 1990-2006.

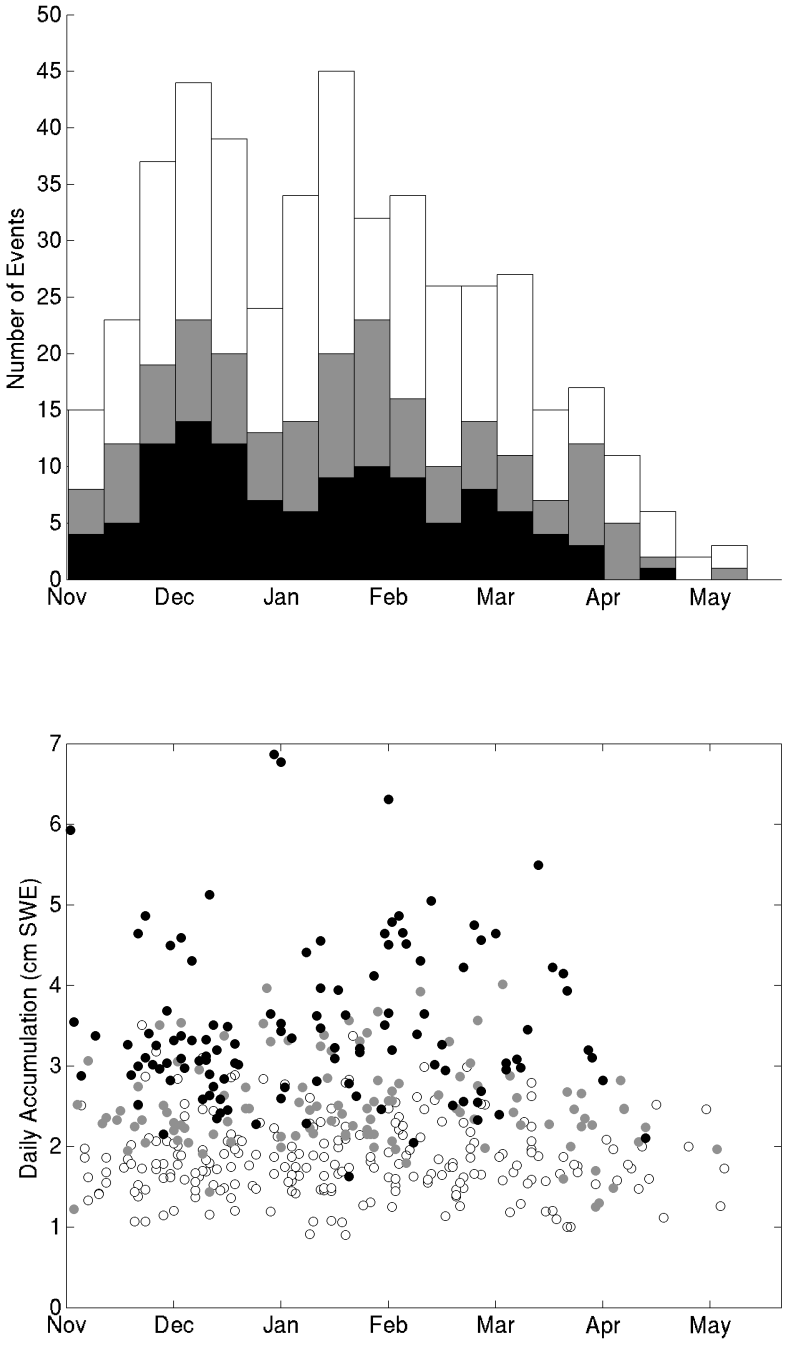


Figure 3.12. Timing of large accumulation events, water years 1983-2006. Top – histogram of frequency of occurrence of large events. Largest 20 events are shown by the height of the white bar; largest 10 events correspond to the gray bar; the largest 5 correspond to the black bar. Bottom – timing and magnitude of large accumulation events. Black represents the largest 5 events; gray the next largest 5 events (ranked 6$^{th}$-10$^{th}$); and, empty circles correspond to the 11$^{th}$-20$^{th}$ snowiest days.

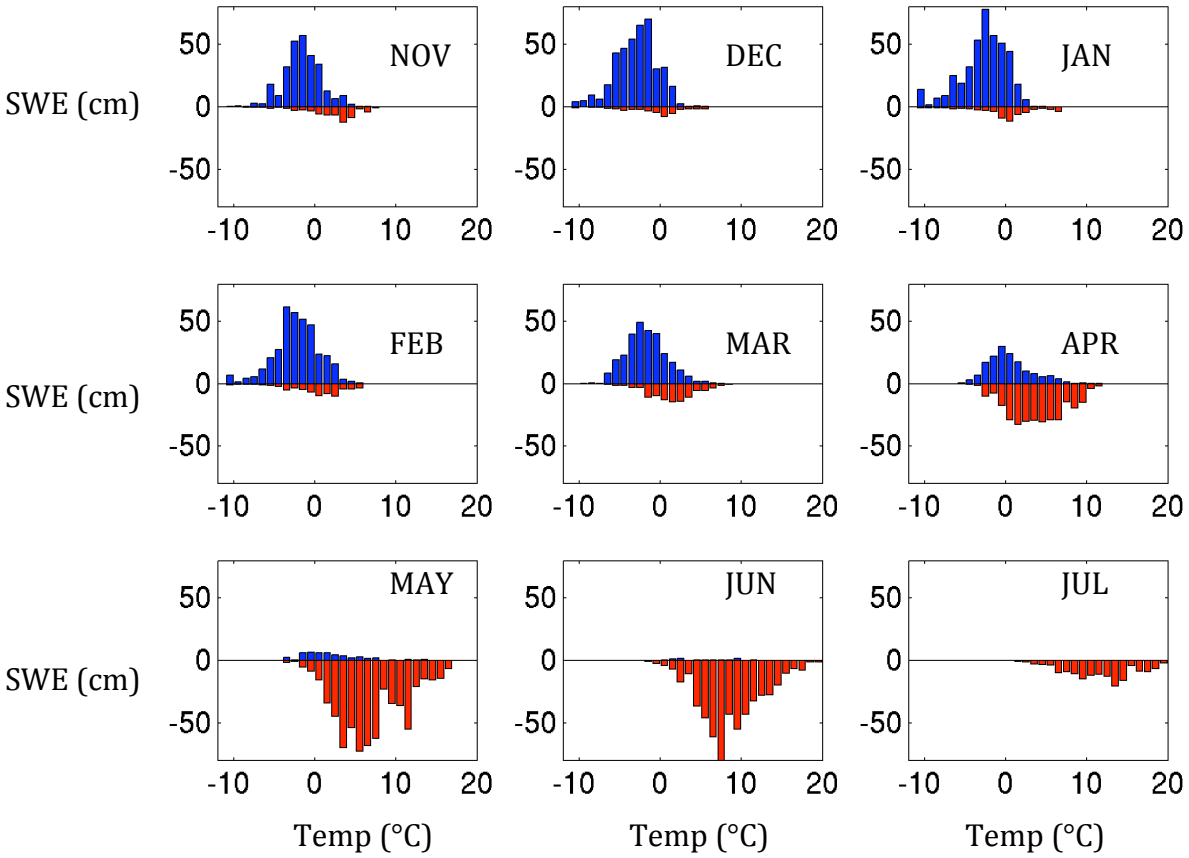


Figure 3.13. Daily accumulation (blue) and loss (red) for the months November-July for the water years from 1990-2006. Accumulation and loss have been binned by 1°C intervals. Bar heights indicate the sum of all events occurring in a temperature bin for the 17 year period.

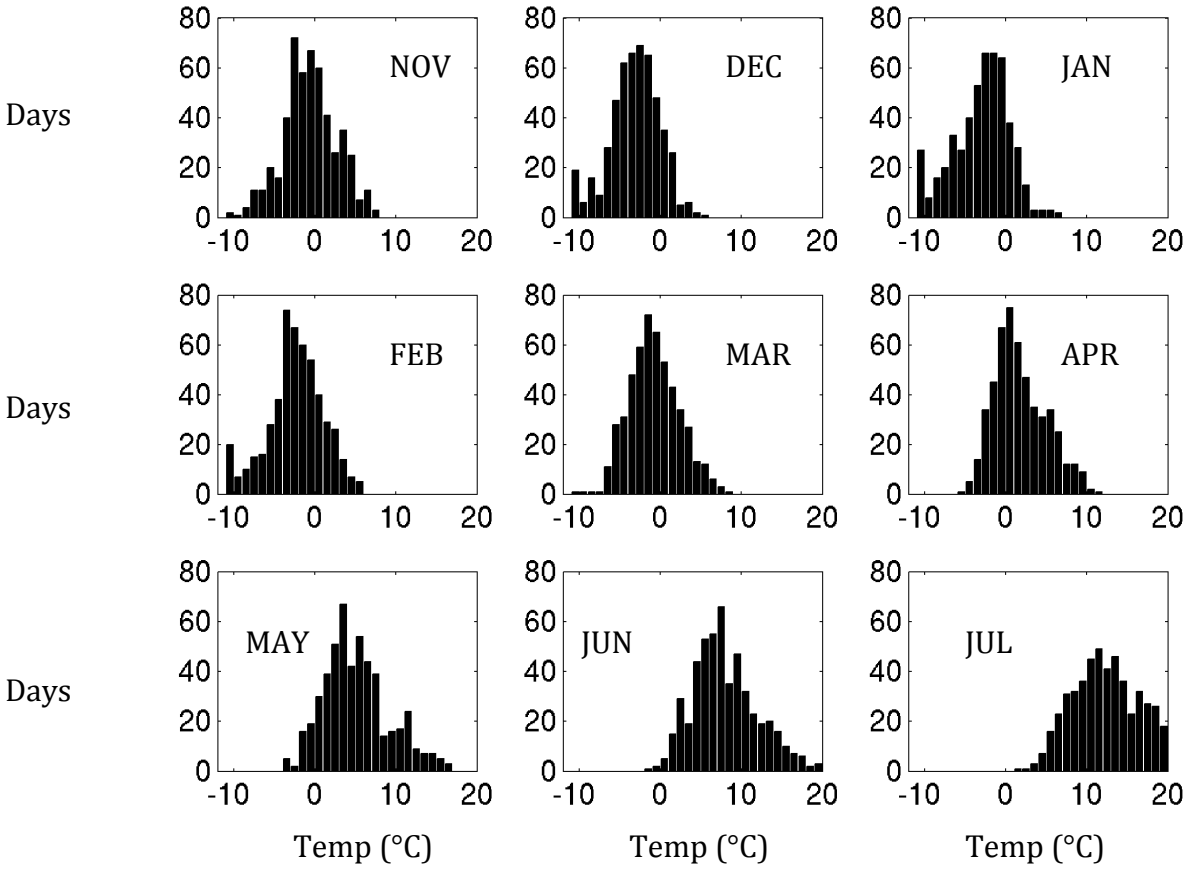


Figure 3.14. Histograms of daily mean temperature for November-July for the water years 1990-2006. Bin intervals are 1°C. Bar heights indicate the total number of days when the mean temperature fell within a bin.

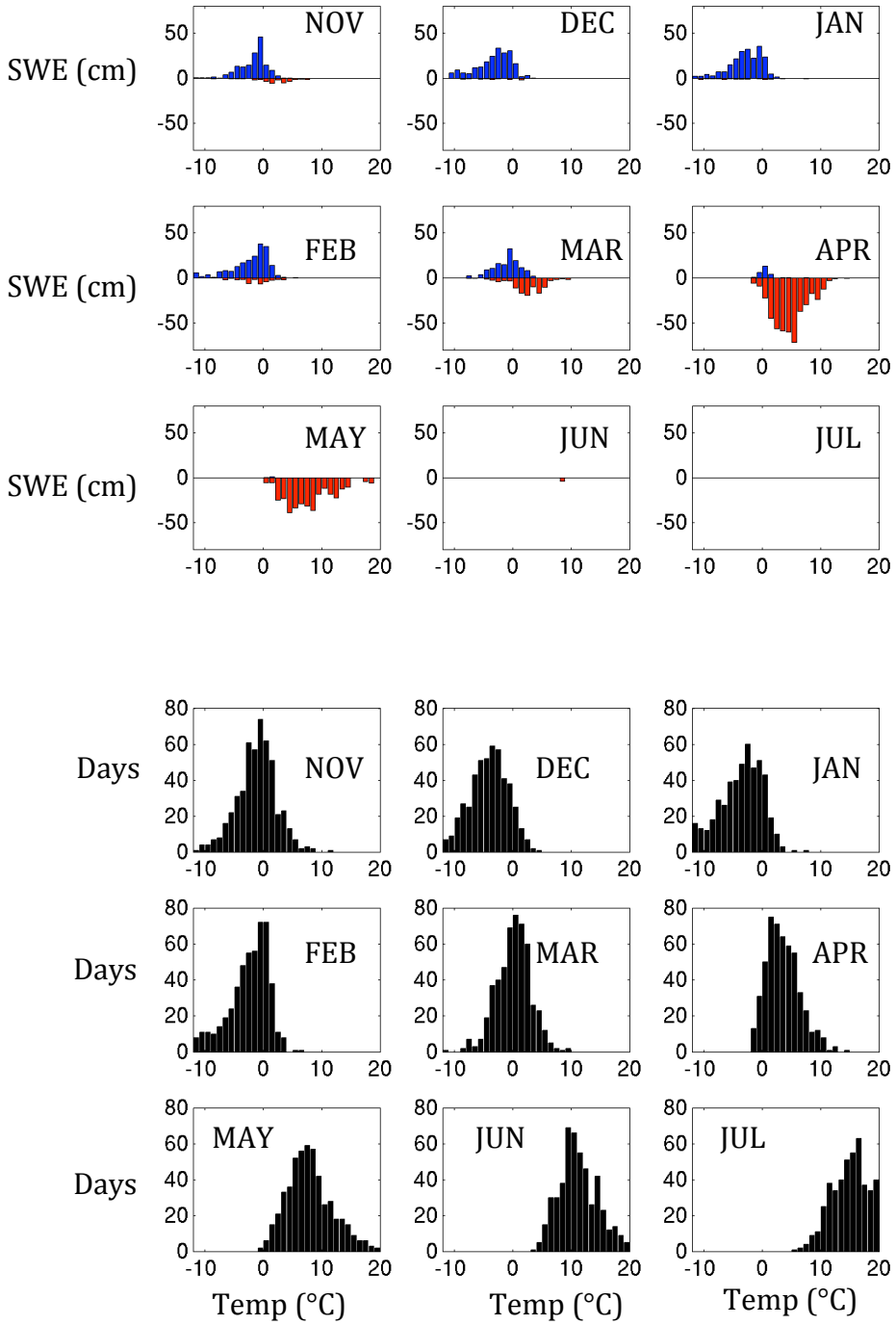


Figure 3.15. SWE accumulation and loss versus daily mean temperature (as in Fig. 3.13) and histograms of daily mean temperature (as in Fig. 3.14) for the Pope Ridge SNOTEL station (elevation 1079 m).

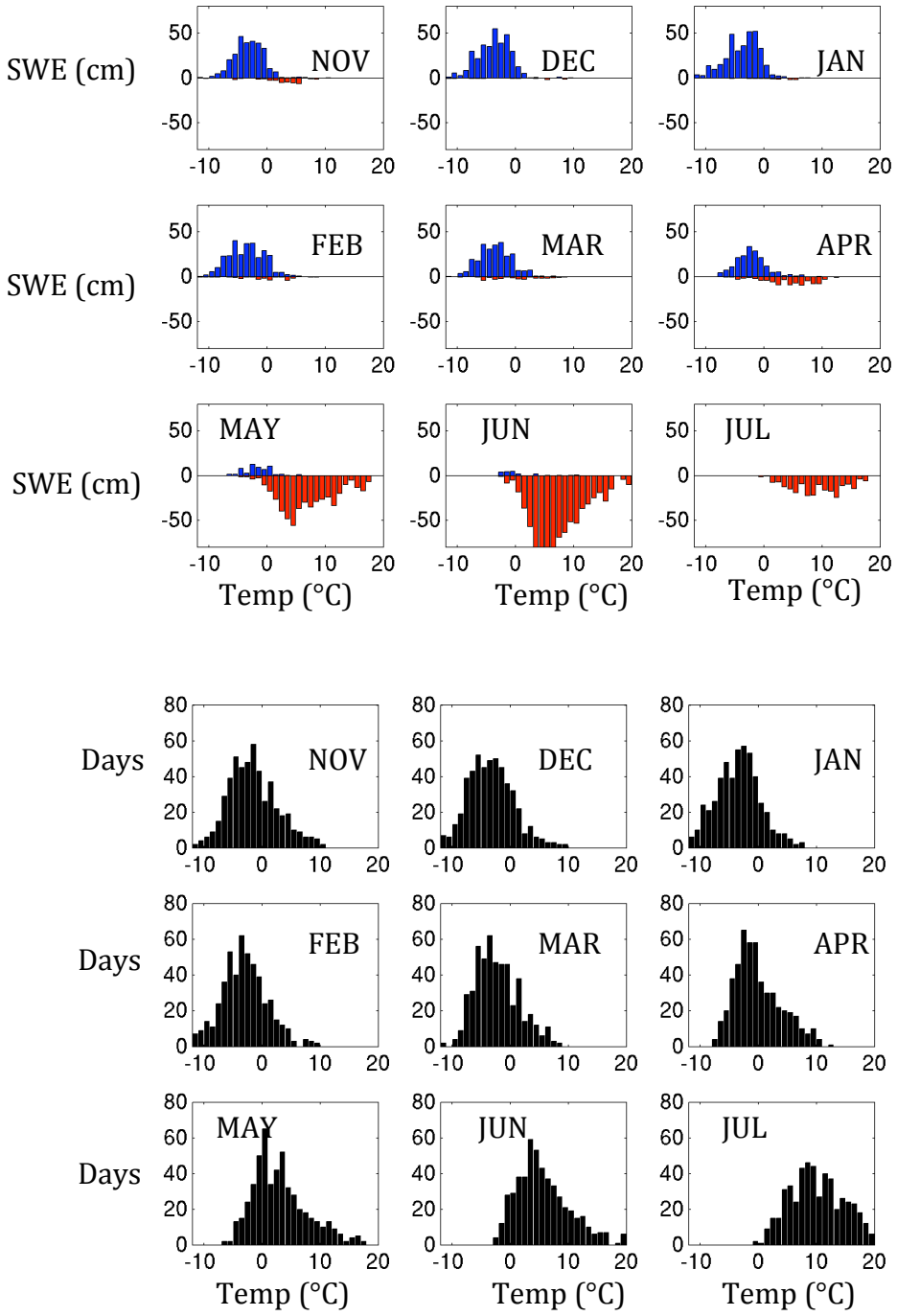


Figure 3.16. SWE accumulation and loss versus daily mean temperature (as in Fig. 3.13) and histograms of daily mean temperature (as in Fig. 3.14) for the Corral Pass SNOTEL station (elevation 1829 m).

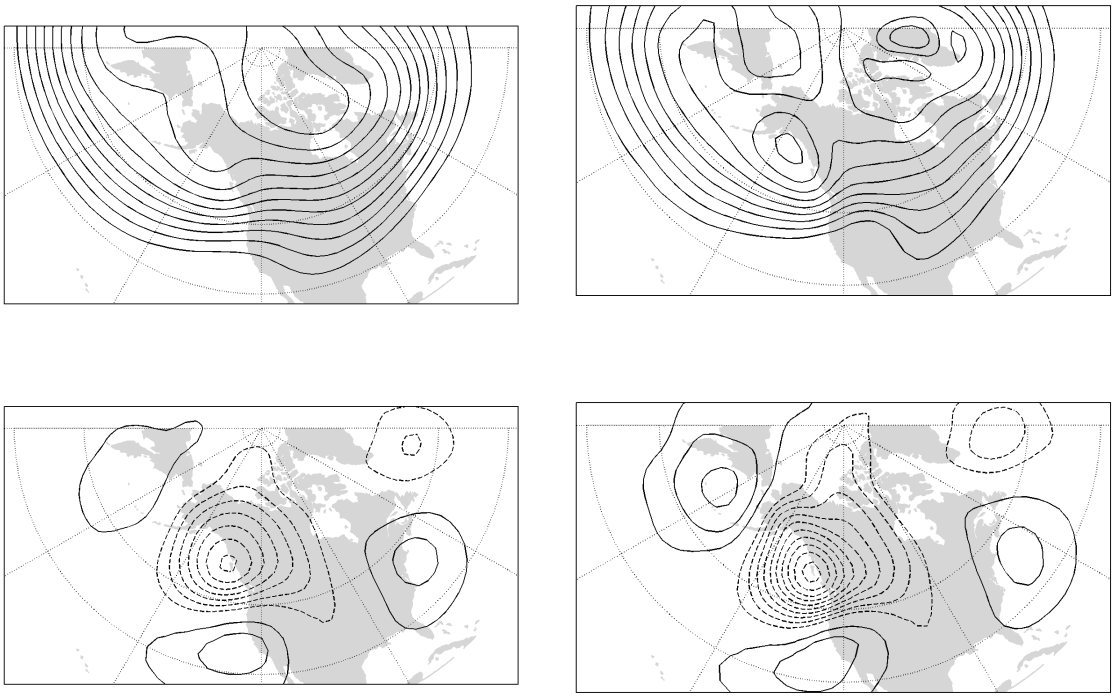

Figure 3.17. Composite maps of the 500-hPa and 850-hPa geopotential height fields (upper left and right, respectively) and anomalies (lower left and lower right, respectively) for the 10 days of greatest accumulation from each year for the water years 1983-2006. Contours for the composite maps are 510 dam to 570 dam with an interval of 6 dam; contours for the anomaly maps have an interval of 2 dam with positive (negative) anomalies shown as solid (dashed) lines.

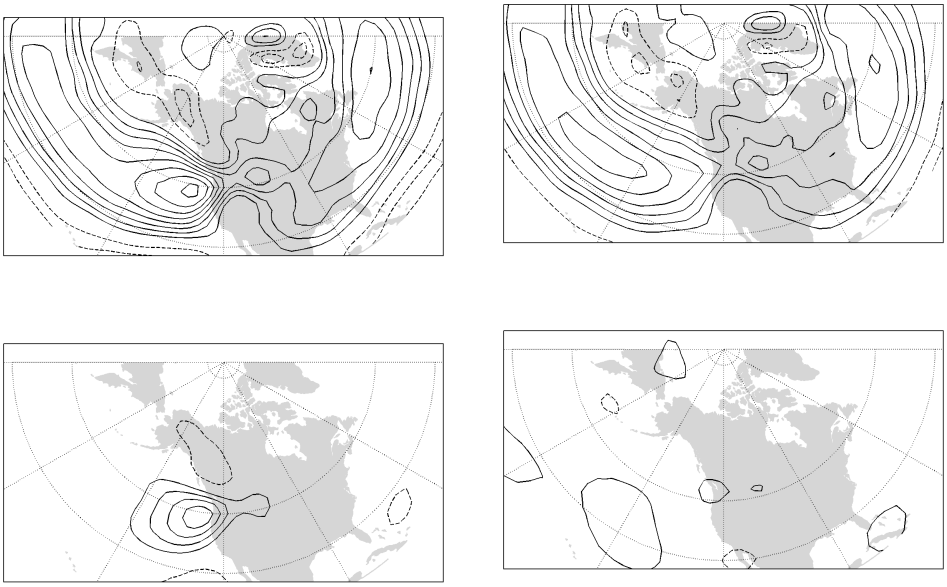

Figure 3.18. Maps of the u-component of the wind on the 850-hPa pressure surface. The top panels represents a composite of the 10 days of greatest accumulation (left) and 10 days of greatest loss from each winter from 1983-2006; the bottom panels represents the anomalies for the same days of accumulation (left) and loss (right). All contour intervals are 2 m/s.

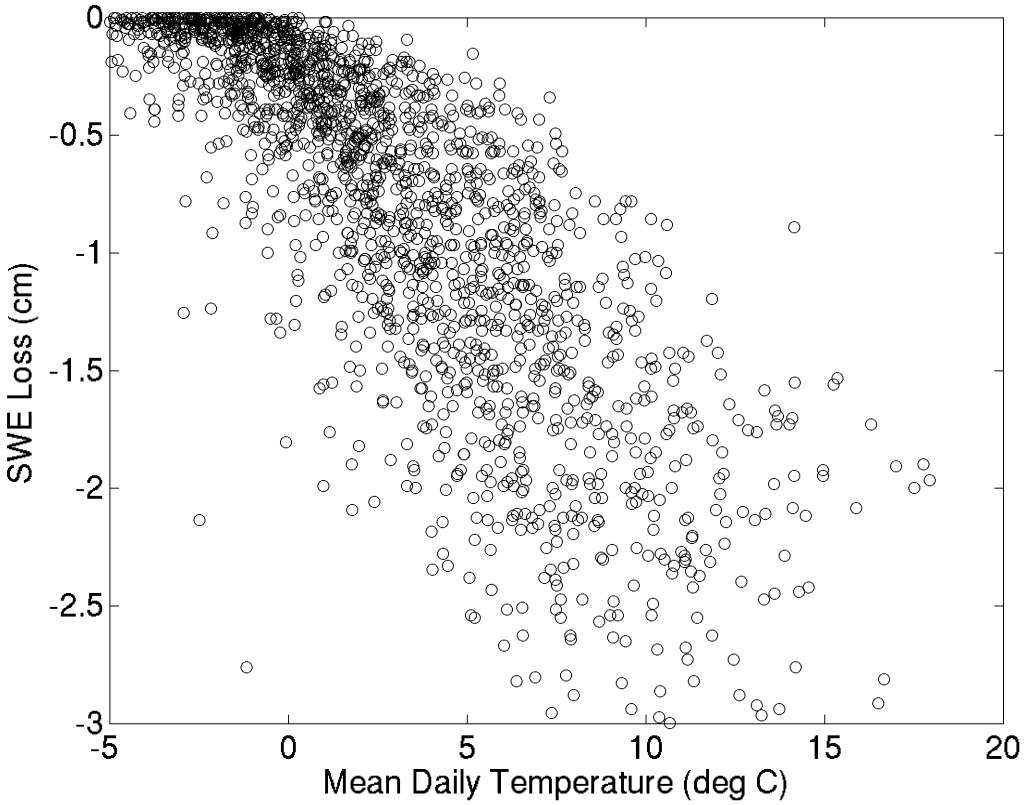


Figure 3.19. Daily SWE loss versus daily mean temperature, March-June, water years 1990-2006. SWE loss and temperatures taken from the indices representing all 30 SNOTEL stations.

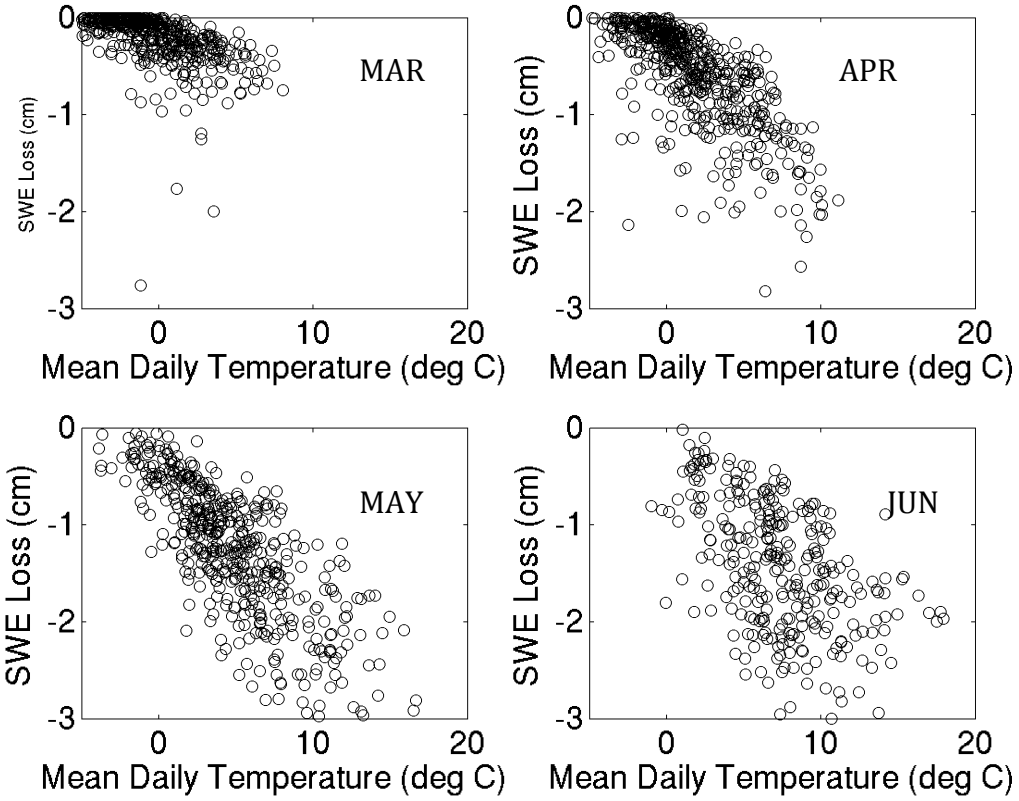


Figure 3.20. As in Figure 3.19, but the data have been composited by month.

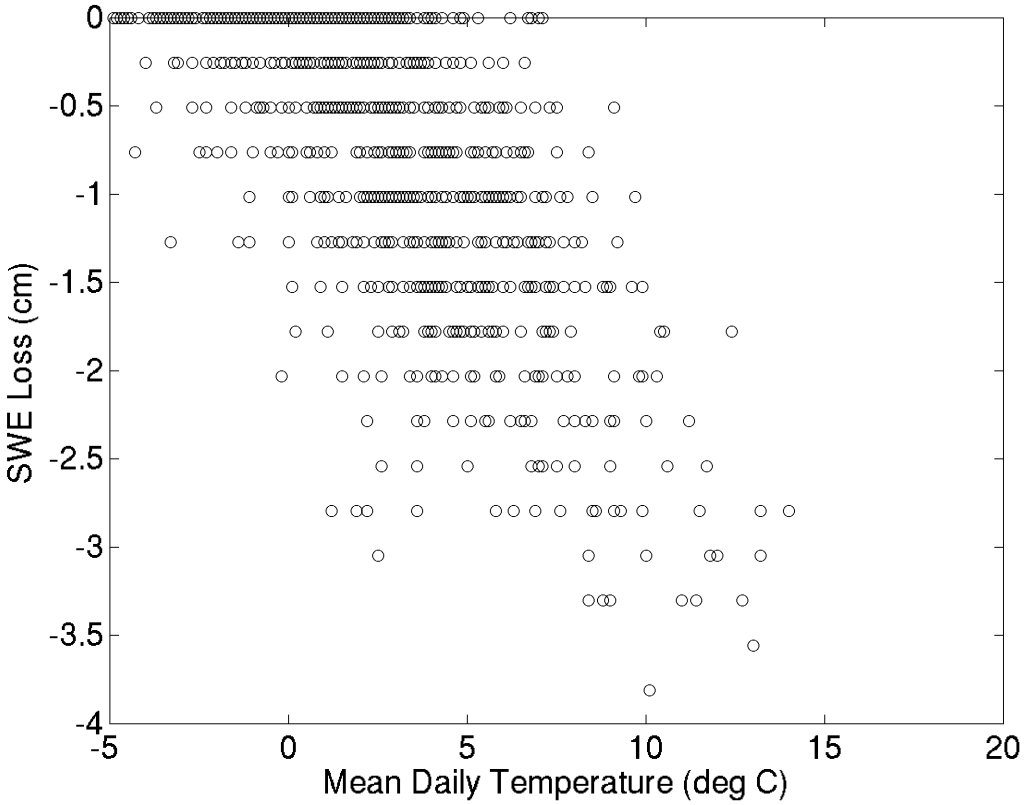


Figure 3.21. Daily SWE loss versus daily mean temperature at Pope Ridge SNOTEL (elevation 1079 m) for the months of March, April, and May, water years 1990-2006.

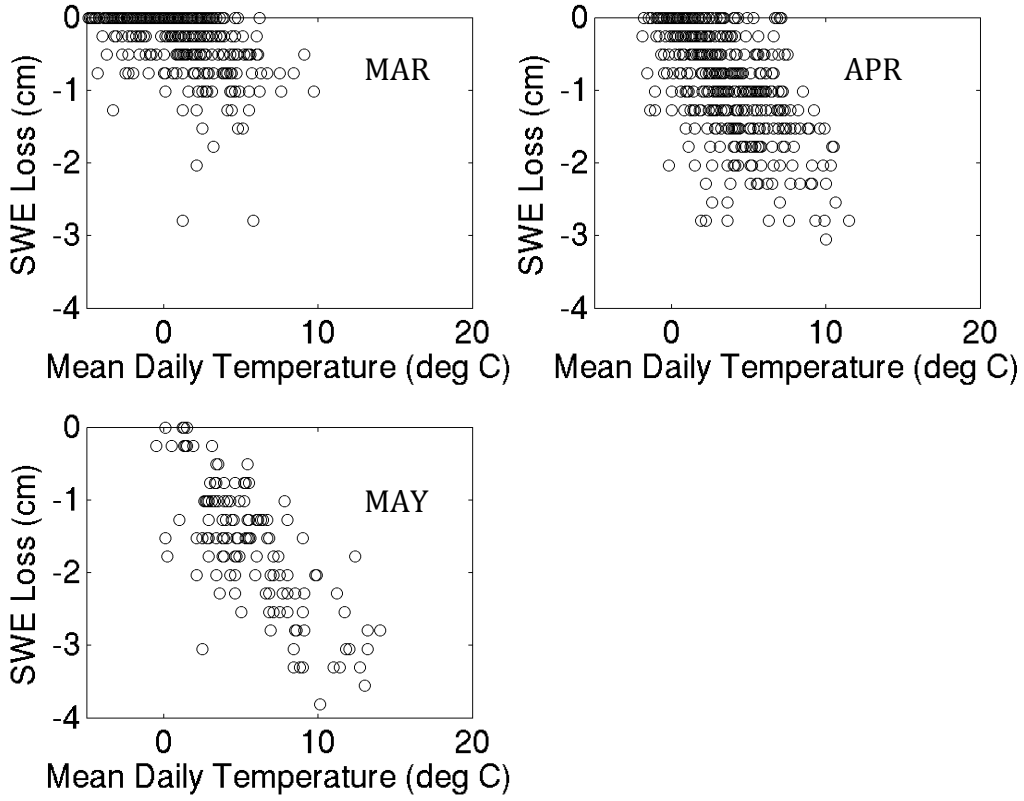


Figure 3.22 As in Figure 3.21, but the data have been composited by month.

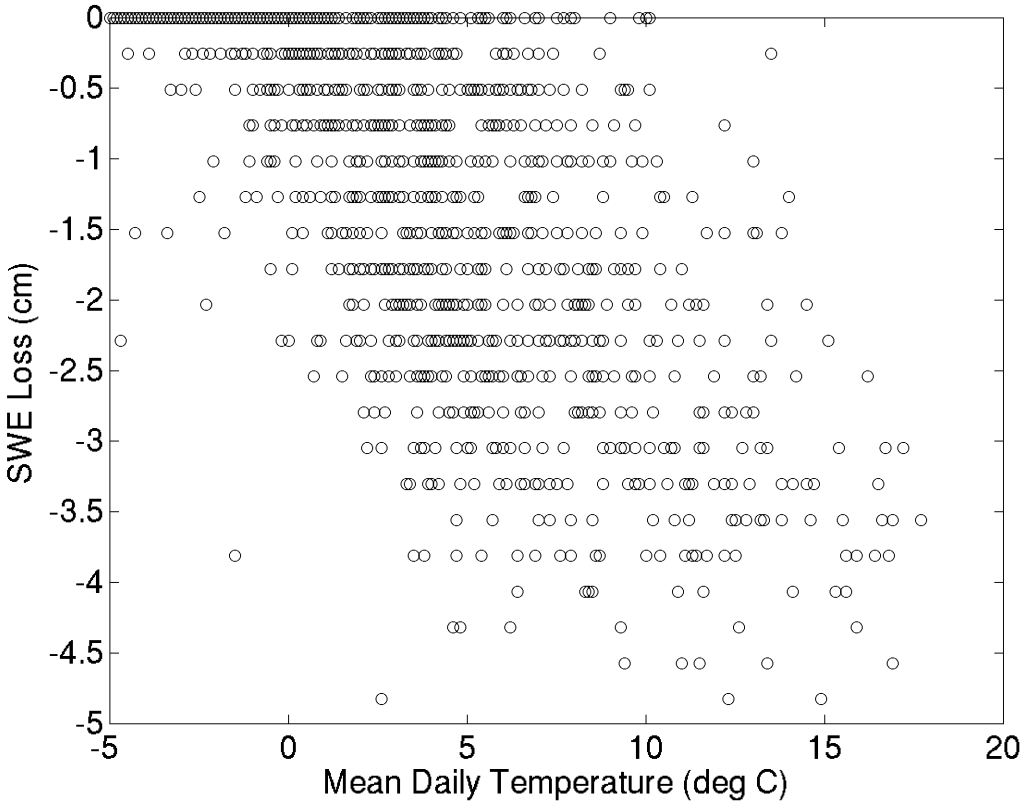


Figure 3.23. Daily SWE loss versus daily mean temperature at Corral Pass SNOTEL (elevation 1829 m) for the months of April, May, June, and July, water years 1990-2006.

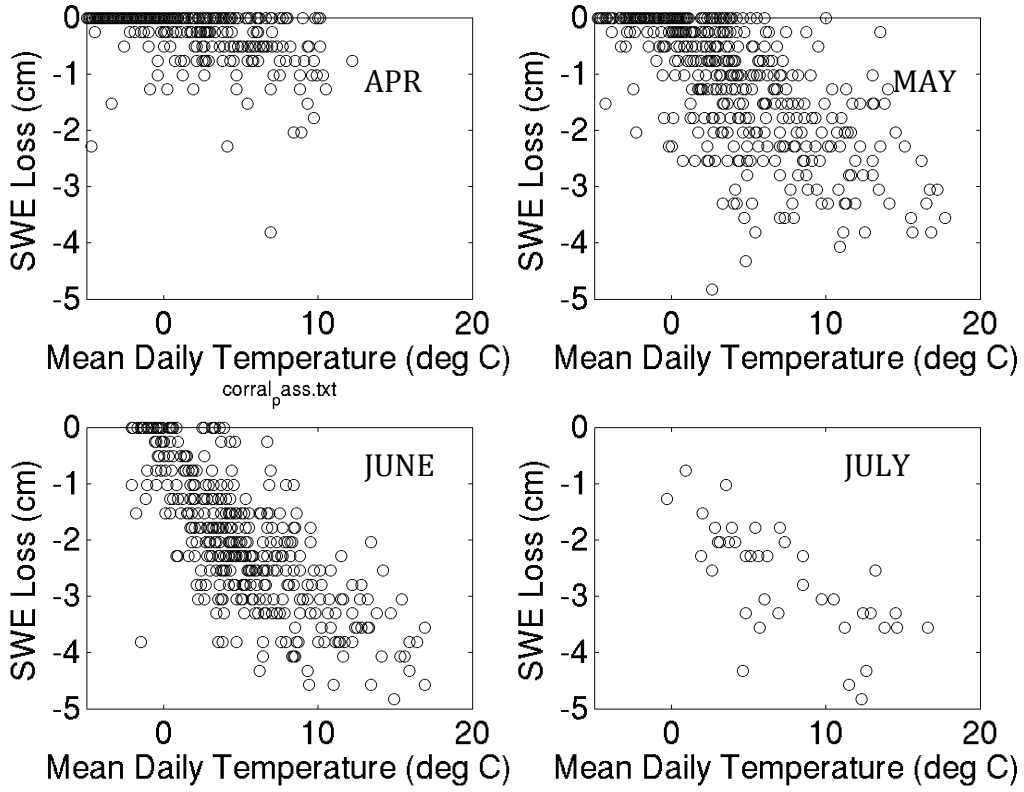


Figure 3.24 As in Figure 3.23, but the data have been composited by month.

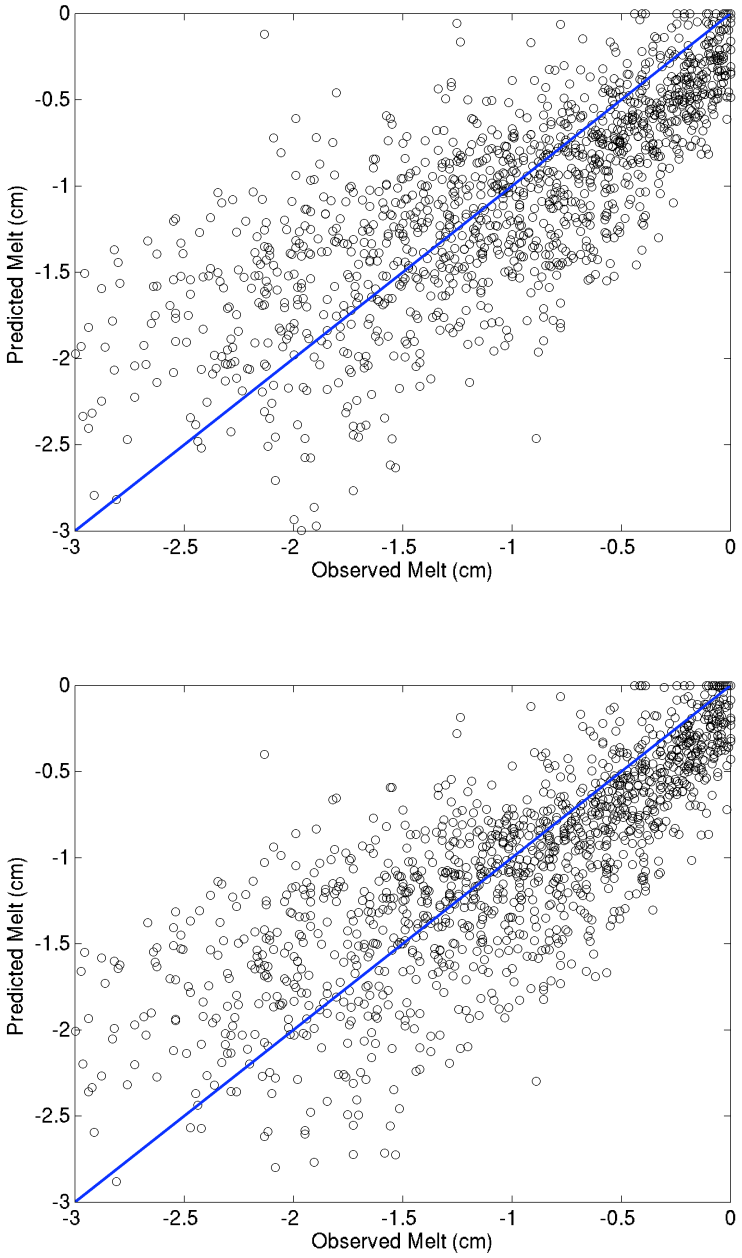


Figure 3.25. Comparison of observed daily melt and predicted daily melt during April, May, and June for the water years 1990-2006. The predictions in the top panel correspond to the degree-day model with no memory; the predictions in the bottom panel correspond to the degree-day model in which an *e*-folding time of 1 day is applied to the temperature time series.

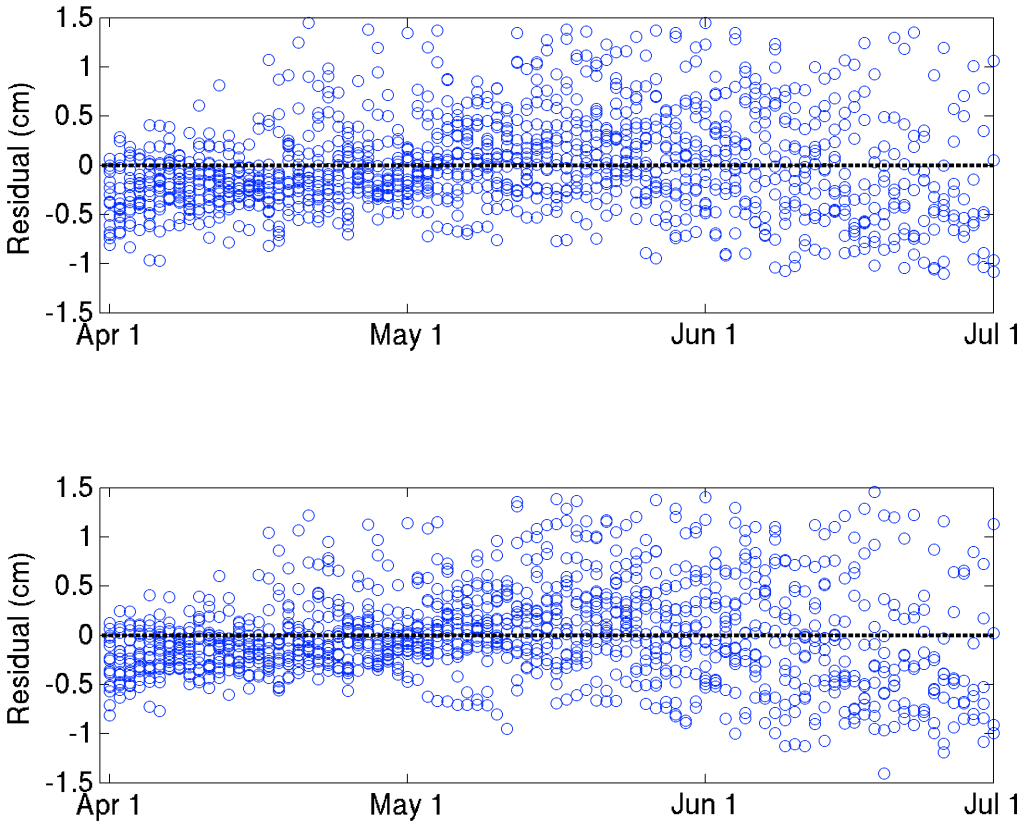


Figure 3.26. Timing and magnitude of the residuals (predicted melt minus observed melt) associated with the degree-day model during April, May, and June for the water years 1990-2006. Positive values indicate where the model has underpredicted the amount of melt, and vice versa. As in Fig. 3.25, the top panel corresponds to the degree-day model with no memory; the bottom panel corresponds to the degree-day model where an *e*-folding time of 1 day is applied to the temperature time series.

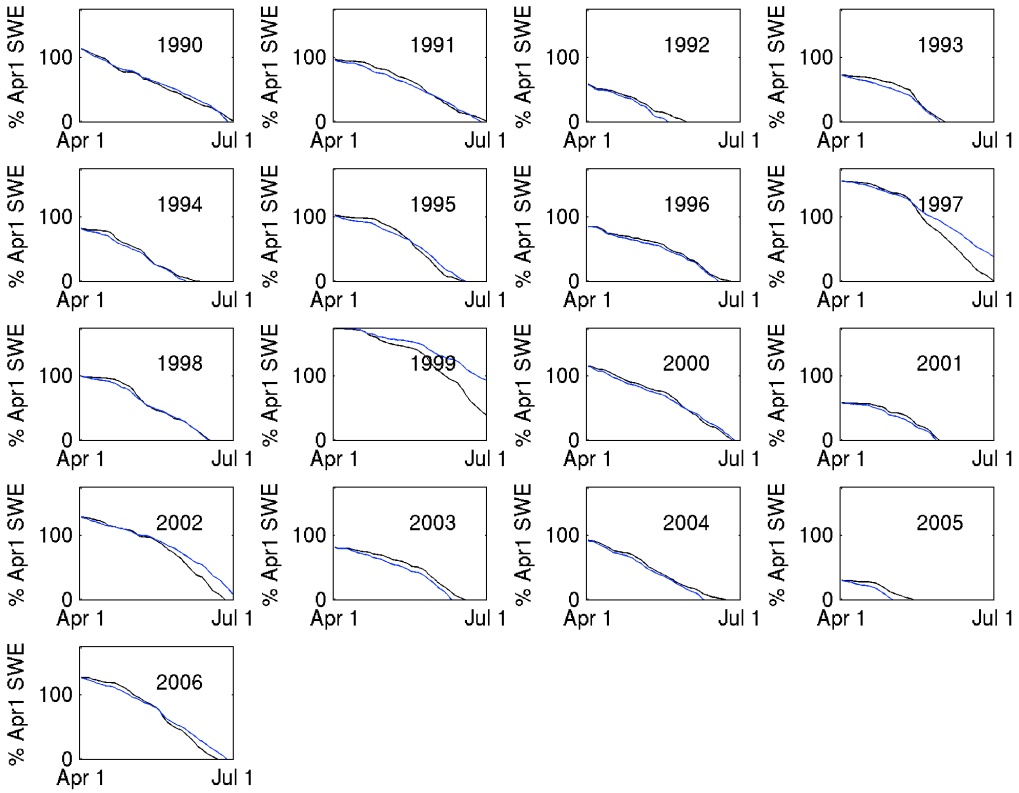


Figure 3.27. Cumulative SWE losses following April 1 for the water years 1990-2006. The black line corresponds to the observed cumulative loss; the blue line corresponds to the predicted cumulative loss based on a degree-day model with no memory. The units for the ordinate correspond to percent of mean April 1 SWE, which is equal to 85 cm SWE.

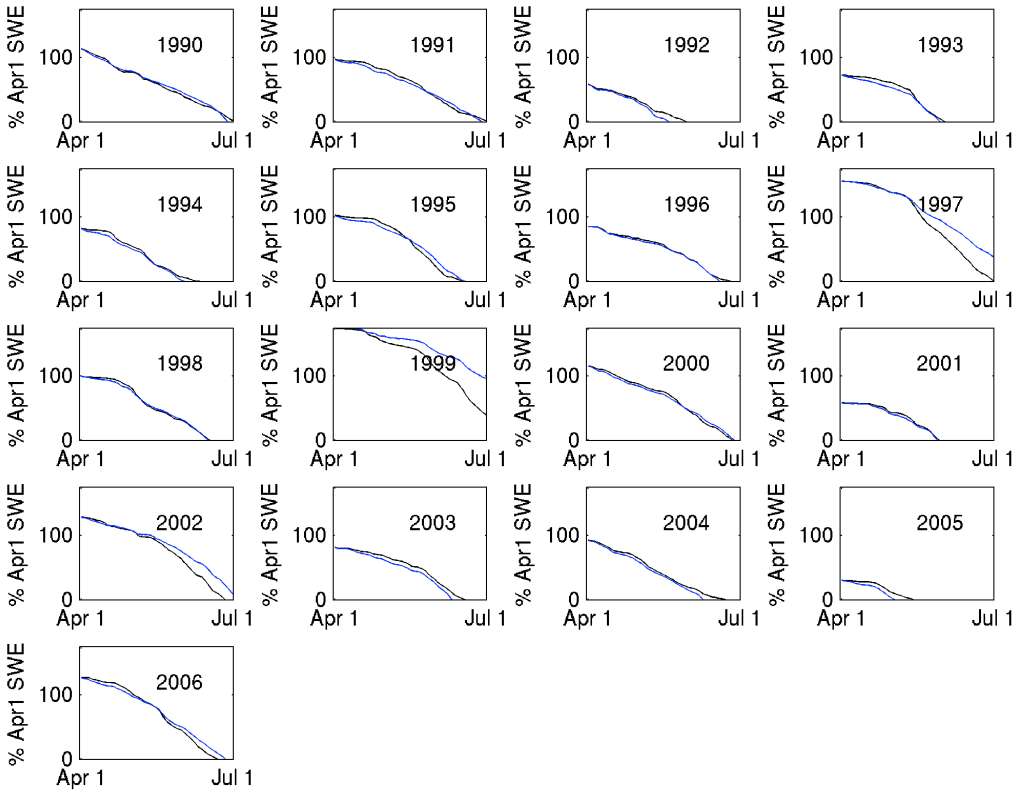


Figure 3.28. As in Fig. 3.27, but the blue line corresponds to predictions from a degree-day model in which an *e*-folding time of 1 day is applied to the temperature time series.

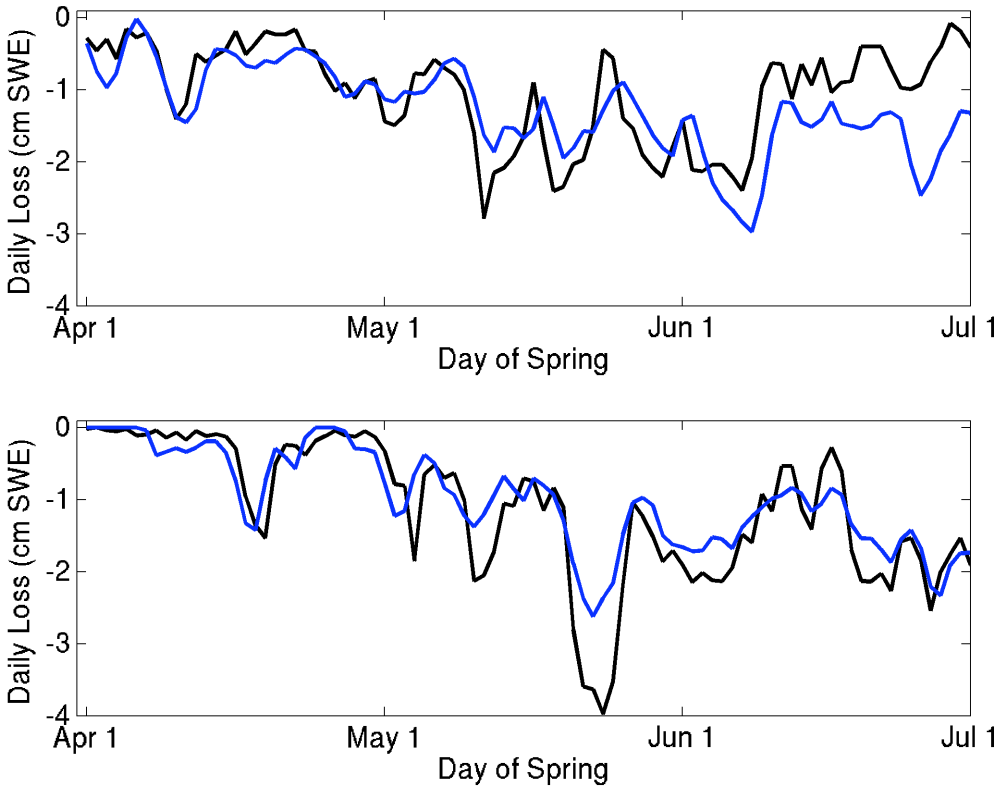


Figure 3.29. Daily time series of observed (black) and predicted (blue) SWE loss for 2007 (top) and 2008 (bottom). Predictions have been made with the degree-day model in which an *e*-folding time of 1 day is applied to the temperature time series.

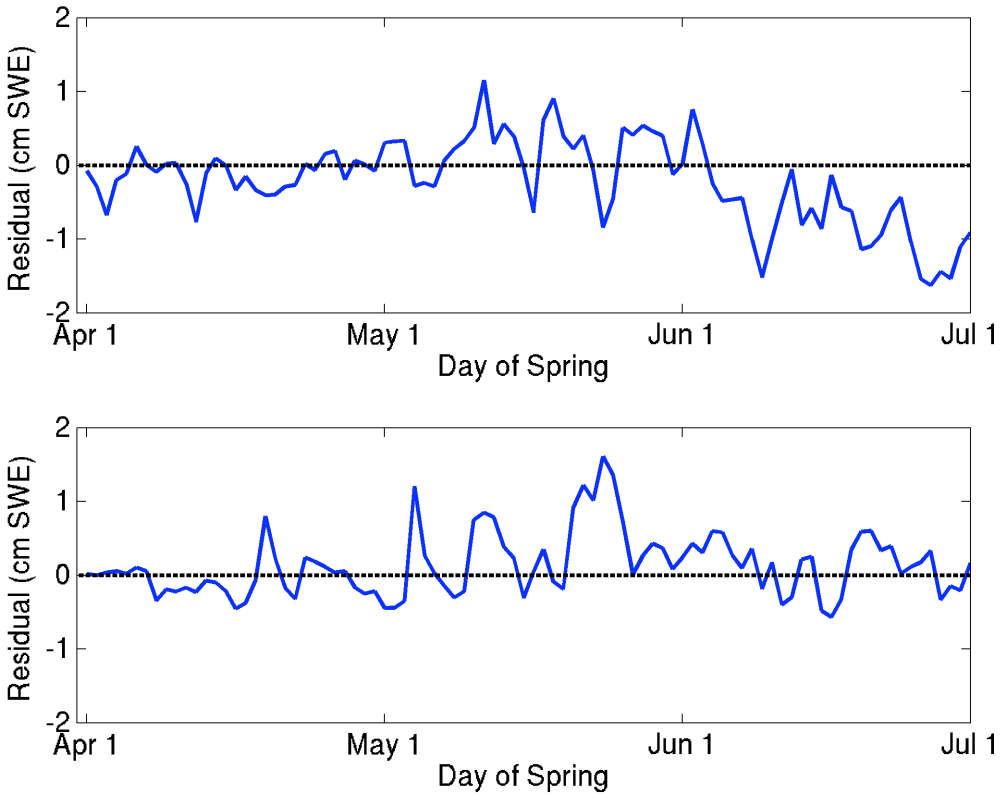


Figure 3.30. As in Fig. 3.29, except for the residual melt (predicted melt minus observed melt) for 2007 (top) and 2008 (bottom). Positive values indicate where the model has underpredicted the amount of melt; negative values indicate an overprediction by the model. Predictions have been made with a degree-day model in which an *e*-folding time of 1 day is applied to the temperature time series.

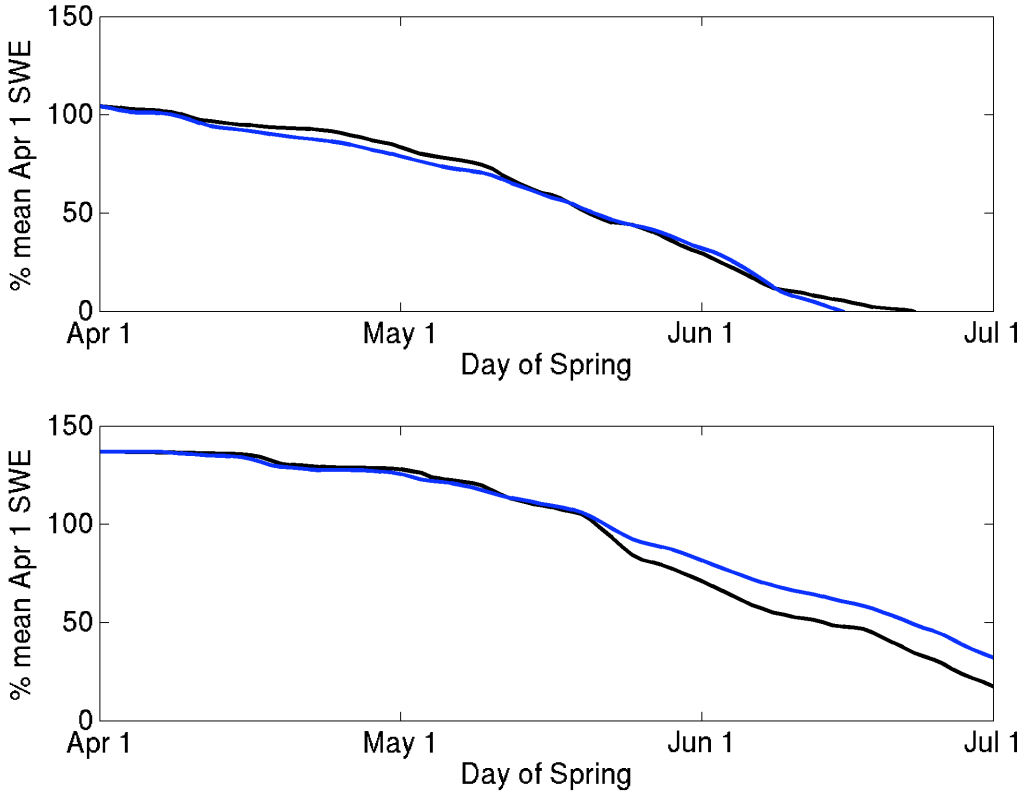


Figure 3.31. Observed (black) and predicted (blue) cumulative losses following April 1 for 2007 (top) and 2008 (bottom). Predictions have been made with the degree-day model in which an *e*-folding time of 1 day is applied to the temperature time series. The units for the ordinate correspond to percent of mean April 1 SWE, which is equal to 85 cm SWE.

Table 3.1. Snowpack Telemetry (SNOTEL) Stations of the Washington Cascades.

| Station Name | ID | Elevation (m) | Latitude (°N) | Longitude (°W) |
|---|---|---|---|---|
| ***Stations 1982-2006*** | | | | |
| Blewett Pass | 20B02S | 1302 | 47.35 | 120.67 |
| Bumping Ridge | 21C38S | 1402 | 46.80 | 121.32 |
| Corral Pass | 21B13S | 1829 | 47.02 | 121.45 |
| Cougar Mountain | 21B42S | 975 | 47.27 | 121.67 |
| Fish Lake | 21B04S | 1028 | 47.53 | 121.08 |
| Grouse Camp | 20B11S | 1640 | 47.27 | 120.48 |
| Harts Pass | 20A05S | 1981 | 48.72 | 120.65 |
| June Lake | 22C09S | 1018 | 46.13 | 122.15 |
| Lone Pine | 21C26S | 1158 | 46.27 | 121.95 |
| Lyman Lake | 20A23S | 1798 | 48.18 | 120.92 |
| Morse Lake | 21C17S | 1646 | 46.90 | 121.47 |
| Olallie Meadows | 21B55S | 1128 | 47.37 | 121.43 |
| Paradise | 21C35S | 1561 | 46.77 | 121.73 |
| Park Creek Ridge | 20A12S | 1402 | 48.43 | 120.90 |
| Pigtail Peak | 21C33S | 1798 | 46.62 | 121.38 |
| Pope Ridge | 20B24S | 1079 | 47.98 | 120.55 |
| Potato Hill | 21C14S | 1372 | 46.33 | 121.50 |
| Rainy Pass | 20A09S | 1457 | 48.52 | 120.73 |
| Sheep Canyon | 22C10S | 1228 | 46.18 | 122.25 |
| Spencer Meadow | 21C20S | 1036 | 46.17 | 121.92 |
| Stampede Pass | 21B10S | 1177 | 47.27 | 121.33 |
| Stevens Pass | 21B01S | 1241 | 47.73 | 121.08 |
| Surprise Lakes | 21C13S | 1295 | 46.08 | 121.75 |
| Trough | 20B25S | 1615 | 47.23 | 120.28 |
| Upper Wheeler | 20B07S | 1341 | 47.28 | 120.37 |
| White Pass | 21C28S | 1372 | 46.63 | 121.37 |
| ***Stations 1989-2006*** | | | | |
| Miners Ridge | 20A40S | 1890 | 48.20 | 120.95 |
| Sasse Ridge | 21B51S | 1280 | 47.38 | 121.05 |
| Spirit Lake | 22C12S | 951 | 46.25 | 122.17 |
| Thunder Basin | 20A07S | 1280 | 48.52 | 120.98 |
| ***Other Stations*** | | | | |
| Alpine Meadows | 21B48S | 1067 | 47.77 | 121.68 |
| Beaver Pass | 21A01S | 1103 | 48.87 | 121.25 |
| Burnt Mountain | 21B63S | 1280 | 47.03 | 121.93 |
| Elbow Lake | 21A32S | 975 | 48.68 | 121.90 |
| Huckleberry Creek | 21B62S | 610 | 47.05 | 121.58 |
| Lost Horse | 21C39S | 1524 | 46.35 | 121.07 |
| Meadows Pass | 21B59S | 1067 | 47.27 | 121.47 |
| Mowich | 21C40S | 960 | 46.92 | 121.95 |
| Mount Gardner | 21B21S | 914 | 47.35 | 121.57 |
| Nooksack | 21A36S | 1518 | 48.82 | 121.92 |
| Rex River | 21B17S | 1219 | 47.30 | 121.60 |
| Skookum Creek | 21B60S | 1195 | 47.68 | 121.60 |
| Swamp Creek | 20A41S | 1219 | 48.57 | 120.77 |
| Swift Creek | 22C13S | 1149 | 46.15 | 122.18 |
| Tinkham Creek | 21B20S | 936 | 47.32 | 121.47 |
| Wells Creek | 21A31S | 1280 | 48.85 | 121.78 |

Table 3.2. Statistics for linear regression of daily SWE loss upon daily mean temperature. Only days in which the Cascades index was greater than or equal to 10 cm were used in the analysis.

| Time Period | Slope (cm/°day) | *y*-int (cm) | $r^2$ | *N* (Days) | Total Melt (cm) |
|---|---|---|---|---|---|
| Mar-June, All Days | -0.1369 | -0.4344 | 0.64 | 1814 | 1501.64 |
| Mar-June, Only Melt Days | -0.1375 | -0.4388 | 0.63 | 1728 | 1501.64 |
| Apr-June, All Days | -0.1408 | -0.4701 | 0.60 | 1304 | 1402.01 |
| Apr-June, Only Melt Days | -0.1405 | -0.4728 | 0.59 | 1293 | 1402.01 |
| Mar, All Days | -0.0452 | -0.2300 | 0.28 | 510 | 99.63 |
| Mar, Only Melt Days | -0.0430 | -0.2446 | 0.24 | 435 | 99.63 |
| Apr, All Days | -0.1176 | -0.3869 | 0.54 | 510 | 303.06 |
| Apr, Only Melt Days | -0.1171 | -0.3906 | 0.53 | 499 | 303.06 |
| May, All Days | -0.1522 | -0.5674 | 0.62 | 486 | 644.63 |
| June, All Days | -0.1065 | -0.6860 | 0.29 | 308 | 454.33 |

Table 3.3. As in Table 3.2, but only for the Pope Ridge SNOTEL station (elevation 1079 m).

| Time Period | Slope (cm/°day) | *y*-int (cm) | $r^2$ | *N* (Days) | Total Melt (cm) |
|---|---|---|---|---|---|
| March-May, All Days | -0.1657 | -0.3236 | 0.46 | 1123 | 892.05 |
| March-May, Only Melt Days | -0.1664 | -0.4792 | 0.36 | 704 | 892.05 |
| Mar, All Days | -0.0559 | -0.1976 | 0.20 | 510 | 106.17 |
| Mar, Only Melt Days | -0.0440 | -0.4847 | 0.08 | 186 | 106.17 |
| Apr, All Days | -0.1511 | -0.3900 | 0.24 | 472 | 452.12 |
| Apr, Only Melt Days | -0.1164 | -0.6598 | 0.15 | 382 | 452.12 |
| May, All Days | -0.2382 | -0.3617 | 0.63 | 141 | 333.76 |
| May, Only Melt Days | -0.2284 | -0.4452 | 0.60 | 136 | 333.76 |

Table 3.4. As in Table 3.2, but only for the Corral Pass SNOTEL station (elevation 1829 m).

| Time Period | Slope (cm/°day) | *y*-int (cm) | $r^2$ | *N* (Days) | Total Melt (cm) |
|---|---|---|---|---|---|
| April-July, All Days | -0.1885 | -0.5254 | 0.53 | 1455 | 1719.33 |
| April-July, Only Melt Days | -0.1705 | -0.8628 | 0.37 | 857 | 1719.33 |
| April, All Days | -0.0463 | -0.1645 | 0.23 | 510 | 83.31 |
| April, Only Melt Days | -0.0405 | -0.5022 | 0.09 | 129 | 83.31 |
| May, All Days | -0.1641 | -0.4501 | 0.50 | 507 | 495.05 |
| May, Only Melt Days | -0.1347 | -0.7977 | 0.34 | 328 | 495.05 |
| June, All Days | -0.2237 | -0.9044 | 0.56 | 395 | 907.54 |
| June, Only Melt Days | -0.1923 | -1.1783 | 0.49 | 357 | 907.54 |
| July, All Days | -0.2011 | -1.3384 | 0.55 | 43 | 233.43 |

# 4. CONSIDERATION OF PHYSICAL PROCESSES AFFECTING THE SNOWPACK DURING WINTER

## *4.1 Energy Balance Model*

Examining a simple energy balance model for the snowpack provides a theoretical justification for the observation that snowmelt during the winter is rare, as presented in the previous chapter.

The energy balance equation presented in Army Corps of Engineers (1956; henceforth ACE) is shown in Eqn. 4.1:

$$Q_{\mathrm{NET}} = Q_{\mathrm{RS}} + Q_{\mathrm{RL}} + Q_{\mathrm{S}} + Q_{\mathrm{L}} + Q_{\mathrm{G}} + Q_{\mathrm{P}} - \Delta Q_{\mathrm{PACK}} \qquad (4.1)$$

The heat available for a phase change of the snow ($Q_{\mathrm{NET}}$) is equal to the sum of the heat absorbed from incident shortwave radiation ($Q_{\mathrm{RS}}$), exchange of heat accompanying the emission and absorption of longwave radiation ($Q_{\mathrm{RL}}$), sensible heat flux ($Q_{\mathrm{S}}$), latent heat flux ($Q_{\mathrm{L}}$), exchange of heat from the underlying ground surface ($Q_{\mathrm{G}}$), exchange of heat occurring when liquid precipitation falls on the snowpack ($Q_{\mathrm{P}}$), and any changes in the heat content of the snowpack ($\Delta Q_{\mathrm{PACK}}$). This formalism is exploited by numerous snowpack models, including the Utah Energy Balance Model (Tarboton et al. 1995) and the SNOW-17 model (Anderson 1976, 2006), which is used in the National Weather Service's River Forecast System.

For the Cascades, melting is the most important phase change for the snowpack. While sublimation can occur when atmospheric temperature and vapor pressure are below the triple point of water (0.01°C and 6.12 mb), the amount of

energy required for sublimation of 1 cm of SWE is nearly 26000 kJ/m$^2$. This energy input is far above what is typically experienced by the snowpack on a winter day. Thus, we will focus on melting, which only requires 3344 kJ/m$^2$ of energy to melt 1 cm of snow. For convenience and to be consistent with the time-step of the SNOTEL observations, this can be converted to an average daily flux of 38.7 W/m$^2$. For each of the terms in the energy balance equation, scaling arguments can be made to demonstrate that only rarely is the net energy flux likely to be large enough to melt significant amounts of snow. Under typical winter conditions in the Cascades the heat flux is just less than 10 W/m$^2$ averaged over the course of a day. The heat flux is sufficient to induce melting during relatively rare, short duration events when temperatures rise above 5°C and the relative humidity is high. Additionally, the snowpack's ability to store liquid water prevents most snowmelt from running off. This liquid water can be refrozen during periods when the heat flux is directed away from the snowpack, allowing the snowpack to retain its SWE.

During the following discussion, the equations shown are identical to those presented in ACE. The only differences are that the units have been updated to the SI system. It will be assumed that the snowpack has a thermal quality of 1, which represents the ratio of energy required to produce a given amount of water from snow versus to the amount of energy required to produce the same amount of water from ice at 0°C. Setting the thermal quality equal to 1 is equivalent to assuming that the snowpack is isothermal and responds to heating in the same way as ice at 0°C. For snowpacks that are actually below 0°C, this assumption causes the estimates for melt to be positively biased because more energy is required for melt than

estimated from Eqn. 4.1[1]; for snowpacks with appreciable liquid water, the estimates are negatively biased and less energy will be required for melt than estimated from Eqn. 4.1.

Fluxes are defined as positive if they are into the snowpack, indicating that the snowpack would warm and/or melt; fluxes that are negative are directed away from the snowpack, signifying cooling. Since this analysis focuses on melting and the thermal quality of the snow is assumed to be 1, $\Delta Q_{\mathrm{PACK}}$ is assumed to be equal to zero. In reality, $\Delta Q_{\mathrm{PACK}}$ equals zero *only* when the sum of the other flux terms on the right-hand side of Eqn. 4.1 is positive and the thermal quality of the snow is 1; if the sum of the other flux terms on the right-hand side of Eqn. 4.1 is negative, then $Q_{NET}$ is zero and $\Delta Q_{\mathrm{PACK}}$ is negative and represents the amount of cooling experienced by the snowpack.

*4.2 Shortwave Radiation ($Q_{RS}$)*

Estimates of the average daily solar radiation reaching the surface in the Cascades region during December, January, and February are approximately 50 W/m$^2$ (ECMWF; Gupta et al. 1999). Even on a cloudless day, the greatest amount of insolation is about 100-120 W/m$^2$. The albedo of snow ranges from 50-90% depending on the age of the top layers of snow, with the lower values more typical of snowpack in late winter (ACE). Thus, the amount of absorbed radiation ranges

[1] This explains why the degree-day model often overestimates daily melt during April (Section 3.9) – the thermal quality is likely greater than 1 at the beginning of the melt season.

from 5-25 W/m$^2$ on a typical day, with values as high as to 50-60 W/m$^2$ on a clear day with a relatively older, "darker" snowpack surface.

Since the SNOTEL stations are typically located in clearings, the role of vegetation in intercepting insolation is not considered here explicitly. However, for forested areas, the values for $Q_{RS}$ would be much smaller.

*4.3 Longwave Radiation ($Q_{RL}$)*

Objects emit longwave radiation in accordance to their temperature ($T$) and emissivity ($\varepsilon$), as described by the Stefan-Boltzmann Law:

$$Q_{RL} = \varepsilon \sigma T^4 \qquad (4.2)$$

where $\sigma$ represents the Stefan-Boltzmann constant (5.67e-8 W/m2/°K$^4$). The snowpack's emissivity for longwave radiation is approximately 1, thus it emits longwave radiation much like a blackbody. The atmosphere is not as efficient in emitting longwave radiation, and typical values for the emissivity range between 0.6 and 0.8 (Anderson 2006) for clear-sky conditions, with this value strongly controlled by the humidity. The ACE investigations use a constant emissivity of 0.757. This value comes from an empirically-derived relationship between emissivity and humidity, using the saturation vapor pressure at 0°C (6.11 hPa). Most vegetation is extremely efficient at emitting longwave radiation, and its emissivity can be considered equal to 1. The net flux can be calculated using the following equations:

$$Q_{RL} = (0.757\sigma T_A^4 - \sigma T_S^4)(1 - 0.07872N) \quad (4.3)$$

$$Q_{RL} = (F\sigma T_A^4 + (1-F)0.757\sigma T_A^4) - \sigma T_S^4 \quad (4.4)$$

Equation 4.3[2] represents the longwave flux for various amounts of cloud cover (a fraction between 0 and 1, represented by $N$); $T_A$ and $T_S$ correspond to the air temperature and snowpack temperature in Kelvin, respectively. Equation 4.4 represents the longwave flux for various amounts of forest cover (a fraction between 0 and 1, represented by $F$) under clear skies. Estimates of the longwave fluxes have been calculated by assuming that the temperature of the vegetation is equal to the air temperature, setting $T_S$ equal to 0°C, and using values of 0.3, 0.5, and 0.8 for $N$ and $F$. Results are shown in Fig. 4.1.

Cloud cover acts to reduce the magnitude of the longwave loss for the snowpack. Regardless of cloudiness, the net longwave fluxes in the absence of vegetation are typically negative (top panel Fig. 4.1), unless the air temperature is extremely warm (20°C or greater). The presence of vegetation greatly enhances the longwave flux into the snowpack: 50% forest cover yields positive flux at temperatures just above 8°C.

[2] The constant 0.07872 is an adjustment to the cloud fraction that represents a cloud base of 1 km above the snow surface – higher clouds would have a constant with a larger value. The equations appearing in ACE set this constant to be equal to $0.024Z$, where $Z$ is the height of cloud base in thousands of feet.

Mean daily temperatures from the time series representing the daily average of the 30 SNOTEL stations are usually below zero during mid-winter. The highest temperatures for the daily mean temperature time series for the 17-year period for the same three months range from 5°C to just under 7°C. Thus, the longwave flux is almost always negative during December, January, and February. From Fig. 4.1, one can estimate that for a typical day with temperatures near 0°C, a non-forested area under clear skies could experience fluxes on the order of –100 W/m$^2$, while a forested area under substantial cloud cover would experience a flux on the order of –10 W/m$^2$.

*4.4 Sensible ($Q_S$) and Latent ($Q_L$) Heat Flux*

Sensible and latent heat fluxes are functions of the wind speed and the differences in temperature and vapor pressure between the snow surface and the air immediately above the snow, respectively, as shown in Eqns. 4.5 and 4.6. The sensible heat flux equation also has a correction for the atmospheric pressure ($p$; $p_0$ represents atmospheric pressure at sea level, ~1000 hPa). These equations have been taken from ACE and are relatively crude approximations, because they do not include terms to describe the atmospheric stability (see Storck 2000), resulting in zero flux when stable conditions occur.

$$Q_S = 2.49 \text{ W/m}^2/^\circ\text{C}/(\text{m/s}) \, (p/p_0)(T_A - T_S)(v) \qquad (4.5)$$

$$Q_L = 11.875 \text{ W/m}^2/\text{mb}/(\text{m/s}) \, (e_A - e_S)(v) \qquad (4.6)$$

The wind speed is represented by $v$; $e_A$ and $e_S$ represent the vapor pressure of the air and snowpack, respectively, with the latter equal to 6.11 hPa for an isothermal snowpack at 0°C. Figure 4.2 shows sample estimates of sensible and latent heat fluxes based on these equations and substituting relatively light wind speeds (0.5 m/s, 1m/s, and 2m/s). At the reference level of 1 m above the snow surface, light winds are likely to occur on most days in the Cascades.

While the relationship between sensible heat flux and temperature is explicit in Eqn 4.5 (i.e., sensible heat flux will be positive for temperatures above freezing), the relationship between latent heat flux and temperature is less direct, as it is predicated on temperature's control over ambient vapor pressure. Latent heat flux will be positive when water vapor from the air condenses onto the snowpack. In order for condensation to occur, the ambient vapor pressure must exceed that of the vapor pressure of the snowpack (~6 hPa); essentially, the air must be nearly saturated and the air temperature must be considerably warmer than freezing.

For the warmest of winter days ($T_A$~5°C), and assuming a relative humidity of 100%, the vapor pressure difference between saturated air and a 0°C snow surface would only amount to 2-3 hPa. Thus, both the sensible and latent heat flux equations require temperatures to be greater than 0°C to cause the fluxes to be positive. For a warm, moist day, sensible heat fluxes on the order of +20 W/m$^2$ and latent heat fluxes as large as +50 W/m$^2$ seem possible. However, as mentioned in the previous section, it is rare for temperatures to be this warm – under more typical conditions, sensible and latent heat fluxes should each be on the order of 10-

20 W/m$^2$, with the positive fluxes for above-freezing temperatures and negative fluxes for below-freezing temperatures.

*4.5 Heat Flux with the Ground Surface ($Q_G$)*

The heat flux between the ground surface and the snowpack can be modeled as a conduction process, as described in Eqn. 4.7:

$$Q_G = k\,(dT/dz) \qquad (4.7)$$

where $k$ is a constant describing the thermal conductivity of the soil and $dT/dz$ is the temperature gradient between the ground surface and the depth of maximum temperature in the sub-surface. Typically, these values are extremely small, yielding a heat flux on the order of 1 to 2 W/m$^2$. Measurements of melt attributable to this heat flux appearing in ACE are typically less than 2 cm per month. Thus, heat exchange with the ground can be considered negligible when making estimates of daily melt.

*4.6 Heat Flux from Precipitation Falling as Rain ($Q_P$)*

Precipitation falling as rain can transfer heat to the snowpack in accordance with the following equation:

$$Q_P = 0.484\ \text{W/m}^2/^\circ\text{C/cm}\ (T_R - T_S)(P) \qquad (4.8)$$

Where $T_R$ represents the temperature of the rainfall, $T_S$ represents the temperature of the snowpack, and $P$ represents the amount of precipitation in cm over a day.

For heavy rain events (~10 cm of precipitation in one day) when temperatures are well above freezing (~ 5°C), the heat flux from rainfall could be on the order of 20 W/m$^2$. However, for more typical rain events of a few centimeters of rain per day, the heat flux is less than 10 W/m$^2$ (Fig. 4.3).

Rainfall can lead to a much larger heat flux if it falls onto a sub-freezing snowpack. Under these circumstances, the rain is likely to refreeze. The latent heat released by the this phase change is equal to the amount of latent heat of fusion, or 3344 kJ/m$^2$ for 1 cm of snow. Considering that the specific heat of snow is approximately 21 kJ/cm SWE/°C, the snowpack can be substantially warmed by the rainfall. For example, 1 cm of rainfall that is refrozen into the snowpack could raise the temperature of a snowpack containing 16 cm of SWE by 10°C, if the heat could be transferred efficiently.

*4.7 Heat Transfer*

Even in the event of a net heat flux into the snowpack, the relatively low thermal conductivity of the snow will require that these conditions persist for several days for appreciable melt to occur throughout the snowpack. Equation 4.9 defines a "relaxation time" ($\tau$) representing the amount of time required for the snowpack to adjust to a temperature perturbation ($T_E$-$T_S$; where $T_E$ is the environmental or air temperature and $T_S$ is the mean temperature of the snowpack). In Eqns. 4.9-4.13, $dT/dt$ represents the warming rate of the snowpack; $k$ is a

constant representing the thermal conductivity (in W/m/°K); *m* is the mass of the snowpack; $C_P$ is the heat capacity of ice at 0°C; *z* is the depth of the snowpack; and ρ is the density of the snowpack. By substituting the expression for the warming rate (*dT/dt*) shown in Eqn. 4.10 and the expression for the temperature gradient between the air and the snowpack shown in Eqn. 4.11, Eqn. 4.9 can be rearranged to yield Eqn. 4.12, which expresses the relaxation time as a function of the snow density, the depth of the snowpack, and the thermal conductivity. Equation 4.13 provides an estimate for the thermal conductivity, and is taken from Sturm et al. (1997), where measurements of thermal conductivity are reconciled with estimates appearing throughout the literature.

$$\tau = \frac{T_E - T_S}{\left(\frac{dT}{dt}\right)} \qquad (4.9)$$

$$\frac{dT}{dt} = \frac{k\nabla T}{mC_P} \qquad (4.10)$$

$$\nabla T = \frac{T_E - T_S}{z} \qquad (4.11)$$

$$\tau = \frac{mC_P z}{k} = \frac{\rho C_P z^2}{k} \qquad (4.12)$$

$$k = 0.138 - 1.01\rho + 3.233\rho^2 \qquad (4.13)$$

Figure 4.4 uses the above equations to estimate the relaxation time associated with snow of various densities[3]. The low density snow (ρ=0.2 g/cm$^3$) is

[3] In a "real" snowpack, density is likely to vary throughout the depth of the snowpack, with deeper layers exhibiting the highest density. For simplicity, the snowpack will be assumed to have a mean density. Also, the estimates of *k* are based on dry snow, and it is assumed that no liquid water is present.

similar to freshly deposited snow; the high density snow ($\rho$=0.6 g/cm$^3$) is likely only to be observed at the end of the winter, following substantial compaction. The conclusion to be drawn from Fig. 4.4 is the relaxation time for a typical mid-winter snowpack (SWE greater than 20 cm; r<=0.4 g/cm$^3$) is greater than 1 day. In order for sufficient heat to be transferred to the bulk of the snowpack and induce melting, temperatures must remain well above freezing for several days. For the relaxation time to be less than 1 day for a snowpack with a low to medium density, very little snow must be present, as might be the case in November or at the lowest elevations in the Cascades.

*4.8 Summary for Winter Conditions*

Combining the scaling arguments made above, the occurrence of melt requires the sum of incoming solar radiation and the downward sensible and latent heat fluxes to be greater than the emission of longwave radiation from the snowpack. Fluxes across the ground surface are negligible, and fluxes with liquid precipitation are important only during the heaviest, warmest rain events. There appears to be a partial cancellation between the absorption of shortwave radiation and the emission of longwave radiation, with the latter bring stronger – under clear skies $Q_{RS}$ could be as high as 60 W/m$^2$; but it would be counterbalanced by $Q_{RL}$ as large as –100 W/m$^2$. While the presence of vegetation reduces the magnitude of $Q_{RL}$, it also reduces $Q_{RS}$, because the forest canopy serves as an effective interceptor of shortwave radiation.

The sensible and latent heat fluxes must play an important role in inducing melt to occur. For these fluxes to be positive, the air temperature must be greater than 0°C, and the vapor pressure must be greater than that immediately above the snowpack (for a snowpack at 0°C ~ 6 hPa). In a basin-averaged sense, temperatures this high occur only rarely during mid-winter (Fig. 3.14): for December, 85% of the days register temperatures below 0°C; for January 82% of the days are below 0°C; and, for February 76% of the days are below 0°C. As a result, vapor pressures greater than 6 hPa are rare.

Thus, the net heat flux into the snowpack on most days during the mid-winter should be negative. Even on days when temperatures are above freezing and relative humidity is high, the net flux is likely on the order of tens of $W/m^2$, when averaged over the course of the day. Only during instances of extremely warm temperatures (>5°C) is the heat flux likely to exceed 38.7 $W/m^2$, the threshold for melting 1 cm of SWE (see Section 4.1).

Even in cases where sufficient energy is being fluxed to the snowpack, the relatively low thermal conductivity of snow requires that warm conditions persist for longer than 1 day for the bulk of the snowpack to become vulnerable to melting. Additionally, even when melt does occur, much of the melt water can be sequestered by the snowpack and refrozen when colder conditions return. ACE indicates that the liquid water storage for a snowpack is 2-5% of the snowpack's mass. Applying this to the basin-averaged snowpack as depicted in Fig. 3.11, this implies that for a mid-winter snowpack (SWE>=40cm), any melt that is less than 2 cm of SWE is likely to be re-absorbed by the snowpack.

*4.9 Justification for a Degree-Day Approach to Modeling Spring Melt*

While this chapter has focused on the rarity of winter melt, scaling arguments can also be applied to the terms in Eqn. 4.1 to justify the use of a degree-day approach to model daily spring melt. Specifically, for the spring melt:

- $Q_{RS}$ can contribute to melt, but is likely only important in the late summer, as daily insolation is restricted by persistent cloud cover during the spring. QRS would still be correlated to temperature, as many of the warmest days would also have the greatest insolation.
- $Q_{RL}$ and $Q_S$ are directly proportional to air temperature and likely represent the leading terms in the heat flux to the snowpack.
- $Q_L$ can still be considered related to temperature, as discussed in Section 4.4. Latent heat flux contributes to melt when condensation can occur; this is only possible when ambient vapor pressure is considerably higher than 6 hPa, which is more likely to occur at high temperature (and cannot occur at temperatures below 0°C).
- $Q_G$ is small and negligible
- $Q_P$ is large only during intense rainfall occurring at temperatures well above freezing. In this way, $Q_P$ is also related to air temperature.

Thus, the use of daily mean temperature to model melting during the spring is justified by examination of the energy balance of the snowpack.

Ohmura (2001) provides a more detailed analysis to reach a similar conclusion. He claims that the dominant input of energy to the snow or ice is the

downward longwave flux. Furthermore, Ohmura (2001) argues that the secondary and tertiary fluxes (shortwave and sensible heat flux) are also related to air temperature, ensuring that a degree-day approach captures the essential physics of melting.

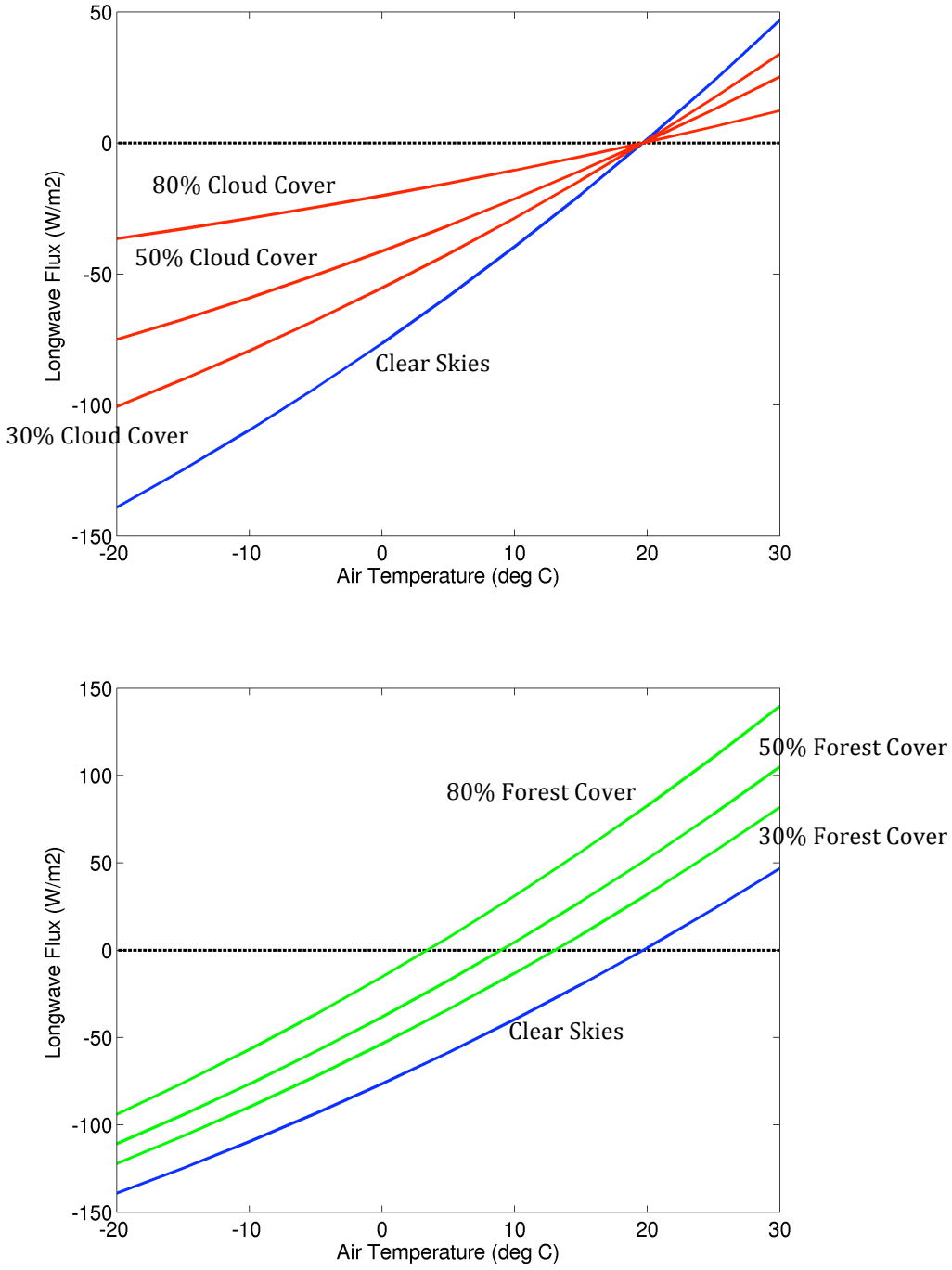


Figure 4.1. Curves depicting the heat flux attributed to longwave radiation versus air temperature. The top panel indicates the flux for an isothermal snowpack at 0°C under clear skies (blue line) and with varying levels of relatively low (cloud base = 1 km) cloud cover (red lines). The bottom panel indicates the flux for the snowpack accounting for various amounts of forest cover (green lines). The blue line is for a vegetation-free area and is identical to the blue line in the top panel.

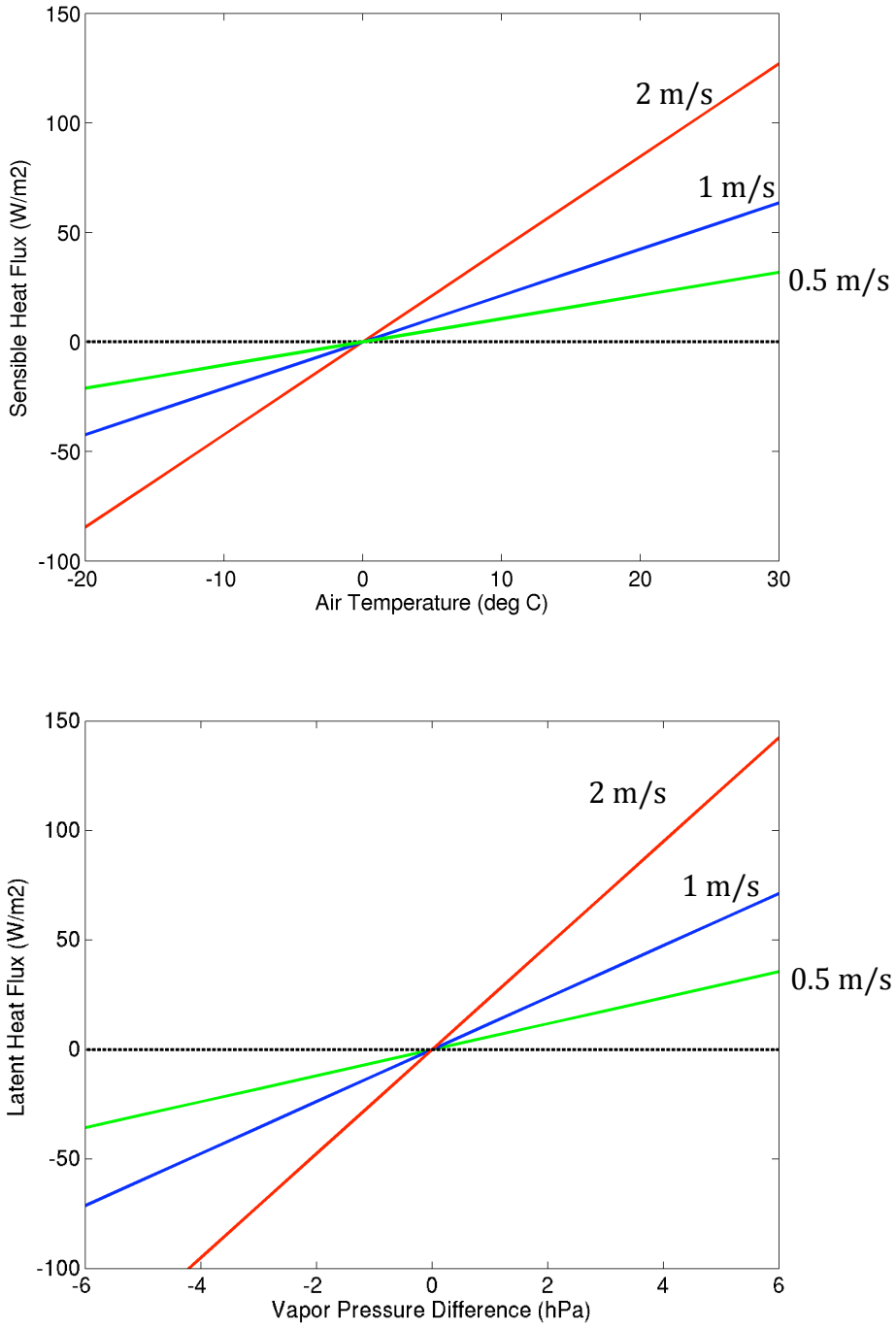


Figure 4.2. Sensible (top) and latent (bottom) heat fluxes for an isothermal snowpack at 0°C. Each colored line represents a different value for the wind speed at the reference level (1m). Green represents a wind of 0.5 m/s; blue represents 1 m/s; red represents 2 m/s.

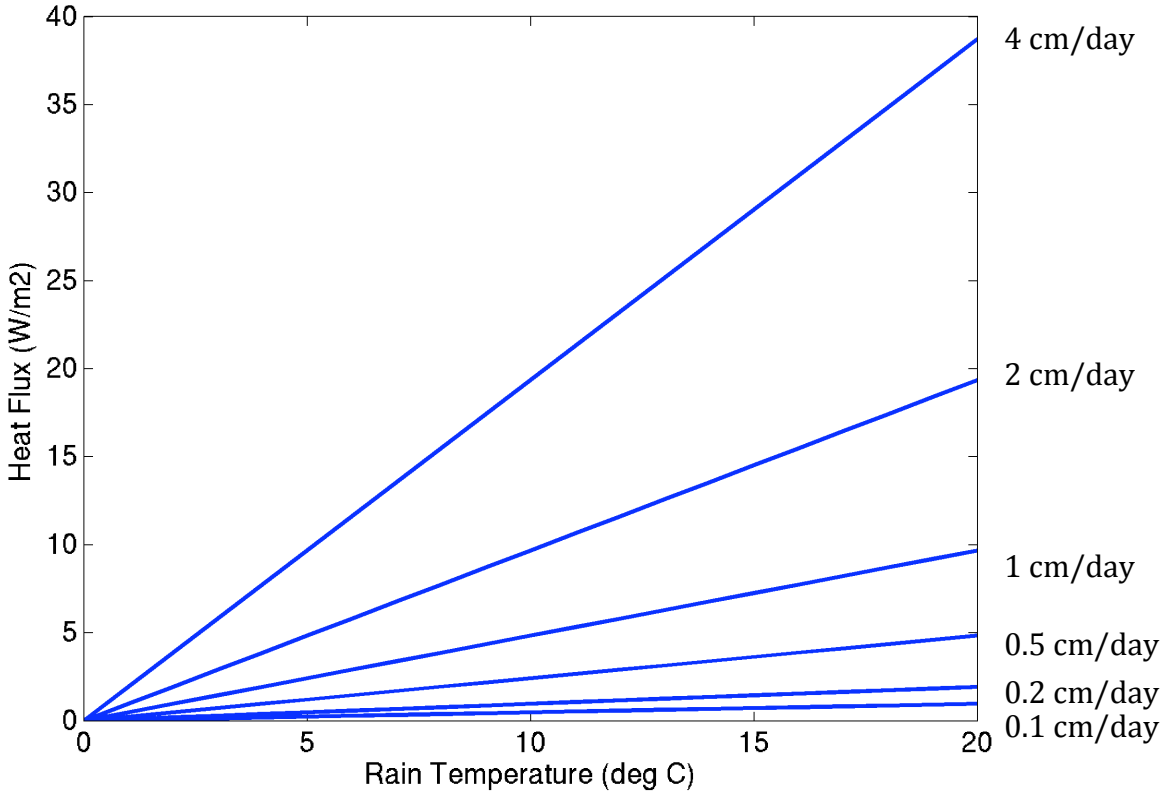


Figure 4.3. Heat flux associated with rain falling on an isothermal snowpack with a temperature of 0°C. Each line represents a different rain rate, ranging from 0.1 cm/day to 4 cm/day.

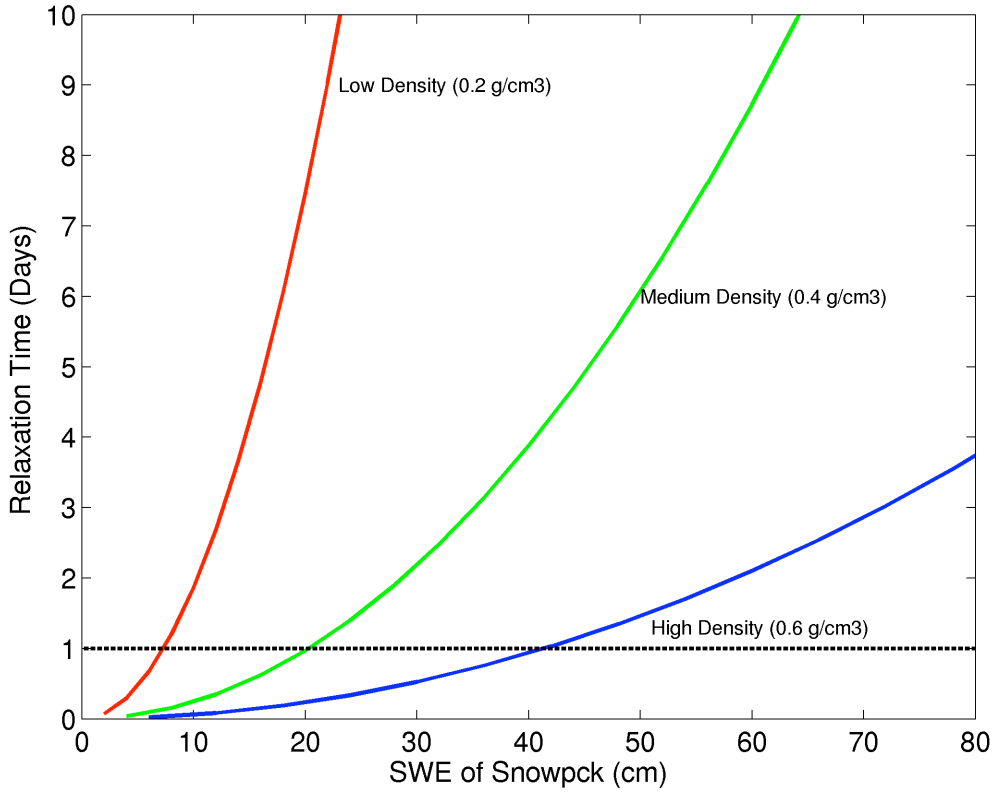


Figure 4.4. Relaxation time (see Eqns. 4.9-4.13) for a hypothetical snowpack as a function of SWE. Three different densities have been considered for the snowpack (0.2 g/cm$^3$ in red; 0.4 g/cm$^3$ in green; 0.6 g/cm$^3$ in blue). A dotted black line marks a relaxation time of 1 day; a snowpack with a relaxation time of less than 1 day would likely melt on the same day if a sufficient heat flux into the snow occurred.

# 5. APPLICATION TO SEATTLE CITY LIGHT PLANNING

## *5.1 Introduction*

In this chapter, the analyses for estimating sensitivity of snowpack to warming (Chapter 2) and characterizing the daily variability of the snowpack (Chapter 3) are applied to the Skagit watershed, a sub-basin within the drainage of the Puget Sound. Seattle City Light (SCL), which provides electricity to the city of Seattle, operates several hydroelectric dams along the Skagit. Both the sensitivity analysis and the information regarding daily variability highlight ways in which SCL operations are vulnerable to climate variability and climate change. These results have implications for long-term planning as well as for season-to-season operations.

## *5.2 Seattle City Light Overview*

Seattle City Light is a public utility that serves approximately 750,000 customers within the Seattle metropolitan area (Fig. 5.1). Hydroelectricity accounts for over 90% of the electricity that SCL provides to its customers (fuel mix for 2007, "Seattle City Light Fingertip Facts" 2008); nuclear accounts for just under 5%; wind just over 3%; coal about 1%; and the remainder (<1%) is a mix of natural gas, biomass, and petroleum. In a typical year, nearly half of this hydroelectricity is generated from SCL-owned dams, while the other half is purchased from the Bonneville Power Administration, the federal agency that markets the power produced by dams along the Columbia River, and from other entities operating dams in the North American West (Figs. 5.2 and 5.3). Of the electricity generated by SCL-owned hydroelectric projects, almost 60% is generated by the Boundary Dam,

located along the Pend Oreille River in northeastern Washington, and nearly 40% by the Ross, Gorge, Diablo, and Newhalem dams which are all located along the Skagit River in northwestern Washington. The remaining ~ 2% is generated by projects on the Cedar and South Fork Tolt Rivers.

*5.3 Focus on the Skagit*

This chapter focuses on SCL's dam operations along the Skagit River. While the Boundary Dam has a greater generating capacity than the dams along the Skagit, the Pend Oreille River has four other dams located along it, each operated by different interests. The Pend Oreille flows through Idaho, Washington, and British Columbia, ultimately feeding into the Columbia River in southern British Columbia. Thus, SCL's ability to unilaterally make decisions regarding the flow of the Pend Oreille is constrained by the operators of upstream dams, as well as by the multitude of water users and dam operators located downstream along the Columbia River Basin. Decisions made for Boundary are subject to multiple state, federal, and international regulations. In contrast, SCL has more latitude in managing its operations along the Skagit. The only other large hydropower project in the Skagit watershed is located on the Baker River (owned by Puget Sound Energy), and since the Baker River is a separate tributary and located downstream of SCL's dams (Fig. 5.3), the operations of the two hydroelectric projects can be considered independently. Additionally, there are fewer water users and diversions of the Skagit than the Columbia River. SCL works closely with downstream groups that have interests in the provision of water and streamflow, such as the Swinomish

Tribe, the City of Anacortes, and the National Marine Fisheries Service. The most important reason for focusing on the Skagit is that the analyses presented in prior chapter apply to the climate of the Washington Cascades. The climate affecting the snowpack and drainage of the Pend Oreille is likely to be more continental in character, and the wintertime variability could be considerably different than that of the Cascades.

*5.4 Estimating the Sensitivity of Snowpack of the Skagit to Warming*

Using the geometric approach (Chapter 2) and the analysis of SNOTEL records within the Skagit (Casola et al. 2009), estimates of the sensitivity to warming can be calculated for the April 1 SWE of the snowpack of the Skagit.

Fig. 5.4 shows the distribution of area with elevation for the Skagit watershed, as shown by the plots for $A(z)$ and the hypsometric curve. Using the same assumptions as were made in Chapter 2 (base of April 1 snowpack located at 600 m elevation; lapse rate = 6.5°C/km; SWE increasing linearly with increasing elevation), the relative loss of water stored by the snowpack accompanying a 1°C warming is estimated to be 19% (Fig. 5.5), assuming no changes in mean winter precipitation that is related to warming.

Compared to the Cascades as a whole, the Skagit has a relatively larger fraction of its area located at high elevation. For the Cascades, the plot of $A(z)$ is fairly constant for elevations ranging from 500 m to 1200 m. The Skagit, on the other hand, exhibits a localized maximum in its $A(z)$ curve above 1000 m, below which the fraction of area actually increases with increasing elevation. Since a

relatively large fraction of the area of the Skagit lies above the present, or the snowline following 1°C warming, the sensitivity for a relatively small amount of warming is less than that for the Cascades. As for the Cascades as a whole, the amount of SWE lost for the first few degrees of warming is nearly a linear multiple of the sensitivity (2°C leads to a 37% loss; 3°C leads to a 53% loss) but the losses taper off with greater warming (4°C leads to a 67% loss; 5°C leads to a 77% loss).

Following the method presented in Casola et al. (2009), the sensitivity can by calculated using the distribution of daily precipitation with respect to temperature. As discussed in Casola et al. (2009) and Chapter 3, the amount of SWE lost during the course of the winter is relatively small. Thus, the accumulated amount of precipitation falling on days when the temperature is at or below 0°C (the inferred accumulated snowfall, as presented in Casola et al. (2009)) serves as a proxy for the accumulated SWE throughout the season. The sensitivity is thus equal to the fraction of the frozen precipitation currently falling at temperatures between –1°C and 0°C.

Figure 5.6 shows histograms for the five SNOTEL stations located in or near the Skagit watershed[1]. Stations at lower elevations exhibit a higher sensitivity, as one would expect (Table 5.1). Considering that the centroid of the snowpack of the Skagit is likely around 1300 m, the sensitivity estimate of 19% of mean April 1 SWE lost of 1°C warming derived from geometrical considerations of the basin is roughly

[1] Technically speaking, Harts Pass is located just outside of the Skagit basin. However, because it is located so close to the crest of the Cascades and the Skagit watershed, it is used by SCL as part of its snow survey.

consistent with the sensitivity estimate (20%; Table 5.1) for the Thunder Basin SNOTEL station (elevation 1316 m).

*5.5 Characterizing the Daily-Scale Variability of Accumulation and Snowmelt*

Using the three SNOTEL stations located in the Skagit watershed that have relatively long periods of record (Thunder Basin, Rainy Pass, and Harts Pass), indices representing the daily accumulation and daily loss of SWE have been calculated for the watershed, using the algorithm described in Section 3.5. Monthly composites of the index values for accumulation and ablation are shown in Fig. 5.7. The corresponding daily mean temperature for the stations is shown in Fig. 5.8.

Figure 5.7 demonstrates that the progression of winter and spring for the Skagit is nearly identical to that of the Cascades as a whole: accumulation dominates from November through March; both accumulation and loss occur during April; loss dominates in May and June, leaving only vestiges of the snowpack, if any, in July. The only noticeable difference is that the distribution of temperature tends to include slightly lower temperatures in the Skagit than for the Cascades as a whole. However, this may reflect the fact that the mean elevation of the three SNOTEL used to calculate the mean temperature for the Skagit is slightly higher than that of the 24 SNOTEL used to calculate the temperature for the Cascades as a whole.

Accumulation tool

The past statistics of snowpack accumulation provide a basis for making mid-winter projections for April 1 SWE. Figure 5.9 shows regressions of the December 1 SWE, January 1 SWE, February 1 SWE, and March 1 SWE upon April 1 SWE for the water years 1990-2006. While the regression relationship between April 1 SWE and December 1 SWE, as well as the relationship between April 1 SWE and January 1 SWE, are quite weak ($r^2$=0.44 and $r^2$=0.57, respectively), the regression relationships for the later months are much stronger ($r^2$=0.90 and $r^2$=0.97, for February 1 SWE and March 1 SWE, respectively). The increase in the strength of correlation through the course of the winter is not surprising, especially given the fact that large accumulation events do not exhibit a preferred time of occurrence within the winter season and that loss is minimal and infrequent (see Chapter 3).

By exploiting the regression relationships for these months, a simple forecast model can be made for predicting April 1 SWE. Uncertainty can be generated for each forecast by examining the distribution of accumulation for past winters – in Fig. 5.10, the ranges that have been added to the predictions represent the 75$^{th}$ and 90$^{th}$ percentiles of the snowiest and least snowy periods associated with each forecast period. While the forecasts made at the beginning of December and January are unlikely to be useful, the relatively narrow range of uncertainty for the February 1 and March 1 forecasts (e.g., for a 90% confidence interval, the range is roughly ± 20% of the long-term mean April 1 SWE for forecasts made in February; for forecasts made in March the range is roughly ± 10% of the long-term mean April 1

SWE) makes them potentially useful for making decisions about the spring snowpack.

It is important to note that the estimates of uncertainty are drawn from the observations for the last 17 water years. While it could be argued that the distribution of April 1 SWE observed during this short period provides a crude estimate of forecast uncertainty, it is important to point out that the last 17 years includes some of the snowiest (e.g. water years 1998, 2000) and least snowy periods (e.g., water year 2005) observed during the last 50 years. Thus, the *range* of estimates observed over the last 17 years provides a representative estimate of the range of historical variability, even if the distribution of values of April 1 SWE over this period might not represent the distribution observed over a longer period of observations or that derived from a hydrological model.

Loss tool

Since the results for the Skagit are similar to that of the Cascades as a whole, the relationship between daily melt rate and daily mean temperature can be exploited to generate a degree-day model for the loss of SWE during the spring. Figure 5.11 shows the plot of daily mean temperature versus daily SWE loss for the Skagit SNOTEL for the months April through June. The regression of the daily loss upon the daily memory-weighted temperature (see Section 3.9) has a slope of –0.2268 cm SWE/°C and a *y*-intercept of 0.7773 cm SWE.

In order to make the degree-day model more suitable for operational purposes, values for the accumulation during April can be added to the model.

During April, a daily accumulation rate ($AA/30$ in Eqn. 5.1) can be prescribed. This daily rate is equal to historical observations of monthly accumulation during April ($AA$), divided by 30 days. Loss during the subsequent months of the melt season are calculated as shown in the degree-day model as presented in Section 3.9, without any terms representing accumulation (Eqn. 5.2). The SWE remaining on the ground on the $i$th day following April 1 ($SWE_i$) is calculated using Eqn. 5.3, using a prescribed value for the April 1 SWE.

For $i$<=30

$$\Delta SWE_i = -0.2268 \text{ cm SWE/°C} * (T_{E\text{-}FOLD})_i - 0.7773 \text{ cm SWE} + AA/30 \quad (5.1)$$

For $i$>30

$$\Delta SWE_i = -0.2268 \text{ cm SWE/°C} * (T_{E\text{-}FOLD})_i - 0.7773 \text{ cm SWE} \quad (5.2)$$

$$SWE_i = \textit{April 1 SWE} + \Sigma\, \Delta SWE_n \text{ (for } n\text{=1 to } i\text{)} \quad (5.3)$$

Figure 5.12 shows how such a model provides a range of projections for rate of loss of SWE during the spring. The following assumptions were made to generate the curves in Fig. 5.12: April 1 SWE was set to the climatological mean value (92 cm); three sets of daily temperature were used (the climatological daily mean, 2°C warmer than the climatological daily mean, and 2°C colder than the climatological daily mean); and, a middle-of-the-road ($AA$ = 9 cm) and a high-accumulation scenario ($AA$ = 15 cm) for April accumulation are included in the model. These values for $AA$ correspond to the median of the monthly April accumulation, and the second highest value of monthly April accumulation (~95$^{th}$ percentile).

The projections of the Skagit show that the melt-out date would fall in mid-June for a year exhibiting spring temperature near that of the climatological mean; a

warm (cold) spring would exhibit an early June (early July) melt-out date. The sensitivities of the melt-out date to the mean temperature (7-8 days per °C) and amount of SWE on April 1 (5 days for ±10% of April 1 SWE) are similar to those for the Cascades as a whole. Accumulation in April can significantly alter the forecast trajectory during April and May, but the projected melt out date is similar to that for a snowpack where all the snow was present on April 1.

*5.6 Applications for Management*

The results presented in the previous sections can be applied to SCL's decision-making and planning for **the coming decades** as well as for **a single water year**.

Long-term Management

Specifically, the key results for **the coming decades** are as follows:

- **In the absence of changes in climatological-mean precipitation, April 1 SWE will likely decline by roughly 20% for each degree Celsius of warming.** Considering a conservative rate of warming of 0.3°C per decade (Salathé et al. 2007), a 20% loss of April 1 SWE is likely to occur over the next 30-40 years, relative to the mean April 1 SWE observed during the period of the 1970's through early 2000's.
- **Less snowpack and warmer temperatures are likely to accelerate the rate of melt during the springtime.** The loss of 20% of mean April 1 SWE would translate to an advance of 9 days for the Skagit melt-out date; a

springtime with temperatures 1°C warmer than those observed over the last two decades would add another 7-8 days to this advance.

Given that the Skagit is a snowmelt-dominated river, the decrease in winter accumulation and enhancement of spring melting will combine to alter the historical timing and magnitude of the springtime streamflow: peak flows are likely to decline; peak flows are likely to occur earlier in the water year; and, late summer flows are likely to decline. This prognosis for the streamflow of the Skagit corroborates projected changes to streamflow in other snowmelt-dominated rivers in Washington (McGuire-Elsner et al. 2009).

For SCL, the projected changes in snowpack and streamflow undermine the effectiveness of current operating protocols if they are extended too far into the future decades. Historical management is designed to capture peak flows that occur in the summer and store a portion of this water for the following winter. Figure 5.13 shows a comparison of mean monthly streamflow on the Skagit with monthly mean streamflow on the nearby Sauk, which lacks man-made diversions and represents "naturalized" streamflow. The difference between the two hydrographs indicates the role of the dams and reservoirs in storing summer flows and releasing water during the winter, the time of peak electricity demand, which typically occurs in January. Thus, if current reservoir refill practices are unchanged, warming and the loss of snowpack are likely to reduce the amount of water that can be carried over from summer to the following winter. Moreover, as late summer flows decrease, it may become more difficult to meet in-stream flow requirements for

salmon on the Skagit and to maintain water levels in Ross Lake for recreational purposes.

SCL's current plans for the coming decades are expressed in the recently reinstituted biennial issuance of an Integrated Resource Plan (IRP)[2]. The IRP provides a 20-year projection of future electricity demand and generation, as well as the anticipated future policy constraints (e.g. changes to existing power exchange contracts, implementation of existing or new environmental laws). The most recent IRP was issued in 2008 and identifies the following issues facing SCL:

- Forecasts of winter load exhibit a steady increase between now and 2027.
- In order to meet a 95% reliability standard (i.e., for SCL to meet the load demands during the month of peak demand, January, with a 95% probability), more energy resources[3] must be added to the system now.
- The passage of Ballot Initiative 937 (I-937) in 2006 requires SCL to supply 15% of its electricity from new renewable sources of energy by 2020.
- The IRP does consider the effect of climate change on the Skagit – modeling results show that climate change will likely increase winter streamflow, move the timing of peak streamflow earlier in the water year, and reduce late summer streamflow.

---

[2] IRP reports were issued in 2006 and 2008 after an 8-year hiatus. The hiatus was due to deregulation (http://www.seattle.gov/light/AboutUs/AnnualReport/2005/). The new reporting schedule also satisfies planning and assessment timetables required by the passage of Ballot Initiative 937 in 2006.

[3] SCL defines both additional generation sources and conservation to be an "energy resource." Thus, implementing conservation practices among customers is considered the "addition" of an energy resource.

To cope with these issues, the latest IRP report recommends enhancing conservation efforts, acquiring a diverse portfolio of power generation from wind, geothermal, biomass, and landfill gas sources, and securing power exchange contracts with Bonneville Power Administration (BPA) and other regional utilities. Although the IRP clearly considers the impact of global warming on SCL's operations, and the proposals to increase conservation and diversify SCL's fuel mix are worthwhile, there are several ways in which SCL's plans for the coming decades could go farther. Specifically, the IRP should:

- **Consider alterations to dam and reservoir operations.** While the addition of energy resources will relieve some demand on the hydroelectricity generated on the Skagit, further consideration should be given to altering dam and reservoir operations. Detailing changes to the future hydrograph of the Skagit seems incomplete without a discussion of options for coping with these changes. Possibilities include beginning reservoir refill earlier in the summer or relying more heavily on storage of fall flows. While these possible alterations in operations are clearly subject to other considerations (maintenance of in-stream flows and Ross Lake levels, seasonal price of power, transfer agreements with other utilities, rate of regional population and demand growth), exploration of potential options would appear prudent, given the relatively large changes projected for the hydrograph of the Skagit due to warming (IRP, Fig. 5.14, bottom panel).
- **Consider incentives for infrastructure investments.** As detailed by Cheng (2009), considerations of climate change have been valuable in enhancing

the incentive for construction of a new tunnel intended to increase potential hydroelectric generation at Gorge Dam. When changes in the timing and magnitude of flow over the coming decades are included in a cost-benefit analysis of the project, the incentive for investing in the tunnel is enhanced. The IRP should consider additional ways that investment in the hydroelectric infrastructure could help boost generation or prevent expected losses in the future (e.g., through sedimentation in reservoirs or replacing aging transmission lines)

- **Incorporate variability and "worst cases" into future projections.** The treatment of climate change in the IRP is overly deterministic. Whereas the discussion and importance of the 95% reliability standard clearly recognizes the role that historical interannual variability has played in affecting generation (Fig. 5.14, top panel), the future is treated only in terms of a shift in mean generation (Fig. 5.14, bottom panel). The envelope of uncertainty embodied in the information of historical variability can be added to the sensitivity information to provide probabilistic projections for spring snowpack, monthly streamflow, and monthly generation. From this range of forecasts, some of the "worst cases" (years with low snowpack, low flows, and low generation) can be selected and used as benchmarks for ensuring system integrity.
- **Extend the timeframe for planning.** The IRP planning range of 20 years is too short. The impacts of warming are likely to become most serious and noticeable in the decades following (2030-2050). Coping with those impacts

will likely require action during the next decade (2010-2020), especially in the case of adding or developing infrastructure.

Management During the Water Year

In order to meet the power demands of its customers, to avoid flood events, and to fulfill targets for in-stream flow monitors, SCL continuously monitors and adjusts its dams operations and reservoir levels within a particular water year. During the winter, weather forecasts can provide up to a week of lead-time in support of management decisions relating to these goals, largely in anticipating the timing and magnitude of major precipitation events. In contrast, forecasts for the spring and summer are based on snowpack information, largely from the snow survey measurements available on April 1. The snowpack information is then used to forecast summer inflows to Ross Lake and Diablo Lake.

The forecast tools presented in this chapter could improve the use of snowpack information. Specifically, two forecasts can be made, one for late winter accumulation and one for the rate of spring and early summer ablation:

- **Forecasts of April 1 SWE can be made using observations as early as February 1.** Forecasts of April 1 SWE made on February 1 are likely to be accurate within a range of approximately ± 20%; forecasts made on March 1 are likely to be accurate within a range of approximately ± 10%.
- **Forecasts of the rate of melt of spring SWE can be made on April 1.** These forecasts provide a trajectory for the SWE for the spring and early summer. Using scenarios regarding mean spring temperature, a range of

trajectories can be generated. If seasonal forecasts of the temperature are available, then one or several of the scenarios could be weighted more heavily than the others in anticipating the rate of melt.

These new tools can add value to SCL's usage of snowpack information in four ways:

- **Both forecasts add lead-time to decision-making.** The current forecasting algorithm begins in April, once snowpack is close to its annual maximum. Using the accumulation tool, a prediction for April 1 SWE can be made on February 1, providing 2 months of additional lead-time. This could be useful for managing late winter dam and reservoir operations or for decisions regarding power purchases and sales for the late winter months. In particular, the forecast would very likely call attention to an impending extreme accumulation season, whether it be extremely high SWE or extremely low SWE. Similarly, the loss tool provides information on April 1 for the late spring and summer, which could be used to make decisions regarding operations and marketing during that period.
- **Spring and summer forecasts are "dynamic" since they are driven by temperature**. The current forecasts of summer inflows to Diablo Lake and Ross Lake are based on the historical climate (e.g., the inflow predicted to occur during a particular period is determined by the amount of SWE present at a given date). The SWE melt trajectories could allow for a companion streamflow or inflow trajectory forecast, where the streamflow or inflow is simulated for each day of the spring and summer as a function of snowmelt.

This procedure is likely to prove more accurate than the current forecasting algorithm, which is based solely on an empirical relationship between SWE and subsequent summer inflow, especially for years exhibiting temperatures that are significantly warmer or colder than the historical mean temperature.

- **Inclusion of uncertainty allows for "cases" or "scenarios" to be developed.** Using different assumptions about accumulation, a user could create cases or scenarios for the upcoming April 1 SWE. For example, the snowiest or least snowy February-March periods on record could be used as a basis for anticipating the range of possible values of April 1 snowpack, rather than focusing exclusively on the prediction of the most likely value. Likewise, using different assumptions about seasonal temperature (the range of 2°C colder and warmer than the long-term climatology has been used in this work for illustrative purposes), a user could generate cases or scenarios for the melt rate. If probabilistic forecasts for the seasonal temperature were available, such as those from the National Center for Environmental Prediction, then the user could incorporate those temperature forecasts as a means of case-building or scenario-building.
- **The simple forecast algorithms are straightforward and relatively low-cost.** While numerical hydrological models are considered to be the state-of-the-art tools for linking information regarding snowpack, climate, and streamflow, their use by SCL typically involves significant cost. The simple tools presented here can be "run" in the span of minutes at virtually no cost (beyond that of aggregating the snowpack data, which is already done by

SCL), allowing them to be updated and re-applied throughout the winter and spring. Furthermore, the complexity of numerical hydrological models may offer a barrier to their application to relatively simple or qualitative questions. The simple models presented here might serve as a first step for SCL planning – if there is some evidence of a particularly worrisome outcome indicated by these simple models, the hydrological models can be applied to the problem to yield more precise, quantitative information.

*5.7 Culture of Seattle City Light*

SCL's interest in climate variability and climate change make it likely that the proposals outlined above could be adopted and implemented with minimal opposition. Throughout its website (http://www.ci.seattle.wa.us/light/) and in a variety of strategic documents (e.g., IRP, 2007 Annual Report subtitled "A Climate of Change") SCL explicitly states its desire deal with climate change, both in reducing its emissions and in being aware of impacts to its hydrolelectric system. SCL has been a key participant in regional climate discussions, ranging from having representatives attend regular research meetings at the University of Washington to coordinating the beginnings of a Skagit River Climate Consortium, a research collaboration of tribal, federal, state, local, and academic researchers and managers that work along the Skagit. The Consortium also demonstrates the relatively positive relationships and functional communication channels that SCL maintains with many organizations that monitor or have jurisdiction over the Skagit, such as the Swinomish Tribe, the National Park Service, the Environmental Protection

Agency, and the US Geological Survey. The organization clearly places value on the latest research related to regional climate variability and change, and is serious about forging partnerships among Skagit stakeholders.

*5.8 Summary*

The snowpack of the Skagit watershed is an important resource for SCL. Understanding the impact of global warming on the snowpack of the Skagit is integral to SCL's long-term planning. Additionally, knowledge of the variability of snowpack within a season can improve the efficiency to SCL's operations within a water year. In particular, the key results of this chapter are as follows:

- **Global warming will likely alter the hydrological cycle of the Skagit, which has serious implications for SCL's planning and operations in the coming decades.** Like the Cascades as a whole, nearly 20% of the April 1 SWE will be lost per 1°C of warming as the proportion of precipitation falling as snow declines. In addition, the spring snowpack is expected to melt more rapidly, advancing the date of the final melt-out and reducing inflow to the SCL reservoirs and streamflow during the late summer. SCL should consider updating its operational protocols and investing in infrastructure improvements to cope with these changes. In addition, these changes in the hydrological cycle emphasize the incorporation of variability as a component of planning (e.g., considering a "worst-case" scenario for snowpack or summer inflow rather than exclusively a shift in the mean). Since these

hydrological changes are likely to play out gradually over the century, it is necessary to extend SCL's planning window beyond the next 20 years.

- SCL can use information regarding the daily variability of the snowpack to **improve its forecasting algorithms used within a single water year**, thereby extending the lead-time afforded to decision-makers. Due to the lack of significant loss of snowpack during the mid-winter, data for past winters can be used to forecast April 1 SWE as early as February 1. In addition, the sensitivity of the spring snowpack to temperature can be exploited to make a dynamic forecast of the rate of spring and early summer ablation, rather than making forecasts strictly based on the historical observations. Updating the spring and summer forecasts to include information about the temperature would enable the development of physically-based scenarios for inflow or streamflow. Both of the proposed forecast tools offer efficient and low-cost methods of incorporating climate information into seasonal planning and operations.

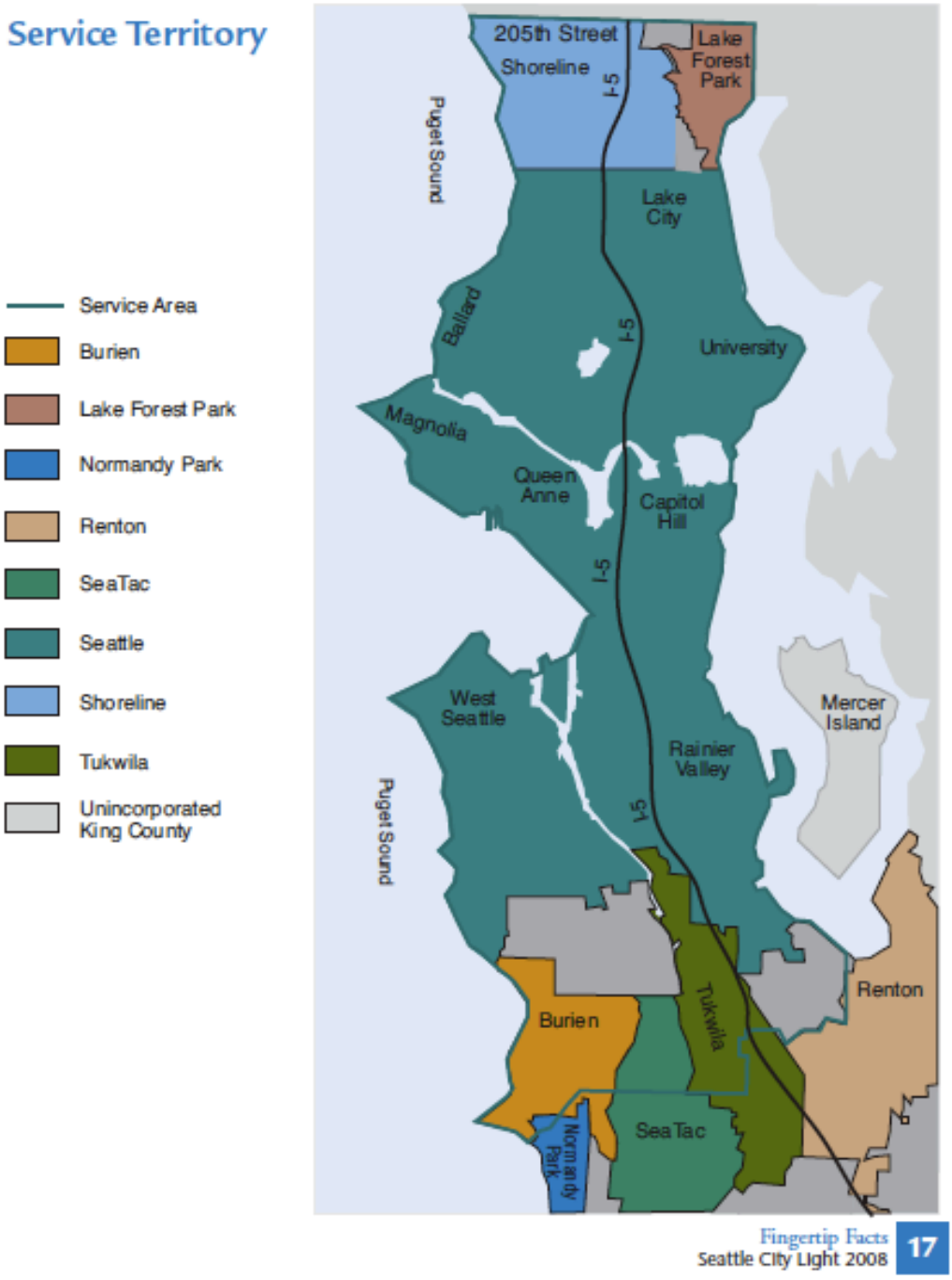


Figure 5.1. Seattle City Light service area map. From "Seattle City Light Fingertip Facts " (2008).

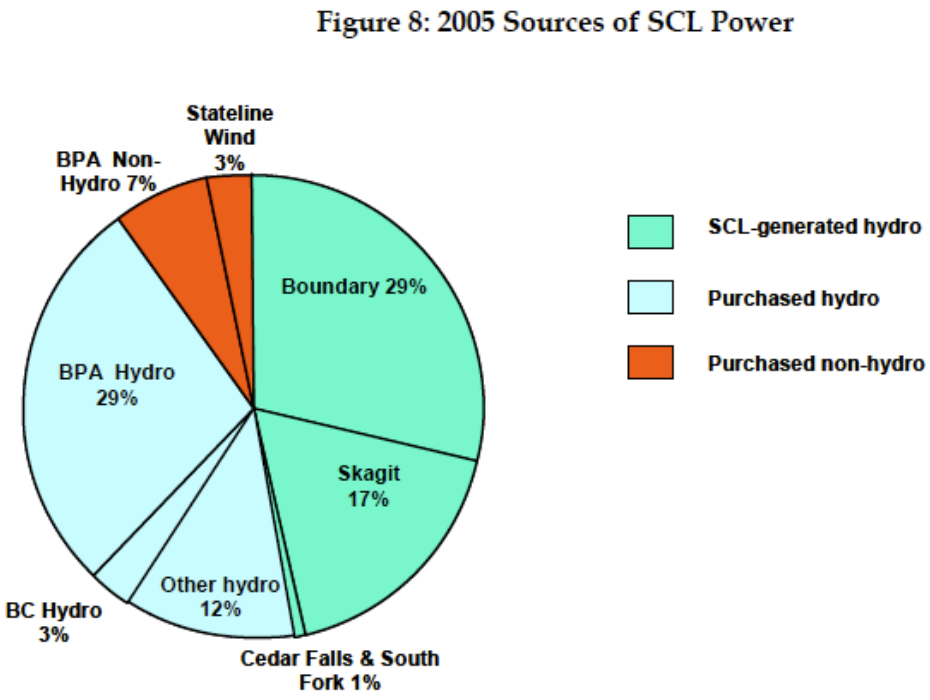


Figure 5.2. Seattle City Light's sources of power for 2005. Figure 8 from "Seattle City Light – Proposed 2008 Strategic Plan" (2008).


Figure 5.3. Locations of Seattle City Light energy resources. Top: Regional Map, from SCL, Intgrated Resource Plan (2008). Bottom: Skagit Watershed Map, from USGS. Blue triangles represent dams: "12175000" corresponds Ross Dam; "12176500" corresponds to Diablo Dam; "12177700" corresponds to Gorge Dam. The two other downstream dams are controlled by Puget Sound Energy as part of its Baker River Hydroelectric Project.

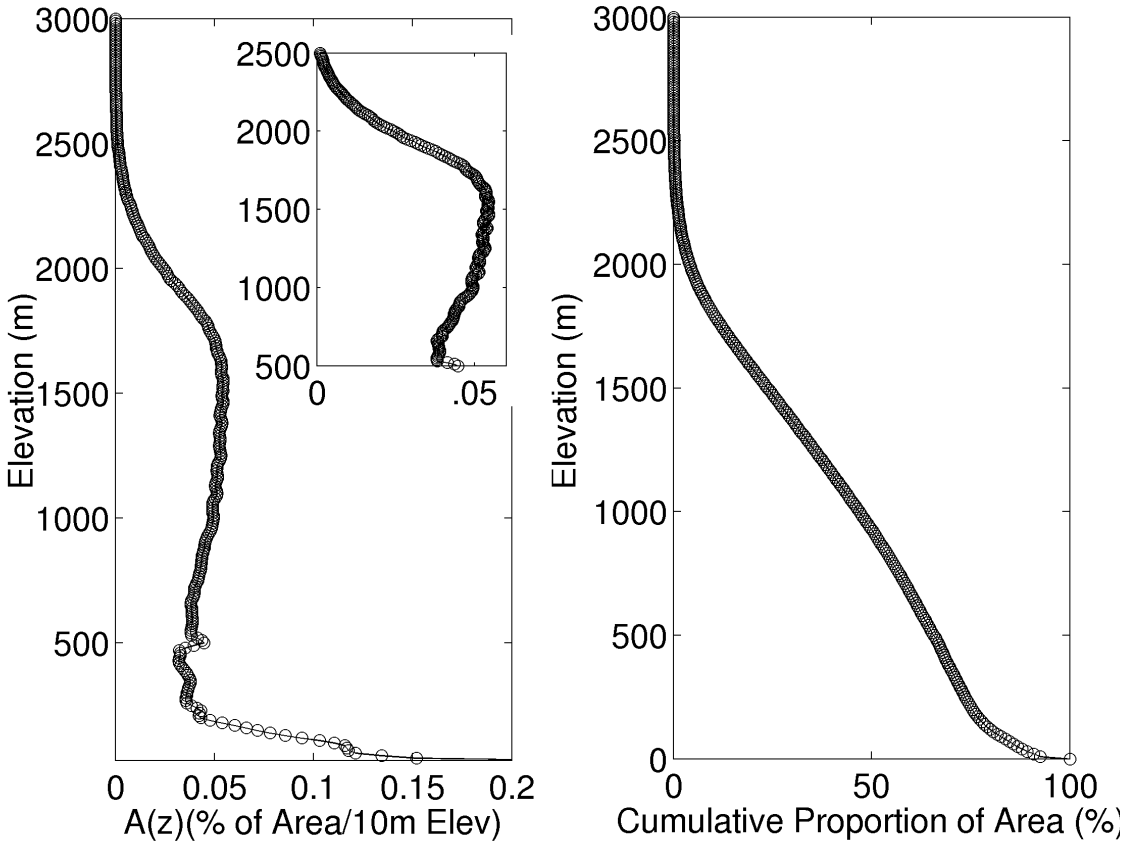


Figure 5.4. Distribution of area with elevation for the Skagit watershed. Left – the curve for *A(z)*; Right – the hypsometric curve.

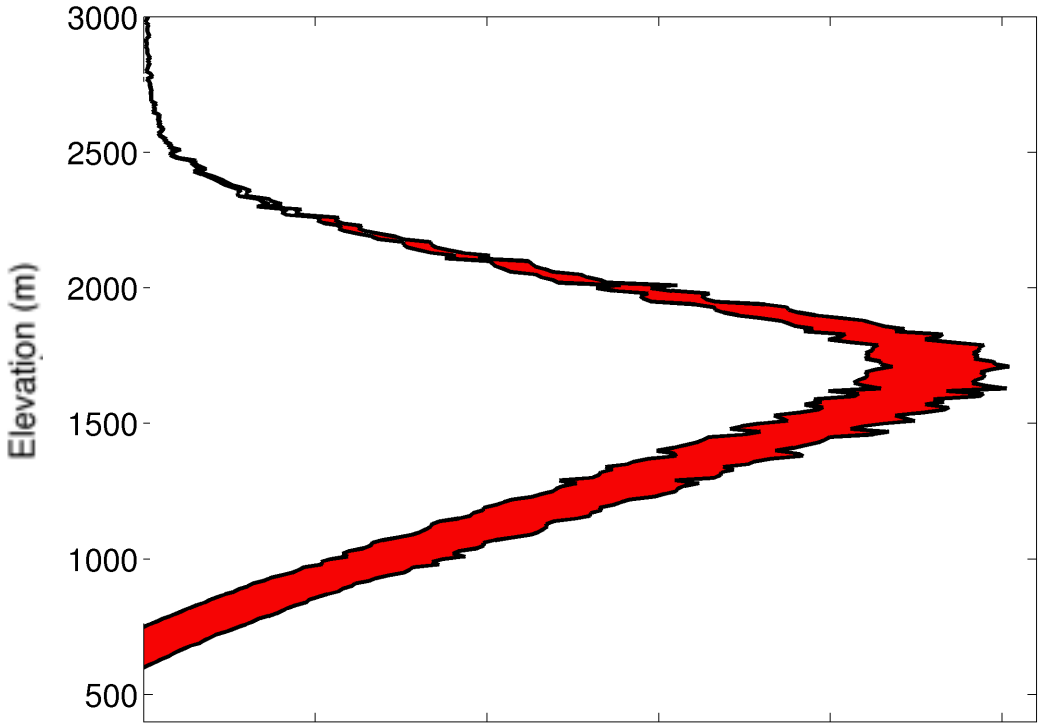


Figure 5.5. Results of the geometric approach for estimating SWE lost in the Skagit watershed for 1°C warming. Outer curve represents the volume of snow-water (snow-water storage or SWS) per 10 m of elevation for the base climate; inner curve represents the SWS per 10m of elevation for a 1°C climate. The estimates for SWS are dimensionless; the area in red represents the *relative* loss of snow-water due to warming.

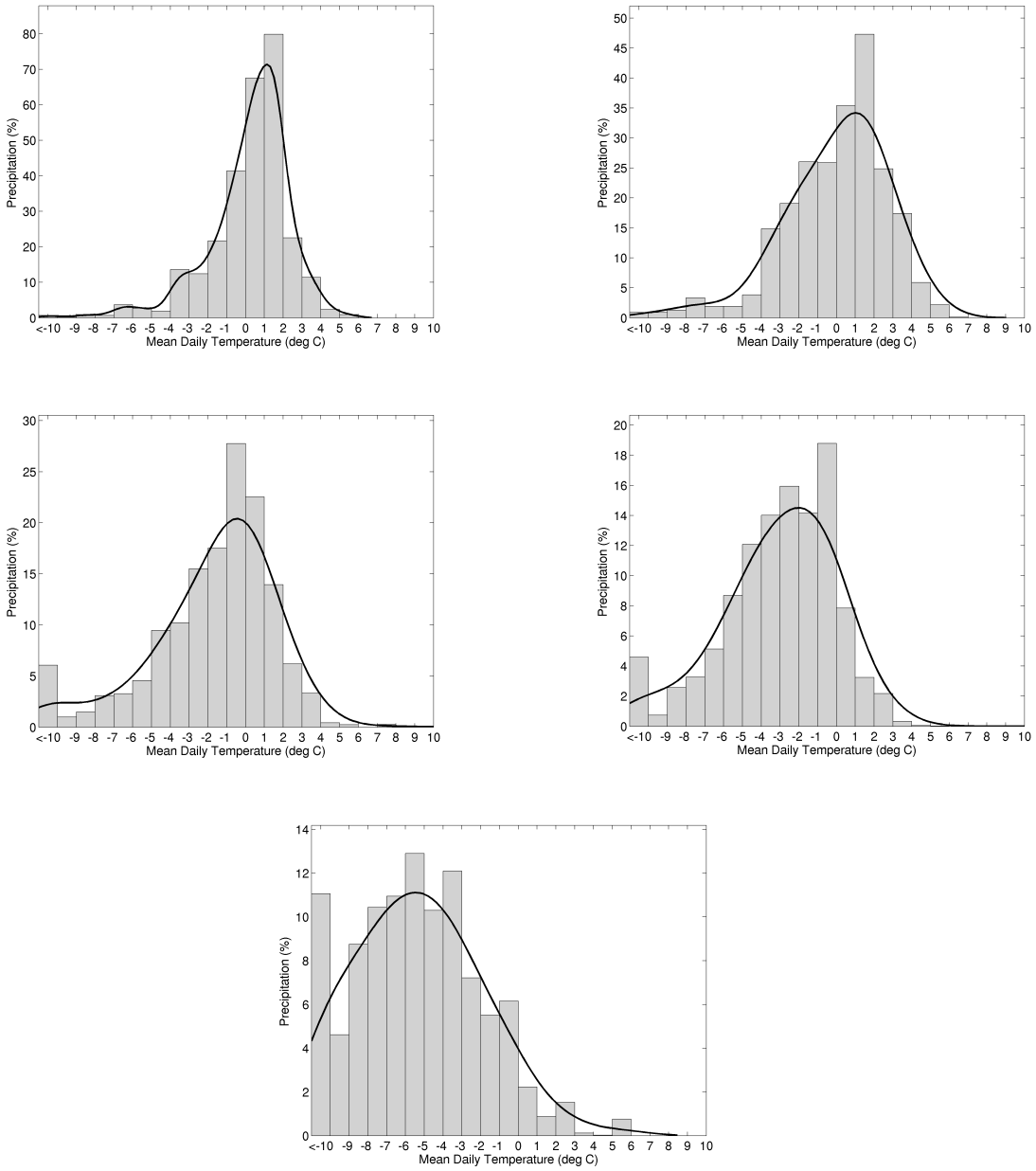


Figure 5.6. Histograms of amount of winter precipitation (November-March) falling versus temperature for various SNOTEL stations in the Skagit watershed (Beaver Pass (upper left, elevation 1103 m), Swamp Creek (upper right, elevation 1219 m), Thunder Basin (middle left, elevation 1280 m), Rainy Pass (middle right, elevation 1457 m), Harts Pass (bottom, elevation 1981 m); see Table 5.1 for station identifiers). The smooth Gaussian curve was fit to the histogram using the histogram data, as performed in Casola et al. (2009).

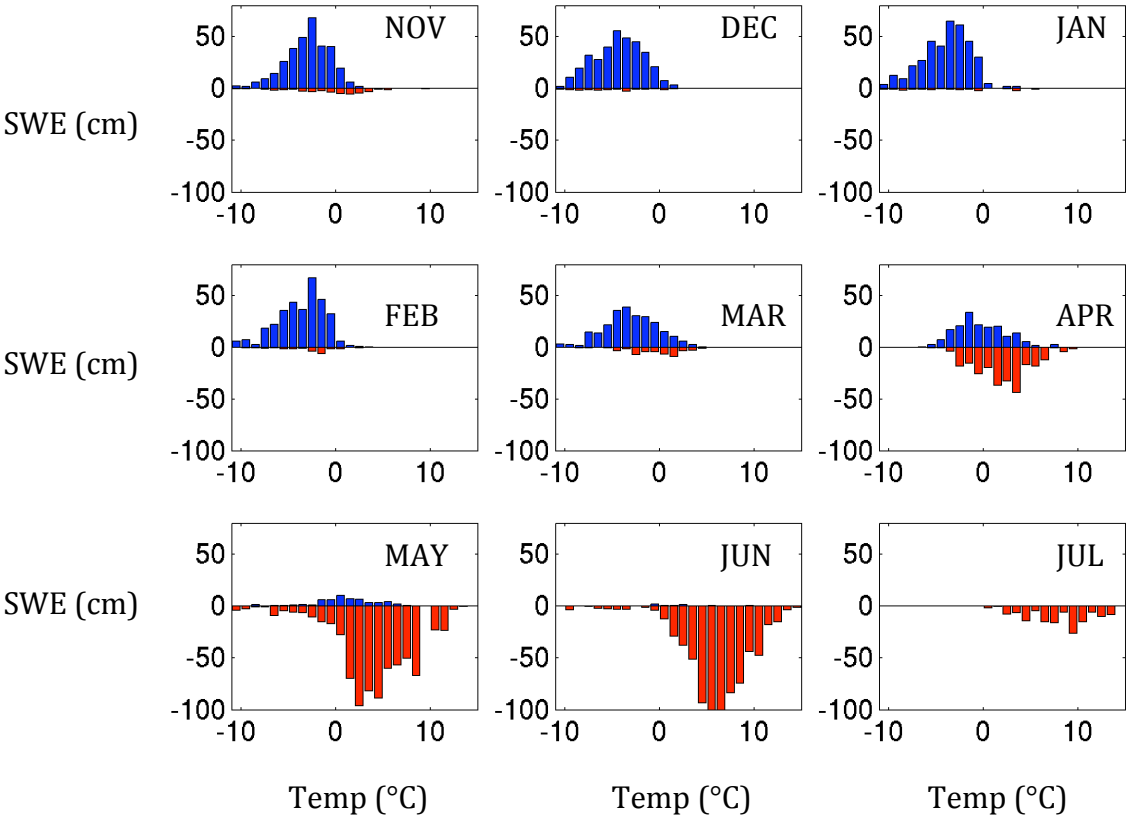


Figure 5.7. Sums of the Skagit indices representing daily accumulation (blue) and loss (red). The sums have been binned by daily mean temperature and composited by month. The Skagit SNOTEL stations used to form the indices are Thunder Basin, Rainy Pass, and Harts Pass (see Table 5.1); the data include the water years 1990-2006.

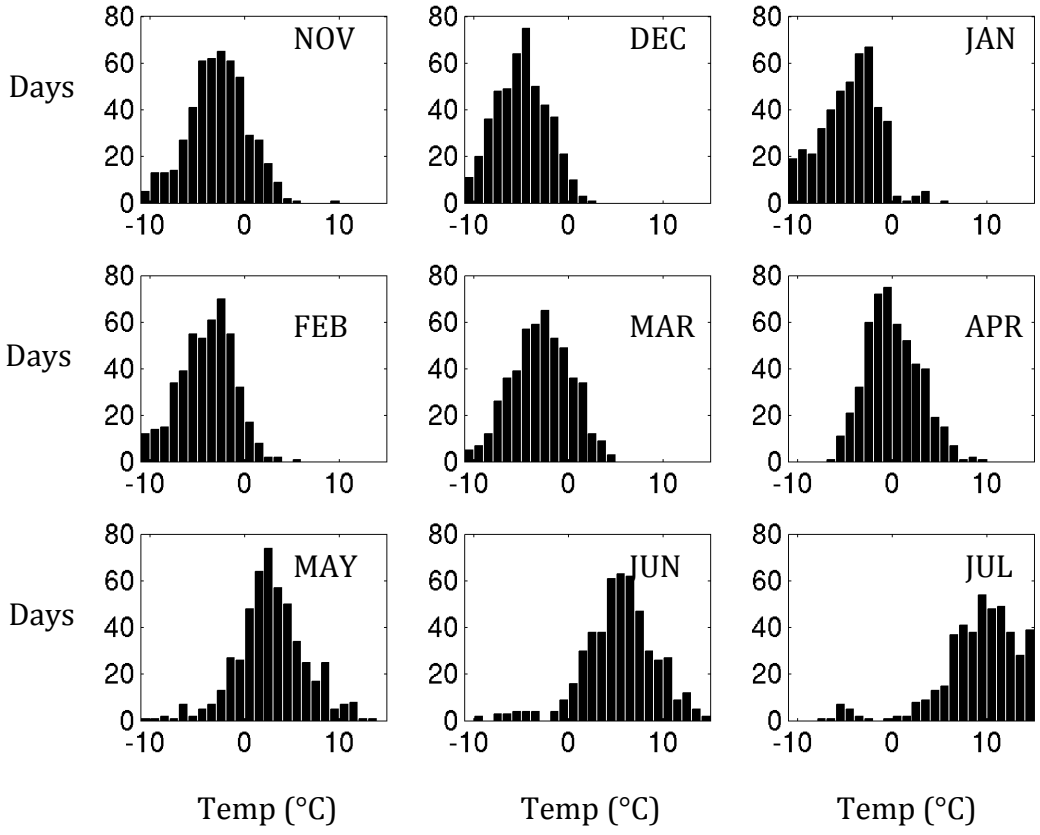


Figure 5.8. Histograms of daily mean temperature composited by month as observed at Skagit SNOTEL for the water years 1990-2006.

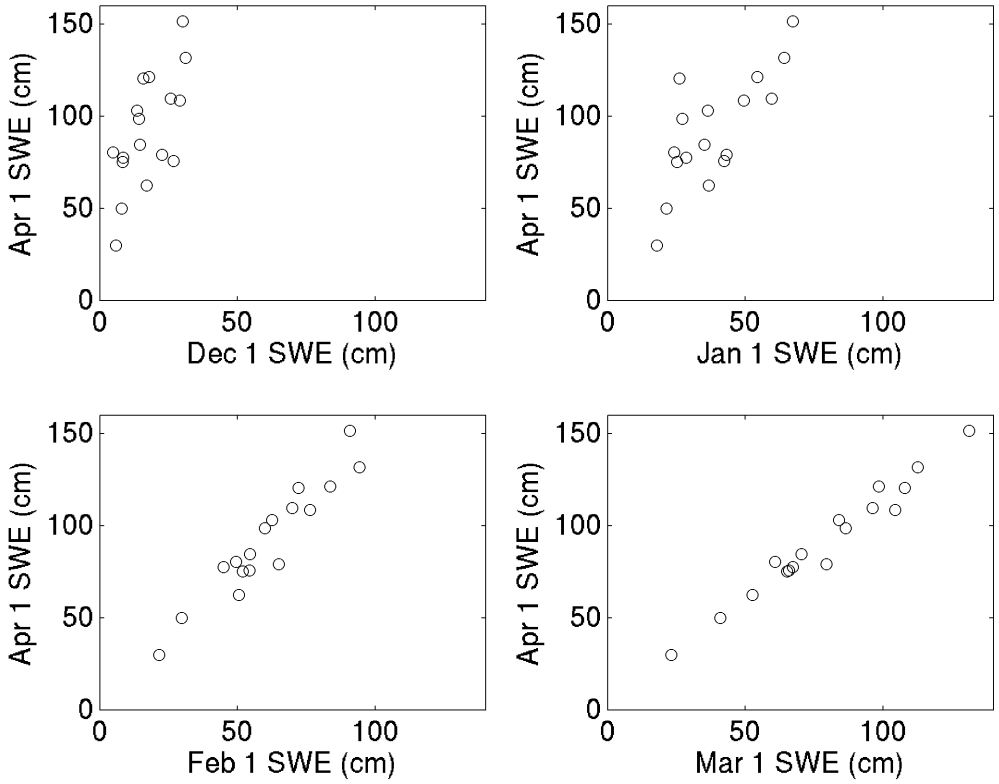


Figure 5.9. Regression of December 1 SWE versus April 1 SWE (upper left); January 1 SWE versus April 1 SWE (upper right); February 1 SWE versus April 1 SWE; and, March 1 SWE versus April 1 SWE for the Skagit SNOTEL, water years 1990-2006.

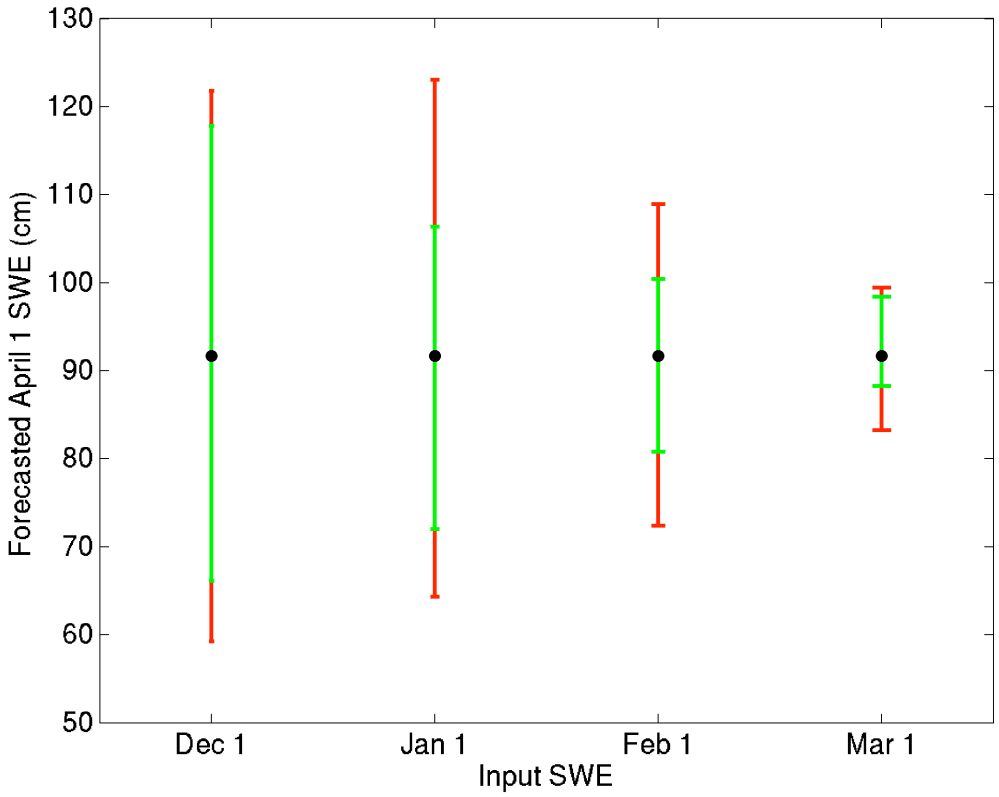


Figure 5.10. Forecast model for April 1 SWE. Dots indicate the prediction for April 1 SWE made using mean values for December 1 SWE, January 1 SWE, February 1 SWE, and March 1 SWE and the regression equations shown in Table 5.2. Green error bars represent 75% confidence limits; red error bars represent 90% confidence limits. Both sets of error bars were generated from historical observations of accumulation following the forecast date.

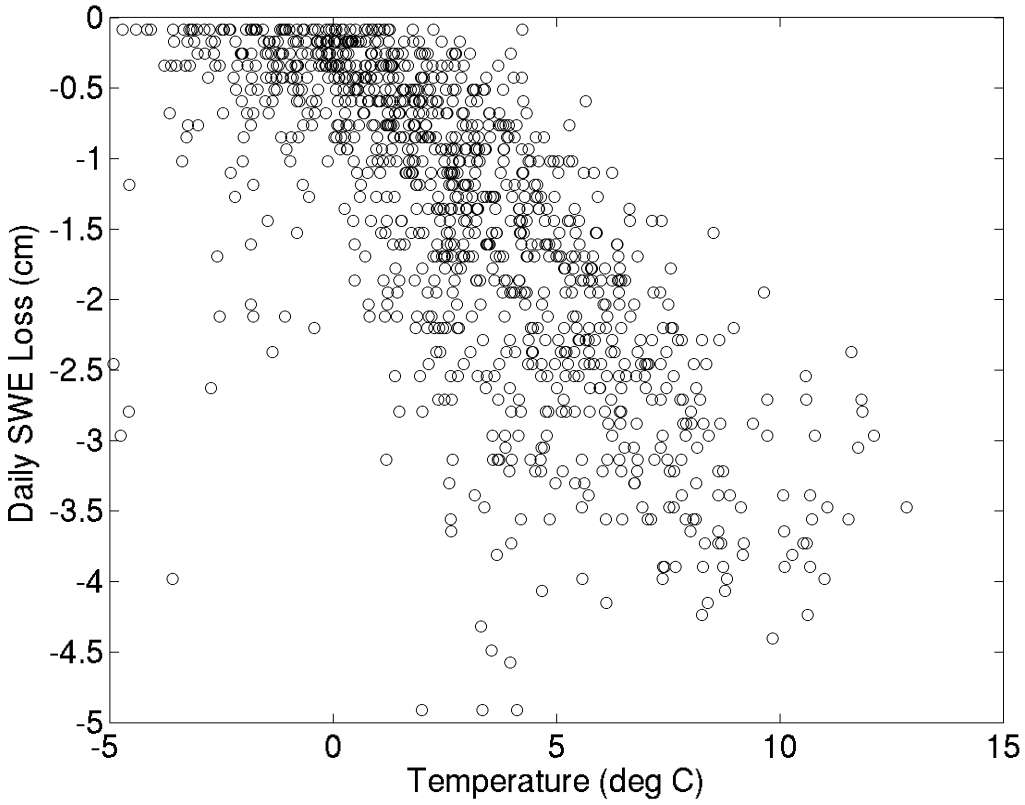


Figure 5.11. Daily SWE loss versus daily mean temperature for the Skagit SNOTEL, April-June, water years 1990-2006.

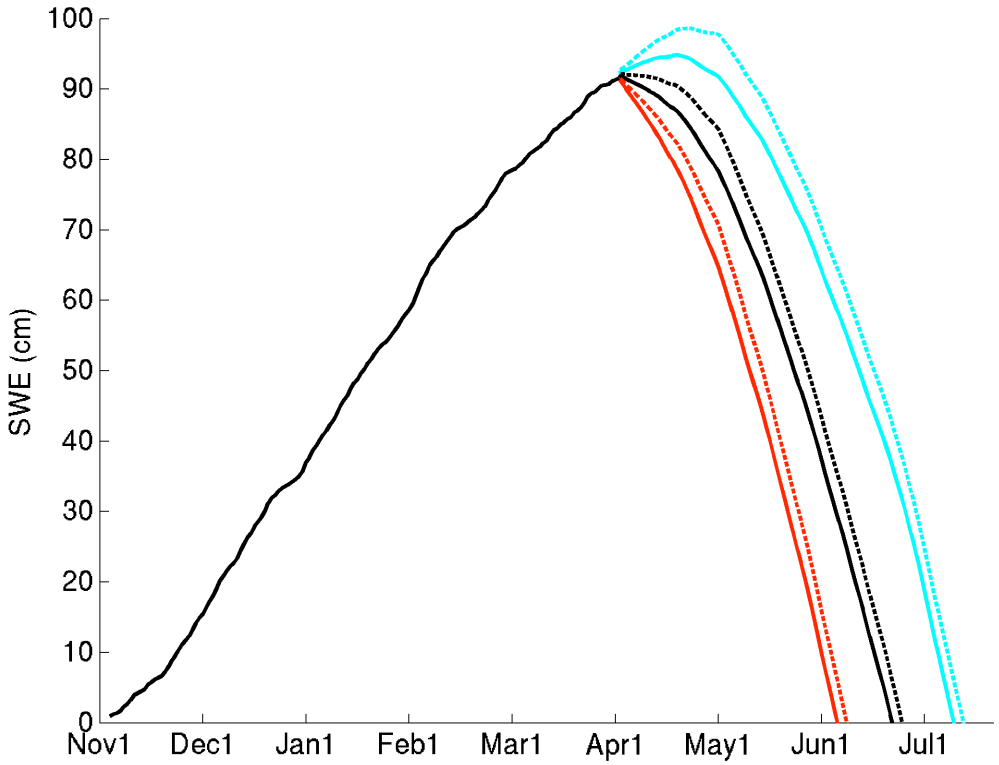


Figure 5.12. Degree-day melt model for the snowpack of the Skagit watershed. Prior to April 1, the thick black line represents the daily mean accumulation for the water years 1990-2006. The solid lines following April 1 represent SWE trajectories for an April experiencing 9 cm of SWE accumulation (a middle-of-the-road scenario). The colors represent different temperatures: black is the climatological mean spring temperature; cyan is 2°C colder than the mean; red is 2°C warmer than the mean. The dotted lines represent high accumulation scenarios (15 cm of SWE accumulating during April).

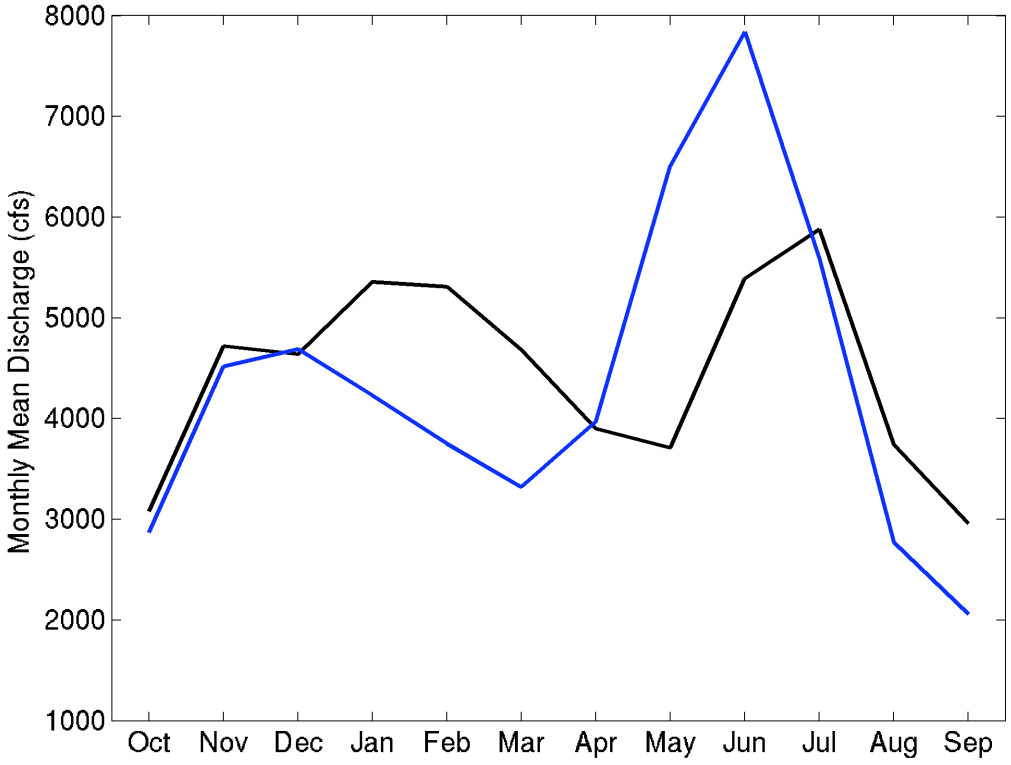


Figure 5.13. Monthly mean streamflow of the Sauk (blue) and Skagit (black) Rivers. The depression of summer flow and increase in winter flow on the Skagit, relative to the Sauk, demonstrate the role of the dams and reservoirs.

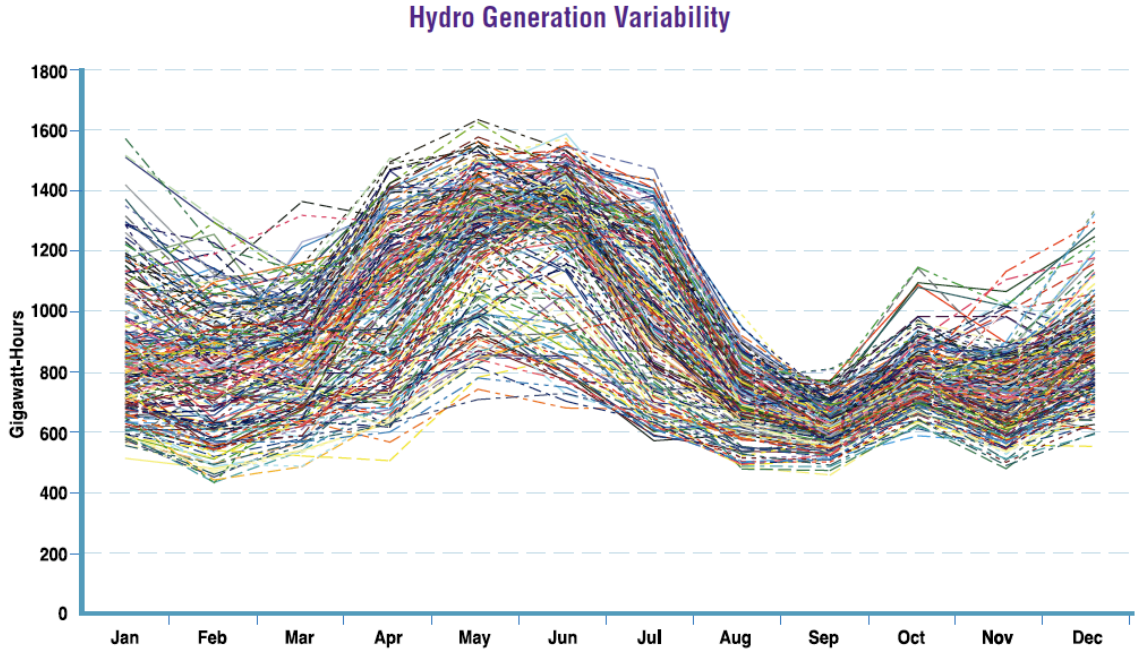


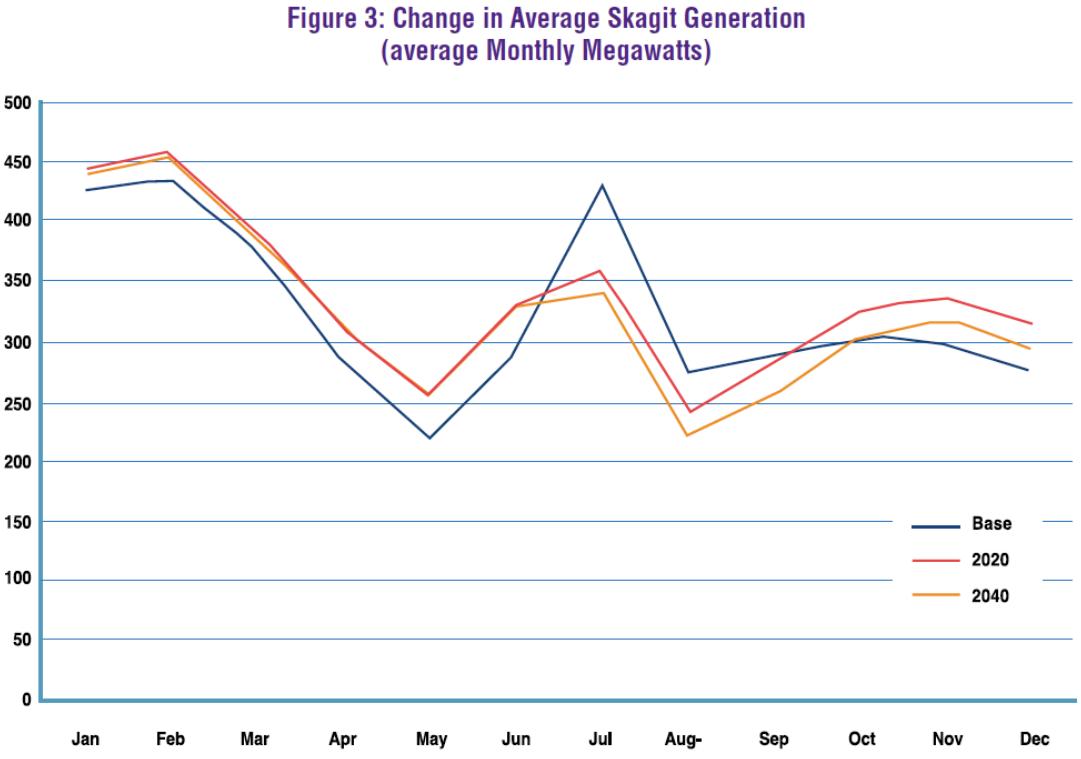


Figure 5.14. Top – Historical variability in generation of hydroelectricity by SCL, from the IRP, Executive Summary (2008). Bottom – Hydroelectricity generated by the SCL dams on the Skagit for the base climate, 2020, and 2040. From the IRP, Appendix G (2008). Note the difference in units (GW-hours vs. MW-months).

Table 5.1. SNOTEL stations in or near the Skagit watershed. The sensitivity estimates is derived from the plots appearing in Fig. 5.6.

| Site | NRCS ID | Elevation | First Water Year | Sensitivity |
|---|---|---|---|---|
| Beaver Pass | 21A01S | 1106 m | 2002 | 41% |
| Swamp Creek | 20A41S | 1197 m | 2000 | 27% |
| Thunder Basin | 20A07S | 1316 m | 1988 | 20% |
| Rainy Pass | 20A09S | 1490 m | 1982 | 12% |
| Harts Pass | 20A05S | 1978 m | 1982 | 4% |

Table 5.2. Statistics for the regressions of monthly SWE values upon April 1 SWE. These values are used to predict April 1 SWE, as shown in Fig. 5.10

| | Slope (cm SWE/cm SWE) | *y*-int (cm SWE) | $r^2$ |
|---|---|---|---|
| December 1 | 2.32 | 51.63 | 0.44 |
| January 1 | 1.51 | 33.31 | 0.57 |
| February 1 | 1.49 | 1.18 | 0.90 |
| March 1 | 1.09 | 5.19 | 0.97 |

# 6. SUMMARY AND FUTURE WORK

## *6.1 Summary*

In order to assess the impact of global warming on a natural resource, it is necessary to separate the effect of human-induced warming from the influences of natural climate variability. In the case of the Cascades snowpack, large swings in precipitation from year to year make it difficult to distill the impact of warming by examining trends in the historical record.

In this dissertation, it is demonstrated through sensitivity analysis (Chapter 2) and the analysis of the SNOTEL record (Chapter 3) that warming is likely to have a significant impact on the snowpack of the Cascades. Ignoring any changes in precipitation due to warming, 1°C of warming will reduce April 1 SWE by roughly 20%, relative to the long-term mean of April 1 SWE. This amount of loss is likely to increase the magnitude and frequency of extremely low snowpack years, which could undermine the typical decision-making protocols of regional water and hydroelectric power managers. In addition, the rate of melt of the snowpack during the spring will be accelerated. Following a 1°C warming, the reduction in accumulation in combination with the increased rate of melting will advance the melt-out date of the snowpack by nearly 2 weeks. For larger amounts of warming (>3°C), the melt season for the Cascades as a whole could begin in March instead of April.

Aside from the impact of warming on the snowpack, investigation of the observations from the Washington Cascades SNOTEL network (Chapter 3) provides insight into the daily and monthly variability of the snowpack. The day-to-day and

month-to-month variations in accumulation and melting can be efficiently represented by indices formed from the average of the daily changes in SWE observed across all stations. These indices show that a relatively large proportion of snowfall occurs during a relatively small number of winter days; melt is rare from December through March and the amount of SWE lost during melt events is typically small; and, daily melt during the spring is proportional to daily mean temperature. The relationship between daily melt and daily mean temperature can be exploited to generate a degree-day model for the rate of melting through the spring and summer. This model provides a reasonable estimate of the cumulative melt during the spring for the snowpack of the Cascades; its performance is slightly improved when a weighted-average of recent daily temperatures is used rather the unweighted daily mean temperature. In particular, this modification improves predictions of daily loss at the beginning of the melt season. Use of the weighted average allows the snowpack to have "memory," which represents the need for the snowpack to raise its temperature prior to the onset of melting.

The results of the sensitivity analysis and SNOTEL analysis are applied to the management and operations of Seattle City Light (SCL). SCL operates three dams located in the Skagit watershed, which is located in the North Cascades. These dams provide nearly 20% of the city of Seattle's electricity. For the coming decades, the impact of warming on the Skagit snowpack is similar to that for the Cascades as a whole – nearly 20% of the April 1 SWE would be lost for 1°C of warming and the rate of spring melt would be accelerated. It is recommended that SCL:

- consider infrastructure investments that might boost hydroelectric generation efficiency or capacity;
- examine alterations to current dam and reservoir operations as a way to adapt to the changes in snowpack;
- tailor the hydroelectric system to "worst case" scenarios associated with warming; and,
- extend their time frame for planning from 20 years to at least 50 years in the future.

Additionally, an accumulation forecast tool and a melt-season forecast tool are presented. The accumulation tool could be used by SCL within a single water year to predict April 1 SWE beginning two months in advance, with updates as warranted by snowfall events. The melt-season tool could be used to estimate the rate of melt throughout the spring, which could be related to spring and summer inflows to the SCL reservoirs. Both tools:

- provide additional lead-time for SCL's in-season decisions;
- introduce a real-time dynamic element to forecasts, which have previously relied solely on statistical relationships based upon historical climate conditions;
- permit the generation of scenarios based on April accumulation and spring temperature; and,
- yield forecast information at minimal cost.

The application of the results of this dissertation to SCL's operations and management illustrates how knowledge of the impacts of climate variability and

change upon a resource can be utilized to identify relevant adaptation options at the regional-scale.

*6.2 Future Work*

Three sets of future research questions are suggested by the results of this work:

1) How does the simulation of spring snowmelt by a distributed hydrological model compare to the predictions of the degree-day model? In particular, the model would indicate which terms in the energy balance equation are most important on the days during which the degree-day model performs poorly. It could then be determined which meteorological conditions and/or snowpack variables are primarily responsible for the forecast errors. Also, does the melt-out date of the snowpack simulated by a distributed model exhibit a similar sensitivity to global warming as estimated using the degree-day model?

2) How does the frequency of large snowfall events in the mountains compare with the frequency of large precipitation events in the lowlands? Would the probability distribution functions of daily snowfall and daily rainfall appear similar? Is there a strong correlation between the size of the leading event and the season-ending accumulated precipitation in the lowlands, as in the mountains? And would these relationships be applicable across the North American West, outside of the Washington Cascades?

3) What is the role of glacial melt in summer streamflow, and how might that role be affected by warming? Warming is likely to enhance glacial melting during the spring and summer. The additional streamflow arising from this glacial melt would partially offset the loss of streamflow from the snowpack. However, this offset is only temporary – once a glacier has lost significant area and mass, it will cease to contribute a significant amount of steamflow. Many of the tributaries that feed the Skagit receive a portion of their input from glaciers, especially during the summer. Estimating the glacial input to streamflow would be necessary to provide a complete understanding of the impacts of warming on the hydrology of the Skagit watershed. As additional motivation, large populations in Asia and South America depend on glacial melt from the Himalayas and Andes for their water supply. Understanding the relationship between warming and glacial melt could be helpful in assessing the impact of climate change on the development of these regions.

**REFERENCES**

American Society of Civil Engineers, 1996: *Hydrology Handbook, 2nd Edition.* Prepared by the Task Committee on Hydrology Handbook of Management Group D of the American Society of Civil Engineers. Manual No. 28. American Society of Civil Engineers, New York, New York. 784 pp.

Anderson, E.A., 2006: *Snow Accumulation and Ablation Model – SNOW-17.* http://earth.boisestate.edu/home/jmcnamar/hydro09/Readings/snow17.pdf

Anderson, E.A., 1976: A Point Energy and Mass Balance Model of a Snow Cover. *NOAA Technical Report NWS 19*, 150 pp.

Army Corps of Engineers, 1956: *Snow hydrology; summary report of the snow investigations.* Portland, Oregon, North Pacific Division, Corps of Engineers, U.S. Army, 437pp.

Bales, R.C., N.P. Molotch, T.H. Painter, M.D. Dettinger, R. Rice, and J. Dozier, 2006: Mountain hydrology of the western United States. *Water Resources Research*, **42**, W08432, doi 10.1029/2005WR004387.

Barnett, T.P, D.W. Pierce, H.G. Hidalgo, C. Bonfils, B.D. Santer, T. Das, G. Bala, A.W. Wood, T. Nozawa, A.A. Mirin, D.R. Cayan, M.D. Dettinger, 2008: Human-Induced Changes in the Hydrology of the Western United States. *Science,* **319**, 1080-1083.

Brohan, P., J.J. Kennedy, I. Haris, S.F.B. Tett and P.D. Jones, 2006: Uncertainty estimates in regional and global observed temperature changes: a new dataset from 1850. *J. Geophysical Research* **111**, D12106

Cayan, D.R., 1996: Interannual Climate Variability and Snowpack in the Western United States. *J. Climate*, **9**, 928-948.

Casola, J.H., L. Cuo, B. Livneh, D.P. Lettenmaier, M.T. Stoelinga, P.W. Mote, and J.M. Wallace, 2009: Assessing the Impacts of Global Warming on Snowpack of the Washington Cascades. *J. Climate*, **22**, 2758-2772.

Casola, J.H. and J.M. Wallace, 2007: Identifying Weatehr Regimes in the Wintertime 500-hPa Geopotential Height Field for the Pacific-North American Sector Using a Limited-Contour Clustering Technique. *Journal of Applied Meteorology and Climatology,* **46**, 1619-1630.

Cheng, W., 2009: Performance of Hydroelectric Projects in the Face of Climate Change: A Case Study of the Skagit Hydroelectric Project. Skagit Climate Change Workshop, Padilla Bay National Estuaries Reserve, March 5, 2009.

Church, Jr., J.E., 1908: *The Mt. Rose Weather Observatory 1906-1907, with notes on the progress of the observatory 1907-1908.* Agricultural Experiment Station, The University of Nevada, Bulletin No. 67, Reno, Nevada. 36pp.

Church, Jr., J.E., 1912: The progress of the Mount Rose Observatory, 1906-1912. *Science,* **36,** 796-800.

Clark, M.P., M.C. Serreze, and G.J. McCabe, 2001: Historical effects of El Niño and La Niña events on the seasonal evolution of the montane snowpack in the Columbia and Colorado River Basins. *Water Resour. Res*, **37**, 741-757

Colle, B.A., C.F. Mass, and K.J. Westrick, 2000: MM5 precipitation verification over the Pacific Northwest during the 1997-1999 cool seasons. *Weather and Forecasting,* **15,** 730-744.

Cornwall, W., 2008: UW Study esamine decline of snowpack. *Seattle Times*, August 6, 2008.
http://seattletimes.nwsource.com/html/localnews/2008094636_climate06m.html

European Center for Medium-Range Weather Forecasts (ECMWF), *European Reanalysis (ERA-40) Atlas (web-version)*. Surface climatologies: Net surface fluxes of solar radiation. Accessed at http://www.ecmwf.int/research/era/ERA-40_Atlas/docs/section_B/parameter_nsfosrpd.html#

Note – information regarding the Reanalysis itself can be found at:

Uppala, S.M., Kållberg, P.W., Simmons, A.J., Andrae, U., da Costa Bechtold, V., Fiorino, M., Gibson, J.K., Haseler, J., Hernandez, A., Kelly, G.A., Li, X., Onogi, K., Saarinen, S., Sokka, N., Allan, R.P., Andersson, E., Arpe, K., Balmaseda, M.A., Beljaars, A.C.M., van de Berg, L., Bidlot, J., Bormann, N., Caires, S., Chevallier, F., Dethof, A., Dragosavac, M., Fisher, M., Fuentes, M., Hagemann, S., Hólm, E., Hoskins, B.J., Isaksen, L., Janssen, P.A.E.M., Jenne, R., McNally, A.P., Mahfouf, J.-F., Morcrette, J.-J., Rayner, N.A., Saunders, R.W., Simon, P., Sterl, A., Trenberth, K.E., Untch, A., Vasiljevic, D., Viterbo, P., and Woollen, J. 2005: The ERA-40 re-analysis. *Quart. J. R. Meteorol*. Soc., **131**, 2961-3012.doi:10.1256/qj.04.176

Fleagle, R.G., 1991: Policy implications of Global Warming for the Northwest. *Northwest Environmental Journal,* **7**, 329-343.

Garen, D.C., and D. Marks, 2005: Spatially distributed energy balance snowmelt modeling in a mountainous river basin: estimation of meteorological inputs and verification of model results. *J. Hydrology*, **315**, 126-153.

Groisman, P.Ya., R.W. Knight, T.R. Karl, D.R. Easterling, B. Sun, and J.H. Lawrimore, 2004: Contemporary Changes of the Hydrological Cycle over the Contiguous United States: Trends Derived from In Situ Observations. *J. Hydromet.*, **5**, 64-84.

Gupta, S.K., N.A. Ritchey, A.C. Wilber, C.H. Whitlock, G.C. Gibson, P.W. Stackhouse, 1999: A climatology of surface radiation budget derived from satellite data. *J. Climate*, 12, 2691-2710.

Hamlet, A.F., P.W. Mote, M.P. Clark, and D.P. Lettenmaier, 2005: Effects of Temperature and Precipitation Variability on Snowpack Trends in the Western United States. *J. Climate*, **18**, 4545-4561.

Howat, I.M., and S. Tulaczyk, 2005: Climate sensitivity of spring snowpack in the Sierra Nevada. *J. Geophys. Res.*, **110**, F04021, doi: 10.1029/2005JF000356.

Jin, J., N.L. Miller, S. Sorooshian, and X. Gao, 2006: Relationship between atmospheric circulation and snowpack in the western USA. *Hydrol. Process.*, **20**, 753-767.

Karl, T.R., C.N. Williams Jr., F.T. Quinlan, and T.A. Boden, 1990: United States Historical Climate Network (HCN) serial temperature and precipitation data. Publication 304, Environmental Sciences Division, Carbon Dioxide Information and Analysis Center, Oak Ridge national Laboratory, Oak Ridge, TN.

Kalnay, E., M. Kanamitsu, R. Kistler, W. Collins, D. Deaven, L. Gandin, M. Iredell, S. Saha, G. White, J. Woollen, Y. Zhu, M. Chelliah, W. Ebisuzaki, W. Higgins, J. Janowiak, K.C. Mo, C. Ropelewski, J.Wang, A. Leetmaa, R. Reynolds, R. Jenne, D. Joseph, 1996: The NCEP/NCAR 40-year reanalysis project. *Bull. Amer. Meteor. Soc.*, **77**, 437-471.

Knowles, N., M.D. Dettinger, and D.R. Cayan, 2006: Trends in Snowfall versus Rainfall in the Western United States. *J. Climate*, **19**, 4545-4559.

Mantua, N.J., S.R. Hare, Y. Zhang, J.M. Wallace, and R.C. Francis, 1997: A Pacific interdecadal climate oscillation with impacts on salmon production. *Bull. Amer. Meteor. Soc.*, **78**, 1069-1079.

McCabe, G.J. and M.D. Dettinger, 2002: Primary Modes and Predictability of year-to-year Snowpack Variations in the Western United States from Teleconnections with Pacific Ocean Climate. *J. Hydromet.*, **3**, 13-25.

McGuire Elsner, M., L. Cuo, N. Voisin, J. Deems, A.F. Hamlet, J. Vano, K.E.B. Mickelson, S.Y. Lee, and D.P. Lettenmaier, 2009: Implications of 21st century climate change for the hydrology of Washington State. Chapter 3.1 in *The Washington Climate Change Impacts Assessment: Evaluating Washington's Future in a Changing Climate*, Climate Impacts Group, University of Washington, Seattle, Washington.

Mote, P.W., A.F. Hamlet, and E. Salathé, 2008: Has spring snowpack declined in the Washington Cascades? *Hydrology and Earth System Sciences*, **12**, 193-206.

Mote, P.W., 2006: Climate-Driven Variability and Trends in Mountain Snowpack in Western North America. *J. Climate*, **19**, 6209-6220.

Mote, P.W., A.F. Hamlet, M.P. Clark, and D.P. Lettenmaier, 2005: Declining Mountain Snowpack in Western North America. *Bull. Amer. Meteor. Soc.*, **86**, 39-49.

Nolin, A.W. and C. Daly, 2006: Mapping "At Risk" Snow in the Pacific Northwest. *J. Hydromet.*, **7**, 1164-1171.

Ohmura, A., 2001: Physical Basis for the Temperature-Based Melt-Index Method. *J. Applied Meteorology*, 40, 753-761.

Rasmussen, L.A., H. Conway, P.S. Hayes 2000: The accumulation regime of Blue Glacier, USA, 1914-96. *J. Glaciology*, **46**, 326-334.

Regonda, S.K., B. Rajagopalan, M. Clark, and J. Pitlick., 2005: Seasonal Cycle Shifts in Hydroclimatology over the Western United States. *J. Climate*, **18**, 372-384.

Salathé Jr, E.P., Y. Zhang, L.R. Leung, Y. Qian, 2009: Regional Climate Model Projections for the State of Washington. *Climatic Change*, submitted.

Salathé, E.P., P.W. Mote, and M.W. Wiley, 2007: Review of scenario selection and downscaling methods for the assessment of climate change impacts on hydrology in the United States pacific northwest. *Int. J. Climatol.,* **27**, 1611-1621.

Seager, R., N. Naik, M. Ting, M.A. Cane, N. Harnik, and Y. Kushnir, 2009: Adjustment of the atmospheric circulation to tropical Pacific SST anomalies: Variaiblity of transient eddy propagation in the Pacific-North America sector. *Q.J.R. Meteorol. Soc.*, *in press*.

Seattle City Light, 2008: Seattle City Light, Fingertip Facts, Your Electric Utility's Customer Information Guide. September 2008. 24 pp.

Seattle City Light, 2008: Integrated Resource Plan. 86pp.
http://www.seattle.gov/light/news/issues/irp/

Seattle City Light, 2008: Integrated Resource Plan, Appendix G, Climate Change in the 2008 IRP. 12pp.
http://www.seattle.gov/light/news/issues/irp/docs/SCLIRP2008_Appendix_G_Climate_Change.pdf

Seattle City Light, Annual Report 2007. 84pp.
http://www.seattle.gov/light/AboutUs/AnnualReport/

Serreze, M.C., M.P. Clark, R. L. Armostrong, D.A. McGinnis, R. S. Pulwarty, 1999: Characteristics of the western United States snowpack from snowpack telemetry (SNOTEL) data. *Water Resour. Res.,* **35,** 2145-2160.

Serreze, M.C. M.P. Clark, and A. Frei, 2001: Characteristics of large snowfall events in the montane western United States as examined using snowpack telemetry (SNOTEL) data. *Water Resour. Res*, **37**, 675-688.

Solomon, S., D. Qin, M.Manning, M.Marquis, K. Averyt, M. M. B. Tignor, H. L. Miller Jr., and Z. Chen, Eds., 2007: *Climate Change 2007: The Physical Science Basis.* Cambridge University Press, 996 pp.

Stewart, I.T., D.R. Cayan, and M.D. Dettinger, 2005: Changes Toward Earlier Streamflow Timing Across Western North America. *J. Climate*, **18**, 1136-1155.

Stoelinga, M.T., M.D. Albright, and C. F. Mass, 2009: A New Look at Snowpack Trends in the Cascade Mountains. *J. Climate*, submitted.

Storck, Pascal, 2000: Trees, snow, and flooding : an investigation of forest canopy effects on snow accumulation and melt at the plot and watershed scales in the Pacific Northwest. PhD Dissertation

Sturm, M., J. Holmgren, M. König, K. Morris, 1997: The thermal condu ctivity of seasonal snow. *J. Glaciology*, **43**, 26-41.

Tarboton, D. G., T. G. Chowdhury and T. H. Jackson, 1995: "A Spatially Distributed Energy Balance Snowmelt Model," in Biogeochemistry of Seasonally Snow-Covered Catchments, ed. K. A. Tonnessen et al., Proceedings of a Boulder Symposium, July 3-14, IAHS Publ. no. 228, p.141-155.

Yang D.Q., B.E. Goodison, J.R. Metcalfe, V.S. Golubev, R. Bates, T.Pangburn, C.L. Hanson, 1998: Accuracy of NWS 8" standard nonrecording precipitation gauge: Results and application of WMO intercomparison. *Journal of Atmospheric and Oceanic Technology*, **15**, 54-68.